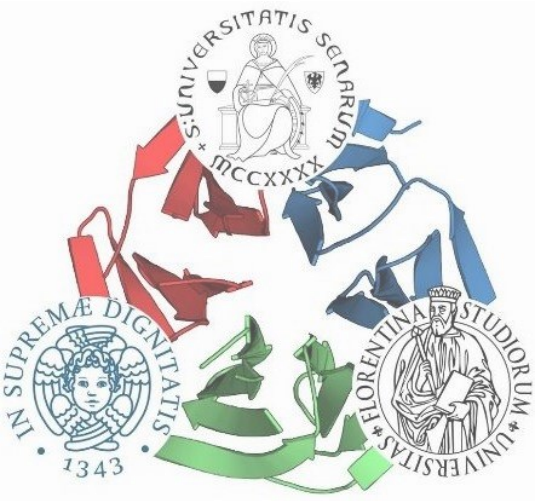

Doctoral Program in Biochemistry and Molecular Biology
Bibim 2.0 – Cycle XXXVI

Investigation on the role of thyroid hormones and their derivatives in different physiopathogenetic mechanisms using HPLC-MS/MS

Candidate
Andrea Bertolini

Supervisor
Prof. Alessandro Saba

Academic year 2022/2023

Abstract

High Performance Liquid Chromatography coupled to Tandem Mass Spectrometry (HPLC-MS/MS) is a versatile analytical technique widely applied in chemistry, biology, laboratory medicine, and biochemistry. This integrated system combines liquid chromatography with tandem mass spectrometry, facilitating the effective separation, identification, and quantification of compounds within complex mixtures. The significance of HPLC-MS/MS extends to various fields, including pharmaceuticals, environmental analysis, and metabolites analysis. This research focused on the application of HPLC-MS/MS for the quantification of thyroid hormones (TH), such as 3,5,3'-triiodothyronine (T3) and thyroxine (T4), along with their metabolites. TH play crucial roles in growth processes, development, and energy metabolism, motivating a comprehensive exploration of their dynamics in different physiological and pathological processes.

The study is organized around four investigations utilizing HPLC-MS/MS as a pivotal instrument with unique pre-analytical approaches and analytical methods to explore diverse matrices. Firstly, the research unveiled neurocognitive dynamics in adult-onset hypothyroidism, employing a rodent pharmacological model. Using an HPLC-MS/MS method, we quantified the total fraction of T3 and T4 in serum samples, validating the experimental plan and providing insights into the impact of various replacement strategies on neurocognitive and neurobiological alterations. Secondly, the thesis delved into TH dynamics in diabetic retinopathy, utilizing HPLC-MS/MS to detect and quantify T3 and T4 in plasma and retina samples from a type 2 diabetes mouse model. This shed light on potential mechanisms, including T3-dependent microRNA/gene regulatory circuits and mitochondrial function. Thirdly, the study addressed iodine dynamics and the role of enzyme dehalogenase 1 (DEHAL1), employing a *Dehal1* KO mouse model. With an adapted method using a derivatization process, our HPLC-MS/MS analysis was able to quantify precursors MIT and DIT in different iodine-supplementation conditions, enhancing understanding of iodine recycling and its consequences. Finally, the thesis investigated *DEHAL1* gene mutations in congenital hypothyroidism, using HPLC-MS/MS to measure MIT and DIT levels in serum and urine of patients from different Sudanese families.

The findings from the pharmacologically induced hypothyroidism model underscored the necessity and sufficiency of levothyroxine (L-T4) alone to restore memory and neuroprogenitors levels to the euthyroid state, challenging the hypothetical impact on

neurogenetic pathways of alternative replacement treatments, such as those implying the use of the metabolite T1AM. Subsequently, we revealed the existence of a local low T3 state (LT3S) in the diabetic retina. This highlighted the TH-dependent response to hyperglycemia-induced stress, unveiling a complex temporal dynamic influencing retinal responses in diabetic retinopathy. Through the development of a new optimized HPLC-MS/MS method, the research uncovered the crucial role of the enzyme DEHAL1 in iodine metabolism within the thyroid gland. Elevated iodotyrosines emerged as biomarkers for the risk of iodine-deficient hypothyroidism, providing translational insights for clinical validation. Eventually, the measurement of serum and urine MIT and DIT emerged as sensitive indicators of iodotyrosines deiodination defects in the presence of *DEHAL1/IYD* mutations, surpassing traditional urine iodine levels and thyroid function tests. This approach offered valuable diagnostic and management insights into dehalogenase-related disorders, emphasizing the importance of personalized and nuanced approaches.

In conclusion, this diverse series of examinations highlighted the instrumental role of HPLC-MS/MS in advancing our understanding of TH dynamics across various physiological and pathological contexts. The precision and versatility of this technique have yielded invaluable insights, paving the way for future research endeavors and potential clinical applications.

Summary

Introduction

1. **High Performance Liquid Chromatography Coupled to Tandem Mass Spectrometry**
   1.1 The basics of chromatography
   1.2 High Performance Liquid Chromatography (HPLC)
   1.3 MS principles

2. **Thyroid hormones**
   2.1 TH synthesis
   2.2 TH transport and regulation
   2.3 TH metabolism

3. **TH in neurogenesis and cognitive disorders**

4. **The homeostatic role of TH in diabetic retinopathy**

5. **The importance of iodine recycling: DEHAL1**

6. **The use of HPLC-MS/MS for the quantification of TH**

Aim

Materials and Methods

7.1 Mouse model of pharmacologically induced hypothyroidism

7.1.1 Serum samples
7.1.2 Statistical analysis

7.2 Diabetic retinopathy in *db/db* mice (a model of type 2 diabetes)

7.2.1 Plasma and retinas of diabetic mice for T3 and T4 quantification
7.2.2 Statistical analysis

7.3 Iodine deficiency model

7.3.1 Plasma and urines samples derivatization process and analysis
7.3.2 Statistical analysis

7.4 Investigating *DEHAL1* gene mutations in congenital hypothyroidism

7.5 Further investigations on TH-related metabolism with molecular biology techniques

7.5.1 Immunofluorescence analysis for hippocampal neurogenesis
7.5.2 Gene expression analysis of neurogenetic markers
7.5.3 Behavioural tests for hypothyroidism effects investigation
7.5.4 Electroretinography and Immunofluorescence analysis in *db/db* mice
7.5.5 MIO-M1 cell culture, mRNA and miRNA genetic analysis and oxidative stress tests in the diabetic retinopathy context

Results

8.1 Generation of a pharmacologically induced model of hypothyroidism

8.1.1 T3 and T4 serum quantification
8.1.2 Behavioural tests results
8.1.3 The impact of different replacement therapies on neurogenesis and neurogenetic pathways

8.2 Visually impaired *db/db* mice does not show alteration in plasma TH

8.2.1 Diabetes leads to notable alterations in TH levels and markers associated with TH signalling in the retina
8.2.2 Genetic and functional insights of *db/db* mice

Figures List

Tables List

Abbreviations

3-T1 = 3-iodo-L-Thyronine

ACF = Acriflavine

AcK = Potassium acetate

ACN = Acetonitrile

AcOH = Acetic acid

AF-1 = Activation function 1

APCI = Atmospheric-pressure chemical ionization

API = Atmospheric pressure ionization

ApoB = Apolipoprotein B

APPI = Atmospheric-pressure photo ionization

βG = βeta Galactosidase

BBB = Blood brain barrier

BRB = Blood retinal barrier

BSA = Bovine serum albumin

BW = Body weight

CAD = Collision gas

cAMP = Cyclic adenosine monophosphate

cDNA= Complementary DNA

CE = Collision energy

CEM = Channel electron multiplier

CH = Congenital Hypothyroidism

CH_2Cl_2 = Methylene chloride

CI = Chemical ionization

CID = Collision-induced dissociation

ClO_4^- = Perchlorate

CNS = Central nervous system

CP = Choroid plexus

CPT2 = Carnitine palmitoyltransferase 2

CSF = Cerebrospinal fluid

CUR = Curtain gas

CxP = Collision exit potential

DBD = DNA binding domain

DCX= Doublecortin

DEHAL = Iodotyrosine dehalogenase

DESI = Desorption electrospray ionization

DI = Discrimination index

DIO = Iodothyronine deiodinase

DIT = Di-iodotyrosine

DNA = Deoxyribonucleic Acid

DNT = 3,5-dinitro-L-Tyrosine

DP = Declustering potential

DR = Diabetic retinopathy

DUOX = Dual oxidase

ED = Equilibrium dialysis

EI = Electron ionization

EMA = European Medicines Agency

EP = Entrance potential

EPM = Elevated Plus Maze

ERG = Electroretinogram

ERK = Extracellular related kinase

ESI = Electrospray ionization

FA = Formic acid

FAB = Fast atom bombardment

FMN = Flavin mononucleotide

fTH = Free TH

Gadph= Glyceraldehyde-3-phosphate dehydrogenase

GC = Gas chromatography

GC-MS = Gas chromatography coupled to Mass Spectrometry

GFAP = Glial fibrillary acidic protein

GH = Growth hormone

GLUT = Glucose transporter

GS = Gas source

GTP = Guanosine-5'-triphosphate

H_2O_2 = Hydrogen Peroxide

HCl = Hydrochloric acid

HIF-1 = Hypoxia-inducible factor 1

HILIC = Hydrophilic interaction liquid chromatography

HG = High glucose

HO = Homozygous

HO-1 = Heme oxygenase-1

HPLC = High Performance Liquid Chromatography

HPLC-MS/MS = High Performance Liquid Chromatography coupled to tandem Mass Spectrometry

Hprt1 = Hypoxanthine-guanine phosphoribosyltransferase

HPT = Hypothalamic-pituitary-thyroid axis

HT = Heterozygous

I = Iodine

I^- = Iodide

I^+ = Iodinium

ID = Iodine deficiency

IQ1 = Focusing lens 1

IS = Internal standard

ISV = Ion spray voltage

ITDD = Iodotyrosine deiodinase deficiency

IYD = Iodotyrosine deiodinase

K67 = 2-acetonyl-1,4-bis[(4-ethoxybenzenesulfonyl)amino]naphthalene

Ka = Association constant

KCN = Voltage-gated K^+ channels

Kdr = Kinase Insert Domain Receptor

Ki67 = Kinase 67

Kit = KIT Proto-Oncogene, Receptor Tyrosine Kinase

Km = Michaelis-Menten constant

KO = Knock-out

KOMP = KO mouse project repository

L1cam = L1 Cell Adhesion Molecule

LAT = L-Type amino acid transporters

LBD = Ligand binding domain

LC =Liquid Chromatography

LID = Low iodine diet

LIT = Linear ion trap

LLE = Liquid-liquid extraction

LOD = Limit of detection

LOQ = Limit of quantification

LT3S = Low T3 state

L-T4 = Levothyroxine

MALDI = Matrix-assisted laser desorption ionization

MAPK = Mitogen-activated protein kinase

MCT = Mono-carboxylate transporter

MeOH = Methanol

MFN2 = Mitofusin-2

mRNA= RNA messenger

MIO-M1 = Moorfields/Institute of Ophthalmology-Müller 1

miRNA/miR = microRNA

MIT = Mono-iodo tyrosine

MRM = Multiple reaction monitoring

MS = Mass Spectrometry

MS/MS = Tandem Mass Spectrometry

NADPH = Nicotinamide adenine dinucleotide phosphate

NaOH = Sodium hydroxide

Neurog2 = Neurogenin 2

NH_4OH = Ammonium hydroxide

NID = Normal iodine diet

NIS = Sodium-Iodide symporter

NF-kB = Nuclear factor kappa-light-chain-enhancer of activated B cells

Ngf = Nerve growth factor

NP = Normal phase

NP-LC = Normal phase liquid chromatography

Nrf2 = Nuclear factor erythroid 2-related factor 2

NTCP = Na+/taurocholate co-transporter

Ntf3 = Neurotrophin 3

OATP = Organic anion transporter polypeptide

OPA1 = Optic atrophy 1

ORT = (Novel) Object Recognition Test

PBS = Phosphate Buffer Saline

PCR = Polymerase chain reaction

PDA = Photo diode array

PERG = Pattern ERG

PGC-1α = Peroxisome proliferator-activated receptor-gamma coactivator

phERG = Photopic ERG

PIK-3 = Phosphatidylinositol 3-kinase

pNF-kB = Phosphorylated NF-kB from

PTU = 6n-propyl-2-thiouracil

PVN = Hypothalamic paraventricular nucleus

QMF = Quadrupole mass filter

qPCR = Quantitative PCR

QTOF = Quadrupole time-of-flight

Qtrap = Quadrupole trap

Qn = Quadrupole n

Rac = Ras-related C3 botulinum toxin substrate

RhoA = Ras homolog family member A

RGC = Retinal ganglion cell

ROS = Reactive oxygen species

ROUT = Robust regression and Outlier removal

RNA = Ribonucleic Acid

RP = Reverse phase

RP-LC = Reverse phase liquid chromatography

RSD = Relative standard deviation

RT = Room temperature

rT3 = 3,3',5'-triiodothyronine or reverse T3

RXR = Retinoid X receptor

SAGE = Serial analysis of gene expression

SAP = Stretch-attend postures

scERG = Scotopic ERG

SCN^- = Thiocyanate

SD = Standard deviation

SEM = Standard error mean

SGZ= Sub granular zone

S-K = Sandell-Kolthoff

SLC = Solute carrier family

SPE = Solid phase extraction

SRM = Selective reaction monitoring

T0AM = Iodothyronamine

T1AM = 3-iodothyronamine

T2 = Diiodothyronine

T2AM = Diiodothyronamine

T3 = 3,5,3’-triiodothyronine

T3AM = Triiodothyronamine

T4 = 3,3’,5,5’-tetraiodothyronine or Thyroxine

TA1 = 3-iodothyroacetic acid

TAAR1 = Trace amine associated receptor 1

TBG = Thyroid-binding globulin

Tbp = TATA-binding protein

TEM = Temperature

Tetrac = 3,5,3’,5’-tetraiodothyroacetic acid

TG = Thyroglobulin

TH = Thyroid hormones

TOF = Time-of-flight

TPO = Thyroid peroxidase

TR = Thyroid receptor

TR = Thyroid responsive element

TRH = Thyrotropin-releasing factor

Triac = 3,5,3’-triiodothyroacetic acid

TSH = Thyroid-stimulating hormone

TTH = Total TH

TTR = Transthyretin

UIC = Urinary iodide concentration

UF = Ultrafiltration

UHPLC = Ultra-high pressure liquid chromatography

UTR = Untranslated region

UV = Ultraviolet

VEGF = Vascular endothelial growth factor

VIS = Visible

VLID = Very low iodine diet

WES = Whole exome sequencing

WHO = World Health Organization

WT = Wild-type

ZO1 = Zona occludens 1

Introduction

1. High Performance Liquid Chromatography Coupled to Tandem Mass Spectrometry

High Performance Liquid Chromatography coupled to Tandem Mass Spectrometry (HPLC-MS/MS) is a powerful analytical technique employed in the field of chemistry, biology, laboratory medicine, and biochemistry for the comprehensive analysis of compounds within complex mixtures. This instrumentation integrates a liquid chromatography system with a tandem mass spectrometer, to achieve effective separation, identification, and quantification of components. In HPLC, a high-pressured liquid mobile phase is utilized to separate compounds based on their affinity for both mobile phase and stationary phase, typically packed into a chromatographic column. The separation of distinct compounds is the result of their competitive interaction with mobile phase and stationary phase, resulting in their separation. Mass Spectrometry (MS) is a technique focused on analysing the mass-to-charge ratio of charged particles. In the context of HPLC-MS/MS, the mass spectrometer is employed as detector to both identify and quantify the compounds separated by HPLC. Tandem Mass Spectrometry (MS/MS) enhances the specificity and sensitivity of compound identification by utilizing two mass analysers in series. The first analyser selects one (or more) specific ion from the mixture, namely precursor ion, while the second analyser examines the fragment ions produced inside a collision cell, placed between the first and the second analyser, from the precursor ion. These latter ions, named product ions, provide structural information about the original compound. The coupling of HPLC with MS/MS combines the separation capabilities of liquid chromatography with the precise and sensitive detection of tandem mass spectrometry. This integration facilitates detailed and accurate analysis of complex mixtures, proving particularly valuable in pharmaceuticals, environmental analysis, and metabolomics, where identifying and quantifying compounds at low concentrations is crucial.

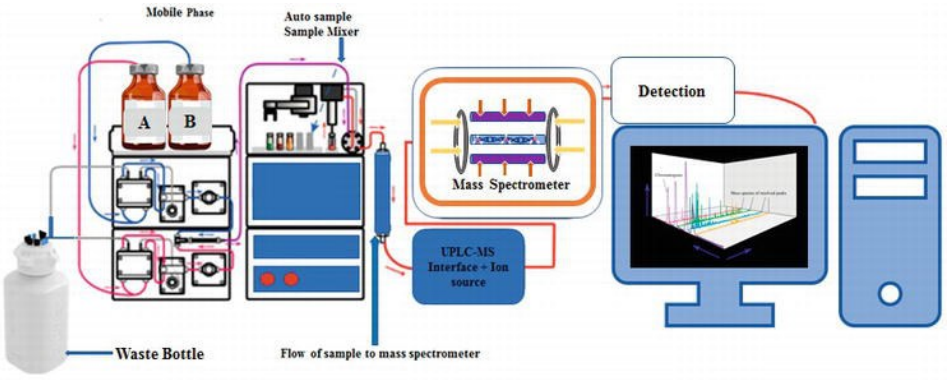

Figure 1. HPLC-MS/MS schematic and representative diagram (adapted from Ashraf SA *et al*. 2019[1]).

1.1 The basics of chromatography

Chromatography is a separation technique that separates and analyses components of a mixture based on their differential distribution between a stationary phase and a mobile phase. The separation process is influenced by various factors, including the molecular characteristics related to adsorption, partition, and affinity, as well as the differences in their molecular weights[2,3]. These differences result in certain components of the mixture remaining in the stationary phase for a longer period of time, causing them to move slowly within the chromatography system, while others quickly pass into the mobile phase and exit the system faster[4]. The chromatography technique is so based on two main components:

1. Stationary phase, which is always composed of either a solid phase or a layer of liquid adsorbed onto the surface of a solid support.

2. Mobile phase, which is always composed of either a liquid or a gaseous component.

The interaction between the stationary phase, mobile phase, and the substances present in the mixture is the fundamental factor that determines the separation of molecules from each other. Partition-based chromatography methods are highly effective in separating and identifying small molecules such as amino acids, carbohydrates, and fatty acids. On the other hand, affinity chromatography techniques, such as ion-exchange chromatography, are more efficient in separating macromolecules like nucleic acids and proteins. Gas-liquid chromatography is employed for the separation of alcohol, ester, lipid, and amino groups, as well as for observing enzymatic interactions. Agarose-gel chromatography is used for purifying RNA, DNA particles, and viruses[5].

In chromatography, the stationary phase refers to either a solid phase or a liquid phase that is coated on the surface of a solid phase, while the mobile phase, on the other hand, is a gaseous or liquid phase that flows over the stationary phase. If the mobile phase is a liquid, it is referred to as liquid chromatography (LC), while if it is a gas, it is called gas chromatography (GC). GC is commonly used for mixtures of volatile compounds while LC is particularly useful for thermal unstable and non-volatile samples[6]. The main purpose of applying chromatography is to achieve a satisfactory separation of the matrix component within a suitable time interval[7].

1.2 High Performance Liquid Chromatography (HPLC)

The term HPLC, or High Performance Liquid Chromatography, denotes a liquid chromatography separation technique conducted under elevated operational pressures, reaching up to hundreds of bars, which can extend into the thousands of bars in ultra-high pressure liquid chromatography (UHPLC) instruments. HPLC is a widely used technique in various fields, including pharmaceuticals, food and beverage, environmental analysis, and forensic science. When coupled to suitable detectors, it can be highly sensitive and detects trace amounts of compounds in complex mixtures. The quantification of a particular compound in a sample can be determined by comparing its peak area or height to that of solutions of the authentic standard of the analyte at known concentrations, or better to a calibration curve built with solutions of the authentic standard at different concentration levels.

In practice, the analytes are dissolved in a suitable liquid mobile phase and then pumped through the stationary phase, which is the core of the HPLC system, where the separation occurs. The stationary phase is contained in a chromatographic column, that is tightly packed with solid particles having size, pores, and surface coating able to interact with the molecules of interest. Each compound interacts differently with both the adsorbent material and the eluent, resulting in a different retention time. Generally, the higher the affinity for the stationary phase (or the lower the affinity for the mobile phase), the later a compound is eluted from the column. Conversely, an analyte with a lower affinity for the stationary phase will be eluted with shorter retention times from the chromatographic column. The nature of interactions is contingent upon the chemical structure of the compound, as well as its physical-chemical properties, including polarity, and the characteristics of both stationary and mobile phases. Therefore, the selection of the stationary phase, as well as that of the mobile phase, is crucial in achieving optimal selectivity for separating the various components of a mixture[8]. Among the many commercially available stationary phases, reverse phase (RP) stationary phases are widely used in HPLC coupled to MS, due to the compatibility of many solvents used in MS, and because it is suitable for separating a wide range of compounds.. Unlike the traditional normal phases, which utilized silica or alumina as the stationary phase, RP stationary phases are coated with siloxane and various alkyl (C8 or C18) or aryl groups on the surface of the silica particles. The terminal portion of the group is responsible for the interaction between the stationary phase and the analytes.

Another separation technique that's been widely used for polar profiling in metabolomics studies is the Hydrophilic Interaction Liquid Chromatography (HILIC). Although it was initially considered a variant of normal phase liquid chromatography (NP-LC) due to historical reasons, the separation mechanism employed in HILIC is more intricate than that of NP-LC. The term HILIC was coined by Alpert in 1990[9], and since 2003, there has been a significant increase in the number of publications concerning it[10]. HILIC employs traditional polar stationary phases like silica, amino, or cyano. However, the mobile phase used in HILIC is similar to that of the RP liquid chromatography (RP-LC) mode[10–15]. It is appropriate for the analysis of compounds in complex systems that consistently elute near the void in RP chromatography. Polar samples exhibit favourable solubility in the aqueous mobile phase utilized in HILIC, thereby overcoming the limitations associated with poor solubility often encountered in NP-LC. HILIC does not necessitate the use of expensive ion pair reagents and can be conveniently coupled with MS, particularly in the electrospray ionization (ESI) mode. In contrast to RP-LC, gradient elution in HILIC commences with a low-polarity organic solvent and elutes polar analytes by increasing the polar aqueous content[16].

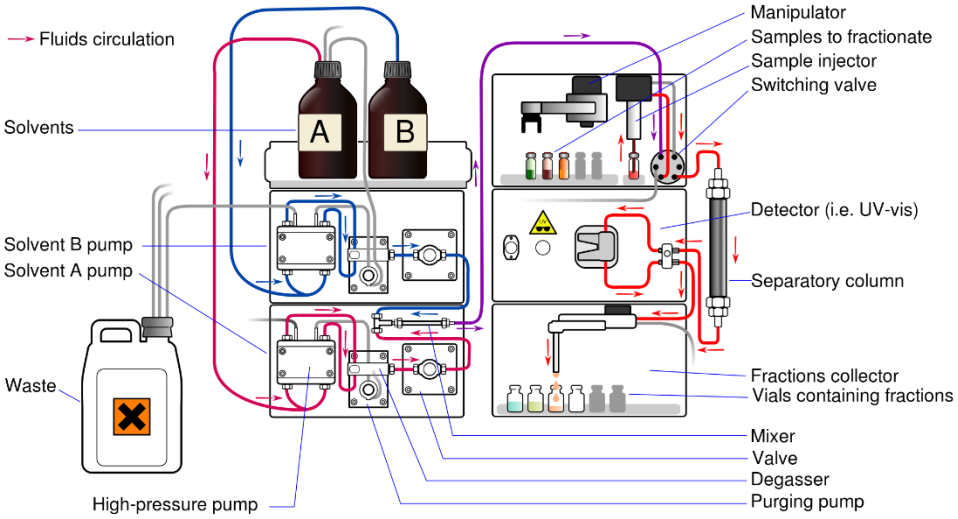

Figure 2. HPLC system layout (adapted from chemdictionary.org)

The HPLC system is structured with several integrated modules, collectively forming what is colloquially referred to as the HPLC tower. This tower typically comprises distinct sections, each serving a crucial role in the chromatographic process. The primary components include a solvent reservoir designed for storing the necessary solvents, a pump that can be either binary (for two pumped solvents) or quaternary (for four pumped solvents), an autosampler for

automated sample injection, a column compartment responsible for housing and maintaining the column temperature, and a detector for the measurement of the separated compounds.

The mobile phase typically consists of a blend of two solvents or two solvent mixtures, commonly comprising an organic phase and an aqueous phase, which are mixed to each other in a solvent mixer included in the pump, in order to make the mobile phase homogeneous. The selection of the mobile phase is contingent upon factors such as the complexity of the mixture, the characteristics of analytes, and the specific chromatographic column employed. In instances where the mixture components are inadequately resolved under isocratic conditions, a gradient condition may be employed, allowing for variations in the mobile phase composition over time. Under isocratic conditions, the mobile phase composition remains constant throughout the chromatographic analysis. In contrast, a gradient condition involves a systematic alteration in the ratio of the organic solvent to water (or vice versa for HILIC), often entailing a gradual increase in the organic solvent concentration until it reaches a point of reversing the relative proportions of the two solvents. The judicious choice between isocratic and gradient conditions is pivotal in optimizing the separation efficiency and resolving power of the chromatographic system, ensuring the accurate analysis of diverse mixtures.

Upon placing the sample in the designated vial, the injection process seamlessly transitions into full automation. The injector efficiently introduces the sample into the continuously flowing mobile phase stream, facilitating its journey towards the HPLC column. The critical parameter influencing the chromatographic process is the retention time, representing the duration required for the mixture of components to traverse the column and reach the detector, thereby displaying a maximum peak height for each compound. This retention time is intricately tied to various factors, including pressure, temperature, the nature of the stationary phase, the solvent composition, as well as the analyte chemical structure.

To monitor the passage of components through the column, various detection methods are employed. Among them, a widely used technique involves ultraviolet (UV) light, where UV or visible (VIS) detectors are prevalent in HPLC due to their stability, operational simplicity, and high sensitivity. UV detectors come in three main types: fixed wavelength, variable wavelength, and diode array detectors (PDA). The PDA, being a UV detector with multiple diodes, resolution elements, or pixels, has the ability to simultaneously detect several wavelengths, making it ideal for comprehensive spectrum analysis. Fluorescence detectors, another frequently used detection method, exhibit remarkable sensitivity to specific component

groups. By employing a specific wavelength to stimulate component atoms, which subsequently emit a light signal, the fluorescence detector utilizes the intensity of the radiated light to determine the concentration of the component. This method finds applicability in a diverse range of materials, including natural substances, pharmaceuticals, petroleum products, and clinical samples[17]. For a more advanced and sensible analysis, the HPLC-MS method integrates mass spectrometers to detect separated compounds eluted from the chromatographic column. This combination produces an ion chromatogram, a three-dimensional representation encompassing retention time, intensity, and mass spectra. Each peak in the ion chromatogram corresponds to a unique component within the mixture. The continual advancements in mass spectrometry technology over recent decades have resulted in the development of highly sensitive instruments, further enhancing the capabilities of this integrated analytical approach.

1.3 MS principles

The fundamental concept of MS involves the generation of ions using an appropriate ionization technique. These ions are then separated based on their mass to charge ratio (m/z) and detected based on their individual m/z values and relative abundance. The general framework followed by all mass spectrometers includes an ion source, a mass analyser (or a series of mass analysers), and a detector.

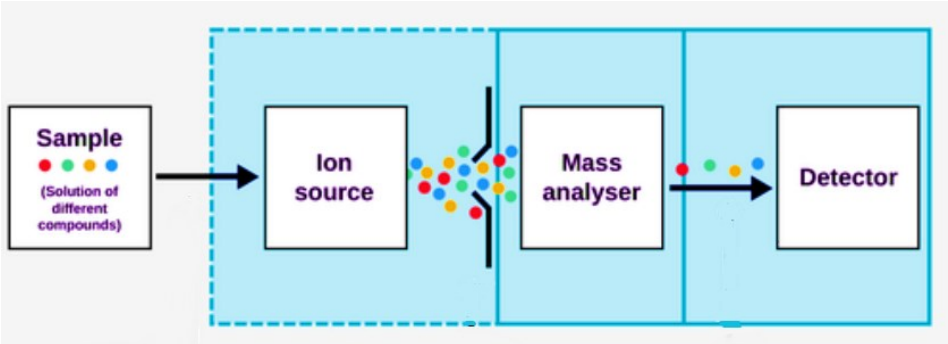

Figure 3. Mass spectrometer scheme (adapted from theory.labster.com).

Briefly, during the ionization step, the ions produced are directed to the high vacuum region of the mass spectrometer, which comprises mass analysers and detector. Within the mass analyser, the ions are accelerated through electric fields, radiofrequencies, and magnetic fields (nowadays used just for selected applications) in order to separate them according to their m/z values. Finally, the detector measures the ion signal intensities, allowing for the determination

of their relative abundances. These data are then plotted to generate the mass spectra and the ion chromatogram[18].

Ionization techniques can be categorized into two main groups: hard and soft techniques. These groups differ from each other based on the amount of residual energy transferred to the molecules. Hard ionization techniques, such as electron ionization (EI), result in a high degree of fragmentation, which is beneficial for structural identifications. On the other hand, soft ionization techniques involve a lower amount of residual energy, which preserve the newly formed ions from an in-source fragmentation. Examples of soft ionization techniques include atmospheric-pressure photo ionization (APPI), atmospheric-pressure chemical ionization (APCI), electrospray ionization (ESI), desorption electrospray ionization (DESI), and matrix-assisted laser desorption ionization (MALDI). Among those operating in the liquid phase, therefore suitable for coupling with HPLC, ESI and APCI are those more commonly used in metabolic and metabolomics studies.

In the past, most ion sources were not compatible with a continuous liquid stream, such as the eluate of an HPLC. However, this changed with the development of ESI by Professor John Fenn in 1989[19] and its optimization by Andries Bruins[20]. ESI, along with APCI, revolutionized the coupling of MS with HPLC and more recently, UHPLC. In ESI, the liquid is dispersed into a spray of electrically charged droplets through a metal capillary exposed to a high electric field. The solvent in this highly charged spray evaporates until the droplets become unstable, reaching the Rayleigh limit. At this point, the droplets undergo deformation, and as their volume decreases, the charge density at the droplet surface increases. Eventually, the electrostatic repulsions become stronger than the surface tension holding the droplets together, causing them to "explode" (Coulomb fission) and form smaller, more stable droplets.

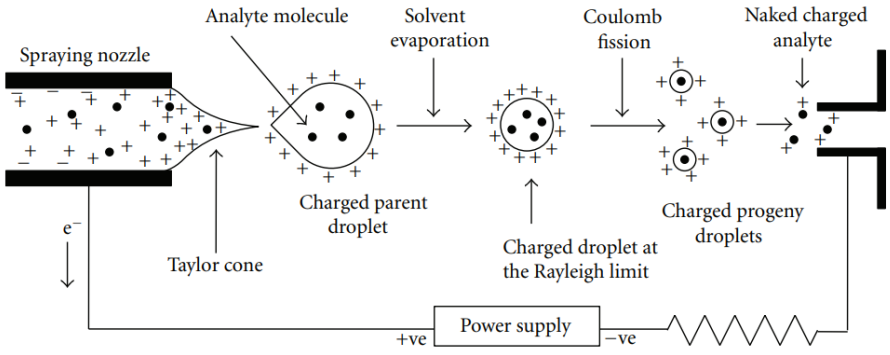

Figure 4. ESI mechanism (adapted from Banerjee S. and Mazumdar S., 2011[21]).

The subsequent desolvation process leads to the release of “naked” sample ions in gas phase from the surface of the charged droplets. For analysis, these ions move to the high vacuum region of the mass spectrometer, driven by the potential cascade in the optical path of the instrument[20,22].

In APCI, a liquid is propelled through a capillary and heated nebulized at the tip. A corona discharge occurs in close proximity to the capillary's tip, initiating the ionization of gas and solvent molecules within the ion source. Subsequently, these ions engage with the analyte, inducing ionization through charge transfer. This method proves effective for small, thermally stable molecules that may not ionize efficiently with ESI[23–25]. For instance, free steroids pose a challenge for ESI due to their neutral and relatively non-polar nature, lacking a functional group capable of carrying a charge. APCI has proven its ionization efficiency, enhancing the sensitivity of HPLC-MS analysis with respect to many steroids[26–28].

Ions are initially generated and then transported into the mass analyser, which serves as the core component of the mass spectrometer. To avoid neutral species to interfere with the detection of the analytes of interest, mass spectrometer dispose of gases (mainly nitrogen) at the very first part of the high vacuum interface to avoid the entrance of non-charged species. The latter are also usually deflected from the following ion path using focusing lenses and differential voltages. The purpose of the analyser is to separate the ions based on their m/z ratio. The selected ions with specific masses are then directed towards the ion detector for counting. The source can produce various types of ions, including molecular ions with positive or negative charge, components of the mobile phase, adducts formed by combining with molecular ions (commonly Na+, K+, NH4+ adducts in positive ions, or Cl-, HCOO-, OH- adducts in negative mode), and fragment ions if in-source fragmentation takes place. There are several types of analysers that can be utilized for ion separation, each employing different methods based on their m/z. These include the quadrupole mass analyser, quadrupole and linear ion trap mass analysers, time-of-flight mass analyser, Fourier transform analysers, and ion cyclotron resonance analyser[25,29].

Quadrupole ion trap analysers utilize three hyperbolic electrodes for the purpose of confining ions within a three-dimensional space through the use of both static and radio frequency voltages. Subsequently, ions are selectively expelled from the trap based on their m/z values, thus generating a mass spectrum. Conversely, it is possible to confine a specific ion within the trap by means of applying an exciting voltage while simultaneously ejecting other ions.

Furthermore, the introduction of an inert gas into the trap can induce fragmentation. An intriguing characteristic of these ion trap analysers is their capacity to repeatedly fragment and isolate ions prior to obtaining the final mass spectrum, thereby allowing for what is known as MSn capabilities. It is also possible to use a quadrupole, namely quadrupole mass filter (QMF), as a trapping system with a prevailing dimension (linear ion trap, LIT), as well as a combination of both QMF and LIT in a single analyser, named QTrap mass analyser[30,31].

The time-of-flight (TOF) analyser functions by propelling ions through a high voltage. The speed of the ions, and consequently the duration their "flight" to the end of a flight tube and then to the detector, relies on their m/z values. If the initial accelerating voltage is pulsed, the detector's output in relation to time can be transformed into a mass spectrum. The TOF analyser is capable of swiftly acquiring spectra with a heightened sensitivity. Additionally, it possesses exceptional mass accuracy, enabling the determination of molecular formulas for diminutive molecules[32,33].

Tandem mass spectrometers incorporating various combinations of mass analysers have been developed. One notable approach involves replacing the third quadrupole in a triple quadrupole mass spectrometer with a TOF analyser, resulting in a hybrid instrument known as a quadrupole time-of-flight (QTOF) mass spectrometer. This QTOF configuration has found extensive application in the field of proteomics, although it possesses certain limitations in scanning functions compared to triple quadrupole instruments. Another innovative design involves configuring the third quadrupole of a triple quadrupole mass spectrometer to operate in a mode where ions are trapped and then sequentially ejected based on their m/z. As already mentioned, this arrangement is commonly referred to as a LIT, and one of the possible overall instrument configuration is denoted as a QTrap instrument. Notably, the end quadrupole in a QTrap instrument can be switched between ion trap mode and conventional quadrupole mode, allowing the instrument to combine advantageous features from both triple quadrupole and ion trap analysers. In ion trap mode, the sensitivity in product ion scanning is significantly heightened, and the ion trap facilitates additional stages of fragmentation, enabling an extended level of fragmentation and mass analysis (MS^3)[34–36].

High-resolution mass spectrometers (TOF, QTOF and Fourier transform based analysers) are suitable for untargeted metabolomics studies. They provide accurate mass measurements, allowing the identification of unknown metabolites. The high resolving power aids in resolving closely spaced peaks and reducing spectral interferences, making these instruments valuable

for comprehensive metabolomic profiling. Triple quadrupole MS is commonly employed for targeted analysis in metabolomics studies. It excels in quantifying known compounds with high sensitivity and specificity[25]. The first quadrupole selects the precursor ion, the second, which basically is a collision cell, induces fragmentation, while the third isolates and detects the specific product ions, allowing for precise quantification.

The choice between a triple quadrupole mass spectrometer and a high-resolution mass spectrometer depends on the specific goals of the analysis. Targeted studies benefit from the sensitivity and specificity of triple quadrupole MS, while untargeted or exploratory studies benefit from the comprehensive capabilities and accurate mass measurements provided by high-resolution MS.

In our experimental work, we specifically used a triple quadrupole analyser, particularly a Sciex 6500+ Qtrap mass spectrometer, working as a triple quadrupole analyser, which is capable of generating MS/MS.

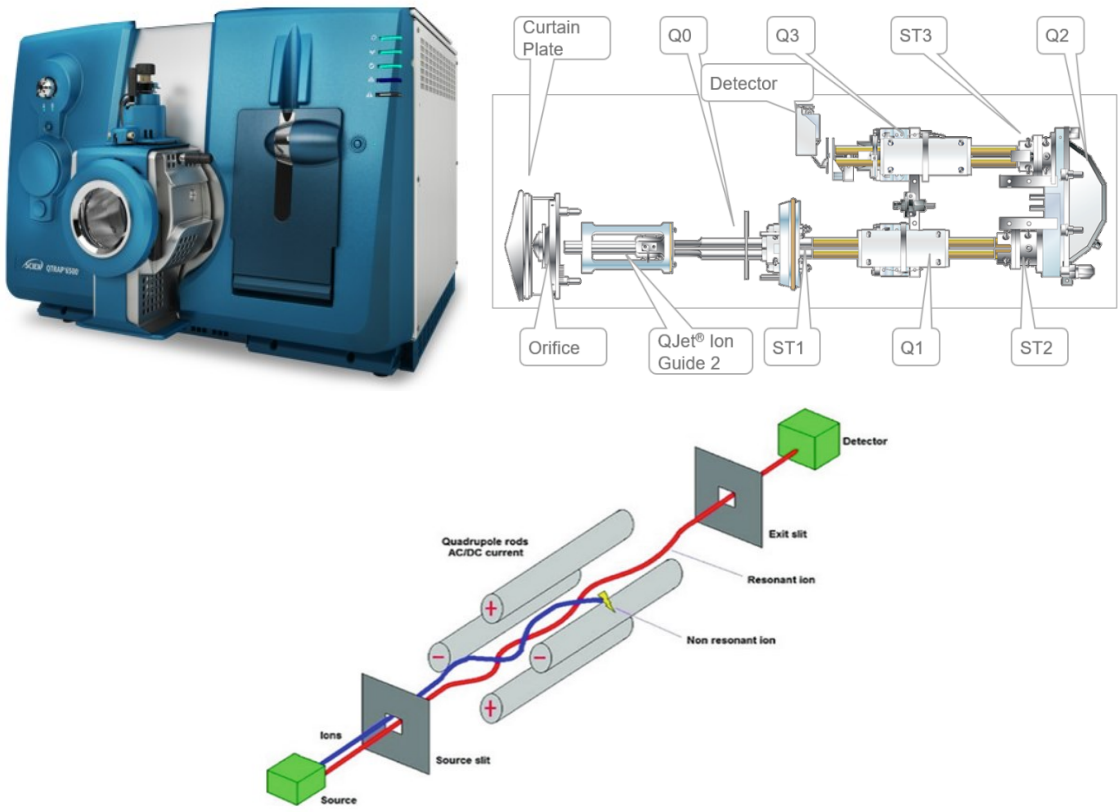

Figure 5. Sciex 6500+ Qtrap mass spectrometer external (A) and (B) internal representation, (C) Representation of the functioning of a quadrupole**.** (A-B adapted from Sciex copyrighted materials, 2018, C adapted from Gandhi K. *et al.* 2022[37]).

The quadrupole analyser consists of four parallel rods onto which direct and varying radio frequency voltages are applied. By adjusting these voltages over time, it becomes possible to scan across a range of m/z values and selectively transmit specific ions through the axis of the rods, thereby creating the mass spectrum. Ions specifically selected by the quadrupole are called resonant and pass through the rods of the quadrupole following a sinusoidal pattern, ions not compatible with the selected voltages values are deflected and diverted from the ion path. MS/MS, on the other hand, involves a specific configuration that enhances the specificity and sensitivity of the analysis. As already stated, this is achieved by placing a collision cell (Q2) between two quadrupoles (Q1 and Q3). Fragmentation within the collision cell typically occurs using an inert collision gas such as Ar or N_2, and this process is known as collision-induced dissociation (CID). Figure 6 illustrates the different scan modes that Q1 and Q3 can operate in.

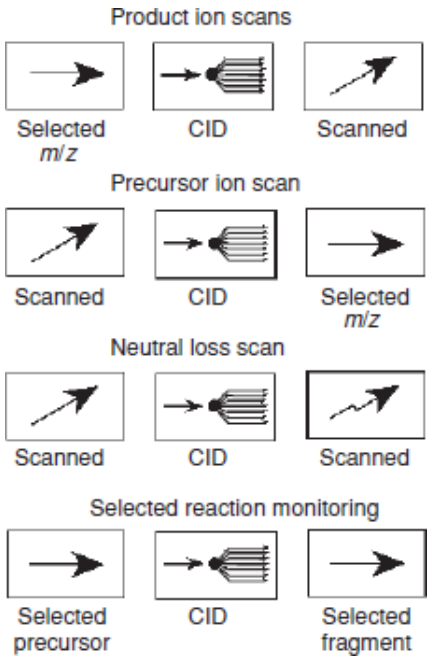

Figure 6. Different quadrupole scan modes in MS/MS (adapted from Hofmann *et al*. 2007[8]).

The first mode, known as the "product ion scan" involves selecting an ion with a specific m/z in Q1 and then fragmenting it in Q2. Q3 is responsible for scanning and detecting all the fragment ions produced in this process. The second mode, called the "precursor ion scan" focuses on a selected fragment ion produced in Q2, while Q1 scans all the masses to identify the precursor ion. Another commonly used mode is the "neutral loss scan" where both Q1 and Q3 scan all the ions within a selected m/z range with a constant mass offset between the two

quadrupoles. This mode detects all the fragmentations that result in a specific neutral fragment. The most frequently used mode is the Selected Reaction Monitoring (SRM), also known as Multiple Reaction Monitoring (MRM). In this mode, there is no scanning involved as both Q1 and Q3 are focused on selected masses. It is important to note that ions selected in Q1 are only detected if they produce a specific fragment through a selected reaction.

Following the analysis conducted by the mass analyser, the ions are subsequently detected and transformed into a practical signal through the utilization of a detector. This device possesses the capability to convert the incident ions into an electric current, which is directly proportional to their abundance. Due to the limited quantity of ions that are released from the mass analyser, it is typically necessary to amplify the signal in order to generate usable signals for data processing. Currently, the electron multiplier is extensively employed among the various types of detectors available. In essence, both positive and negative ions collide with a conversion dynode, thereby initiating the emission of numerous secondary particles. These particles are subsequently converted into electrons and amplified through a cascade effect, resulting in the production of an electric current. This current is then processed by the data system, ultimately generating the mass spectra[8,29].

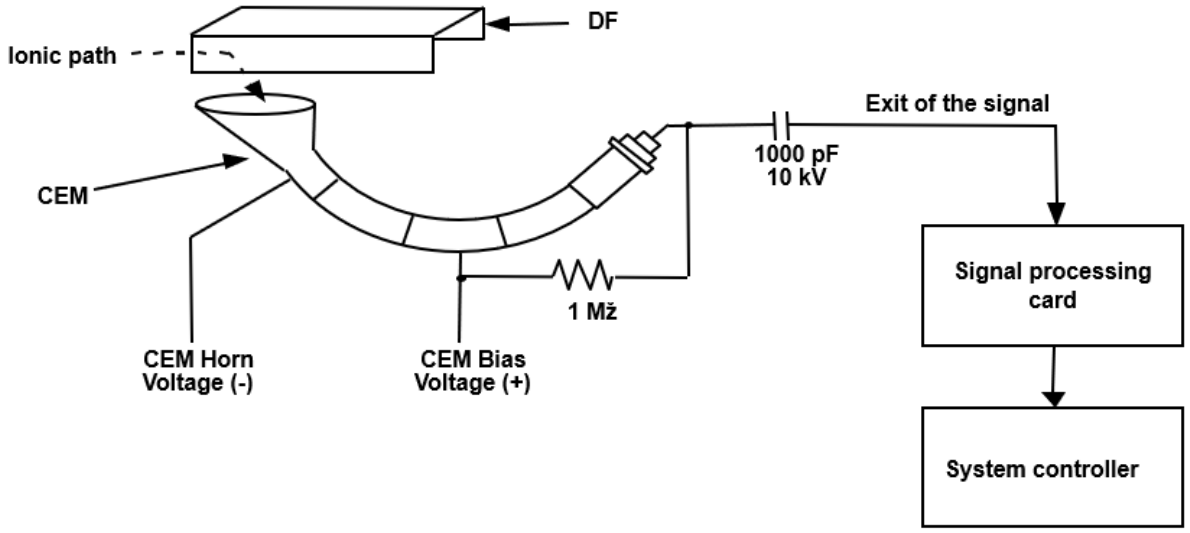

Figure 7. Channel electron multiplier (CEM) detector scheme (adapted from Sciex copyrighted materials, 2018).

2. Thyroid hormones

The term thyroid hormones (TH) specifically refers to 3,3',5,5' tetraiodothyronine (T4 or Thyroxine) and 3,5,3' triiodothyronine (T3), both iodinated tyrosine-based molecules.

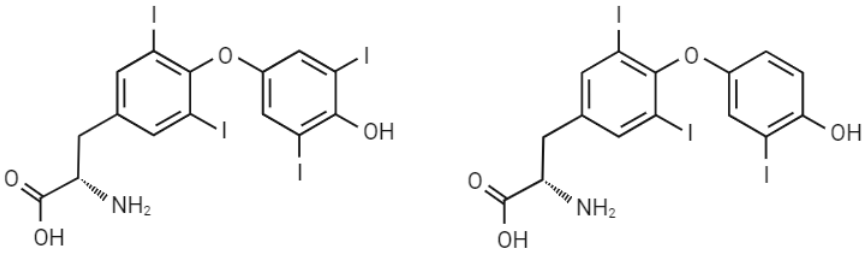

Figure 8. Thyroxine (T4), on the left, and triiodothyronine (T3), on the right (created on Biorender.com).

In humans, the thyroid predominantly produces T4, considered a prohormone due to its conversion into the biologically active T3 in peripheral tissues, exhibiting higher affinity with the nuclear thyroid hormone receptor. Notably, the thyroid contributes to the 20% of circulating T3, maintaining a 1:14 ratio with respect to T4[38,39]. The levels of circulating TH are meticulously regulated by highly sensitive negative-feedback loop mechanisms, both centrally and peripherally. The Hypothalamic-Pituitary-Thyroid axis (HPT) constitutes a fundamental system in maintaining TH homeostasis. Thyrotropin-Releasing Factor (TRH), a tripeptide (pGlu-His-ProNH2), is secreted by the hypothalamic paraventricular nucleus (PVN)[40]. The interaction between secreted TRH and the G-protein coupled receptor TRH-1 on pituitary thyrotrope cells triggers an increase in intracellular cAMP, thereby stimulating the synthesis and release of pituitary Thyroid-Stimulating Hormone (TSH).

TSH, also known as Thyrotropin, is a heterodimeric glycoprotein weighing 28 KDa, composed of α and β subunits, and is secreted by pituitary thyrotrope cells. The proper glycosylation of TSH subunits is essential for their interaction with the G-protein coupled TSH receptor on thyroid follicular cells, initiating the synthesis of TH[41,42]. For the α subunits, there are two sites for glycosylation and for the β subunits, there is only one site[43]. Thyroglobulin synthesis, cellular iodide uptake, TSH bioactivity (i.e., activating the TSH receptors on the surface of follicular thyroid cells), and T3/T4 secretion into the bloodstream are all impacted by the various glycoforms. TSH is the primary diagnostic biomarker of systemic thyroid status due to its pivotal role in thyroid metabolism. Nonetheless, the previously mentioned fluctuations in

the glycosylated chains result in chemical structures that undergo temporal changes. Because of this, TSH measurement is typically based on its biological activity instead of on its concentration, using standard preparations supplied by the World Health Organisation (WHO)[44–47].

2.1 TH synthesis

The synthesis of TH is an intricate process involving a sequence of tissue-specific biochemical reactions. The thyroid's functional unit for de-novo TH biosynthesis is represented by thyroid follicles, comprised of a monolayer of follicular cells known as thyrocytes. The thyrocytes' apical membrane encases the follicle lumen, referred to as colloid, while the basolateral membrane faces the bloodstream[48]. Within the follicles, numerous proteins are present, with Thyroglobulin (TG) being the most highly expressed glycoprotein. TG consists of two homodimers, each approximately 330 KDa in size, and serves as the primary source of TH. Notably, TG contains around 70 tyrosine residues with an average iodine content ranging from 2.5 to 50 atoms of iodine per mole of TG. TSH plays a pivotal role in stimulating TG endocytic uptake into thyrocytes, leading to its lysosomal degradation and subsequent release of TH from the TG polypeptide backbone[49].

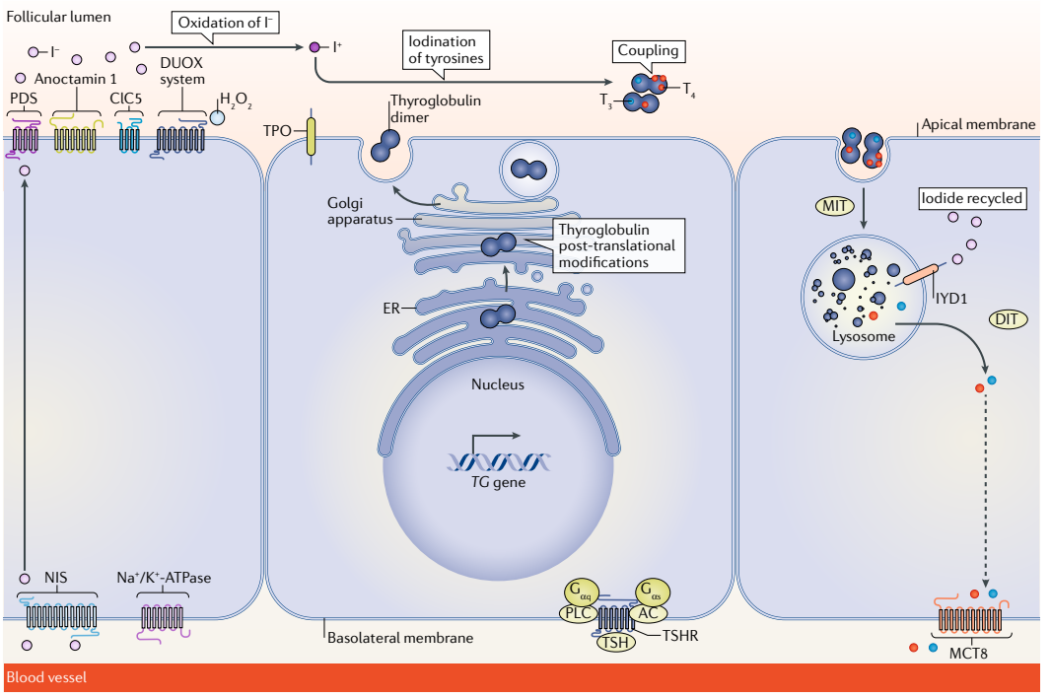

Figure 9. TH synthesis process graphical representation (adapted from Citterio, CE. *et al*. 2019[49])

The sodium-iodide symporter (NIS) facilitates the thyroid gland uptake of iodine at the basolateral membrane of the thyroid cells. NIS is a glycoprotein belonging to the solute carrier family 5 (SLC5A5), which consists of 13 segments. It is in charge of delivering twice as many sodium ions (Na^+) as iodide ions (I^-) into the cytoplasm[50]. The Na^+/K^+-ATPase pump is another essential transmembrane protein that is required for the active transport of iodide against its electrochemical gradient within the cytoplasm. The cytoplasm of thyroid cells can contain up to 30–60 times more iodide than they do normally thanks to the action of NIS. This ensures that the majority of the ingested iodide, a scarce element in the environment, accumulates in the thyroid and is available for TH synthesis[51]. TSH stimulates NIS transcription, translation, and activation by activating the G-protein coupled TSH receptor[52,53]. Competitor NIS inhibitors, such as perchlorate ($ClO4^-$) and thiocyanate (SCN^-), inhibit I^- transport inside the thyrocyte[48].

Iodide is thought to be a major factor in controlling its own accumulation. In 1948, Wolff and Chaikoff discovered that high levels of iodide could reduce its transport and accumulation in the rat thyroid. The "Wolff-Chaikoff effect" was named after this phenomenon[54]. TH biosynthesis can be restored within two days even in the presence of elevated I- levels, thanks to an adaptive mechanism mediated by I^- transport inhibition known as the "escape from Wolff-Chaikoff effect"[55,56]. The presence of two voltage-gated K^+ channels, KCNQ1 and KCNE2, on the basolateral membrane aids in the restoration of electrochemical equilibrium. These channels play an important role in facilitating K^+ efflux outside the cell, emphasising their importance in thyroid function. I^- is transported to the thyrocyte apical membrane and then to the follicle lumen after entering the cytoplasm, a process known as "iodide efflux". Iodide efflux is mediated by the first apical channel found to be mediating it, pendrin[57,58]. TSH regulates pendrin's fast translocation towards the apical membrane through post-translational mechanisms, which increases iodide efflux. Recent research has also revealed that the calcium-activated chloride channel Anoctamin-1 and the chloride channel ClC5 play significant roles in the iodide efflux process[59–61]. I^- ions in the colloid oxidase in order to combine and attach to the TG tyrosyl residues[48].

Thyroid peroxidase (TPO), a crucial enzyme in TH biosynthesis, catalyses this oxidation process. The synthesis of T3 and T4 is dependent on the iodination and coupling of iodotyrosines on TG, which is facilitated by TPO, a glycosylated oxidoreductase. The majority of TPO and its heme-containing active site are found in the follicular lumen, which forms the extracellular process that drives the enzymatic activity. TPO is anchored at the apical

membrane of thyrocytes by the small transmembrane C-terminal region[62–64]. The production of hydrogen peroxide (H_2O_2) by the NADPH oxidase family members dual oxidase enzymes, DUOX1 and DUOX2, is essential for the oxidation of TPO. H_2O_2 facilitates the transformation of I^- into iodinium (I^+) and hypoiodite (IOH^-) ions. These ions subsequently attach themselves to tyrosyl residues on the TG backbone, resulting in the formation of mono- and di-iodo tyrosine (MIT and DIT). The next stage is the thyroid hormonogenic coupling reaction, which is the synthesis of T3 and T4[48,65,66].

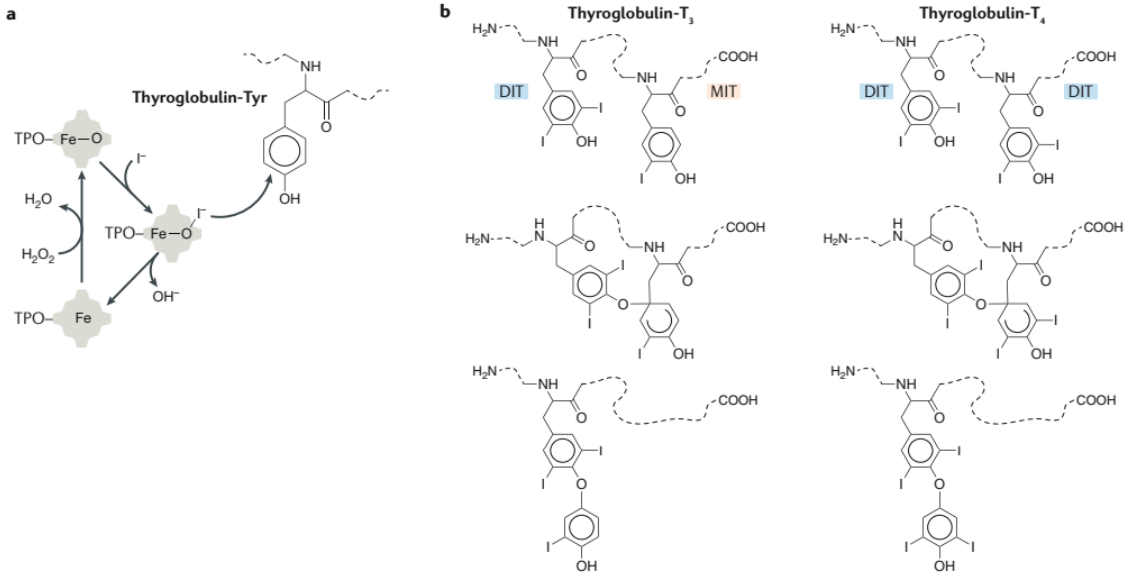

Figure 10. Coupling reaction of TH synthesis (adapted from Citterio, CE. *et al.* 2019[49]).

Although the precise mechanism underlying this process remains unclear, it has been suggested that either an ionic interaction or a free radical intermediate play a role. The process of hormoneogenic coupling involves the transfer of an iodophenoxyl group from MIT or DIT, referred to as the "donor" to a DIT residue, referred to as the "acceptor" producing T3 and T4, respectively[67]. As a byproduct of the reaction, a dehydroalanine remains in the "donor" position. It appears from kinetic models of iodination and hormonogenic coupling reactions that the formation of T3 and T4 requires correctly oriented iodotyrosines in space. Furthermore, these models show a preference for the biosynthesis of T4, the primary thyroid product, from the 25-30 Tyr residues iodinated by TPO[48,68]. Under normal conditions, TG contains about 2.5 T4 residues and 0.7 T3 residues. T4 biosynthesis is followed by intrathyroidal T3 biosynthesis, which results from the union of an MIT and a DIT residue. Notably, the majority of circulating

T3 is not produced by T4 deiodination on TG, but rather by TSH-stimulated peripheral actions of peripherally active deiodinases, namely DIO1 and DIO2[69].

Synthesised TH bound to TG is stored in the colloid until TSH levels rise and it is internalised into thyrocytes via endocytosis processes. Through the proteolytic activity of endopeptidases, newly formed lysosomes within thyrocytes release T3 and T4, as well as uncoupled MIT and DIT. Deiodination of released MIT and DIT molecules occurs enzymatically, yielding I^- and Tyr residues that can be reused in TH biosynthesis. An enzyme known as iodotyrosine dehalogenase (DEHAL1 or IYD) catalyses this vital recycling process[70]. TH must be released into the bloodstream, a process that was previously thought to occur through passive diffusion due to the lipophilic nature of TH. Recent research, however, has revealed that TH enters the bloodstream via a series of transporters found on the basolateral plasma membrane of thyrocytes.

2.2 TH transport and regulation

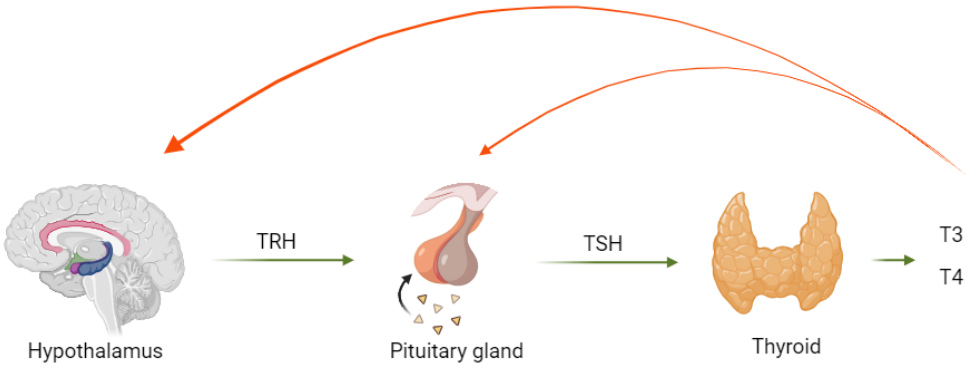

Figure 11. HPT axis (created on Biorender.com).

The increase in circulating T3 and T4 initiates a highly sensitive negative feedback mechanism that regulates the HPT. This feedback loop results in a reduction in the synthesis TRH at the hypothalamus and TSH at the pituitary gland[71]. At a transcriptional level, TH exerts inhibitory effects on the synthesis of TRH and both subunits of TSH. Furthermore, TH has been reported to impede post-transcriptional modifications of TSH and its release[72]. Conversely, a decrease in circulating TH rapidly triggers the secretion of TRH and, subsequently, TSH. This cascade of events leads to an increase in TH synthesis and secretion, aimed at normalizing circulating hormone levels[73]. Given the highly hydrophobic nature of TH, several carrier proteins facilitate their transport and distribution through the bloodstream and cellular compartments[74].

Approximately 95% of circulating TH are bound to thyroid-binding globulin (TBG), transthyretin (TTR), and albumin, with the remaining 5% bound to minor carriers like lipoproteins or available in the circulation as free TH (fTH).

TBG, a liver-synthesized glycoprotein, consists of a single 56 KDa polypeptide chain. It has one binding site for TH, with association constants (Ka) of $1x10^{10}$ M^{-1} and $4.6x10^{8}$ M^{-1} for T4 and T3, respectively. The binding of T4 to TBG induces conformational changes that increase its stability. Since TBG carries the majority of TH (~70%), qualitative and quantitative abnormalities of TBG significantly impact total circulating TH levels[75,76].

TTR, previously known as thyroxine-binding pre-albumin, is a 55 KDa protein circulating as a stable homo-tetramer of identical subunits of 127 amino acids each[77]. Subsequent to the discovery of its TH-binding properties, TTR has been shown to exist partly as a complex with retinol-binding protein, playing a role in vitamin A transport[78]. TTR has two TH binding sites, with Ka values of $2x10^{8}$ M^{-1} and $1x10^{6}$ M^{-1} for T4 and T3, respectively. The lower affinity for TH compared to TBG allows rapid dissociation from TTR, suggesting its association with the immediate delivery of T3 and T4. TTR carries 10 to 15% of protein bound T4 and is primarily synthesized in the liver, with minor synthesis in the central nervous system (CNS). It plays a crucial role in transporting and delivering T4 in the cerebrospinal fluid (CSF), where it serves as the main TH-transporting protein[79].

Albumin binds approximately 5% of circulating TH with lower affinity compared to TBG and TTR, with Ka values of $1.5x10^{6}$ M^{-1} and $2x10^{5}$ M^{-1} for T4 and T3, respectively[76]. Despite these lower affinities, the significant contribution of albumin to TH transport is attributed to its high abundance in human serum. Albumin is proposed to act as a fast TH resource during rapid exchanges in capillary transits[80].

TH transporters, found in diverse solute carrier families, are not exclusive to thyroid-related functions and are widely distributed in various tissues[81]. The mono-carboxylate transporters (MCT) family, with 14 members, includes MCT8 and MCT10, both aiding TH transport across the plasma membrane[82,83]. MCT8, crucial for TH uptake into the brain, is highly specific for TH transport. MCT10, functioning as an aromatic amino acid transporter, exhibits slightly higher efficiency in transporting T3 but lower efficiency in transporting T4[81,84]. MCT8 is expressed in various tissues, playing a specific role in T3 transport across the blood-brain barrier (BBB); pathogenic mutations in its gene are implicated in various diseases[82]. The liver Na^{+}/taurocholate co-transporter (NTCP), part of the solute carrier gene family (SLC10A), is

involved in the enterohepatic circulation of bile acids. Recognizing TH sulfate derivatives, NTCP transports them to the liver, where DIO1 deiodinates and rapidly degrades iodothyronine sulfate[85]. L-Type amino acid transporters (LAT), including LAT1 and LAT2, are heterodimeric proteins crucial for TH transport. LAT1, primarily found in the brain, placenta, and tumours, efficiently transports T3, while LAT2, prevalent in the kidney, colon, and intestine, exhibits different tissue distribution[86–88]. The organic anion transporter polypeptide (OATP) family, with 12 transmembrane domain proteins, transports various compounds, including TH. OATP1C1, a member of this family, specifically transports T3, rT3 (3,3′,5′-triiodothyronine, reverse T_3), T4, and sulfate T4 derivatives, with its physiological relevance in several tissues still unknown[81,89].

TH play essential roles in diverse processes, encompassing tissue development and the control of cellular metabolism. These effects of TH operate through two distinct mechanisms: a genomic pathway, involving the interaction of TH with nuclear thyroid hormone receptors (TR), and a nongenomic pathway characterized by swift onset, where TH engages with plasma membranes and other receptors[90]. The nuclear receptors TR function as ligand-dependent transcription factors, regulating the transcription of target genes upon activation by TH.

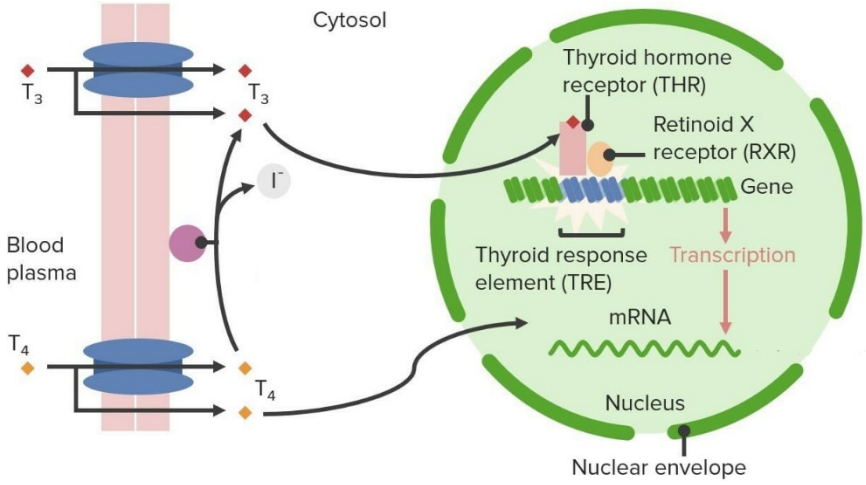

Figure 12. Genomic regulation of TH (adapted from Oiseth S. *et al,* 2022[91]).

T3 binding to TR can either increase or decrease the rate of transcription of target genes. TR can bind to thyroid hormone response elements (TRE) in the promoter region of TH target genes constitutively within the nucleus[92]. Even in the absence of TH, TR remains bound to TRE, repressing or silencing the basal transcription of positively regulated target genes[93]. TR

can exist as a monomer in the absence of its ligand, as homodimers when coupled with another TR, or as heterodimers when coupled with the retinoid X receptor (RXR)[94]. *TRA* and *TRB* genes encode for the two nuclear receptors TRα and TRβ, respectively. Not all TR proteins in mammals function as nuclear receptors, and their potential alternative splicing can give rise to the synthesis of other proteins, albeit with unknown physiological roles. Among the TR isoforms, four functional receptor variants have been identified: TRα1, TRβ1, TRβ2, and TRβ3. These isoforms display distinctive expression patterns during development and in adult tissues. TRα1 and TRβ1 are widely expressed, with the former predominantly found in the brain, heart, skeletal muscle, and brown adipose tissue, and the latter prevalent in the brain, liver, and kidney. TRβ2 exhibits a predominant expression in the pituitary gland, hypothalamus, and cochlea, while TRβ3 is primarily located in the kidney, liver, and lung, exhibiting functional characteristics in rats[95,96]. Notably, TRβ plays a pivotal role in mediating most TH effects on metabolism, making it an ideal pharmacological target for addressing metabolic disorders, particularly those related to lipid metabolism, as well as certain brain diseases. In the pursuit of developing ideal thyromimetic drugs, it is imperative for these pharmaceutical agents to exhibit high selectivity for TRβ. This selectivity is crucial in avoiding potential adverse effects on bone and the heart, underscoring the importance of precision in pharmacological interventions targeting TR[97].

The nongenomic effects of TH deviate from classical TR-mediated TH actions by not necessitating gene transcription and protein synthesis, although they may involve the modulation of gene transcription. These nongenomic mechanisms often rely on signal transduction systems and may implicate various elements, including novel TH membrane receptors, extranuclear TRβ, or truncated isoforms of TRα[90,98].

One such novel receptor, distinct from classical TR, is found on integrin αVβ3, a plasma membrane structural protein highly expressed in tumour cells and dividing endothelial cells. Integrin αVβ3, lacking structural homology with TR, binds TH near the Arg-Gly-Asp binding site[99]. T3 binding activates phosphatidylinositol 3-kinase (PIK-3), directing TRα into the nucleus and promoting the transcription of the hypoxia-inducible factor 1 (HIF-1) gene. TH can also interact with the integrin receptor, activating extracellular-related kinase 1 and 2 (ERK-1 and ERK-2), responsible for transducing TH signals in cancer cells. Furthermore, the interaction of both T3 and T4 with integrin αVβ3 is implicated in their demineralizing action[90]. TH rapidly stimulates PIK-3 and Rac activity on the plasma membrane through interaction with TRβ, leading to the activation of voltage-dependent potassium channels, thereby reducing

excitability and hormone secretion[100]. PIK-3 activation by T3 has direct and indirect effects on the transcriptional increase in HIF-1, glucose transporter 1 (GLUT-1), and MCT4 transporter[93]. Additionally, both T3 and T4 can stimulate mitogen-activated protein kinase (MAPK) activity, promoting angiogenesis. MAPK activation leads to the phosphorylation of the tumour protein p53, resulting in a decrease in its transcriptional activity. In the nucleus, the activated kinase forms a complex with TRβ and phosphorylates its serine. T3 is also responsible for numerous nongenomic actions on plasma membrane proteins, contributing to the basal activity of some ion pumps such as $Ca2^{+}$-ATPase, Na^{+}/K^{+}-ATPase, and Na^{+}/H^{+} antiporter[101]. Recent studies focusing on astrocyte cells have unveiled the involvement of truncated TRα isoforms, specifically TRΔα1 and TRΔα2, in the regulation of actin cytoskeleton modelling. The latter plays a pivotal role in the developmental program of the brain[98]. In response to T3, truncated TRα isoforms have been observed to be imported into the mitochondrial inner membrane, where they directly stimulate oxidative phosphorylation processes[93].

2.3 TH metabolism

Upon entering the cell, TH can undergo tissue-specific metabolism involving further deiodination, deamination, decarboxylation, sulfonation, and conjugation reactions.

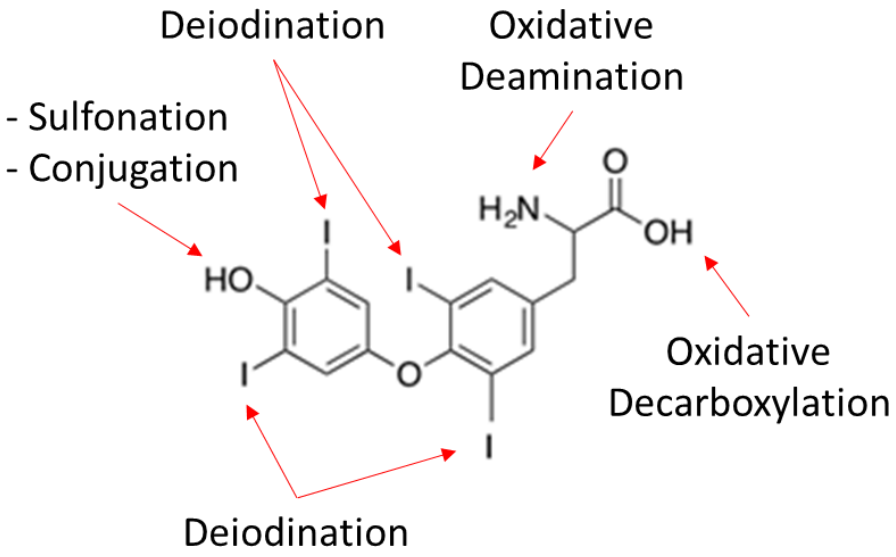

Figure 13. Specific reaction sites of TH (created on Biorender.com).

Mechanisms controlling TH levels operate intracellularly as well and involve the thioredoxin enzyme family, specifically the iodothyronine deiodinases (DIO)[39]. The three isoforms, DIO1, DIO2, and DIO3, play a crucial role in regulating both the levels and activity of TH by removing iodine from T4 precursors[69]. The isoforms exhibit distinct tissue localization and biochemical characteristics[74]. DIO1, located in the plasma membrane, primarily operates in the liver, thyroid, and kidneys, converting T4 to T3. In contrast, DIO2, situated in the endoplasmic reticulum, is responsible for T3 formation in the brain and is expressed in key thyroid-responsive tissues[102]. DIO3, involved in the inactivation of both T4 and T3 (to metabolites, rT3 and 3,3'-diiodothyronine (3,3' T2), respectively), is present in the plasma membrane and is mainly expressed in the brain, placenta, and pancreas[39].

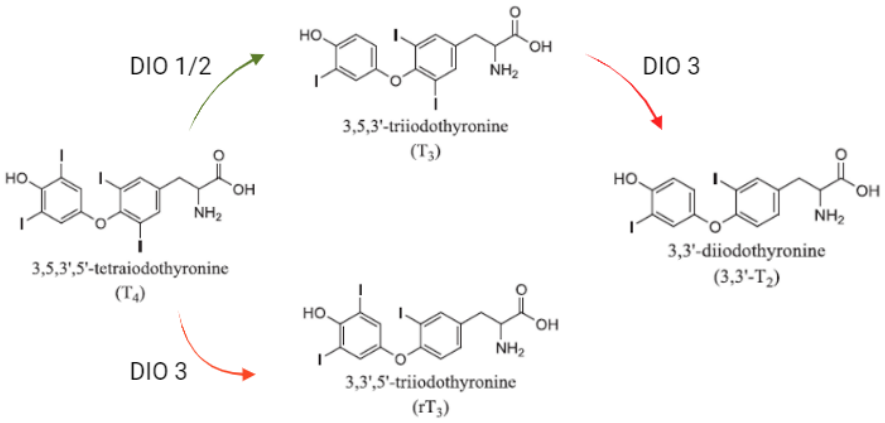

Figure 14. Main DIOs activity (created on Biorender.com).

The diverse regulatory features and tissue localization of these isoforms contribute to the intricate control of TH levels in response to various physiological signals and developmental cues. As already reported above, most of the human circulating T3 is not produced by the thyroid gland, but it is the result of the deiodination activity in the extrathyroidal tissues, catalysed mainly by DIO2 and, to a minor extent, by DIO1[103]. T3 itself is an important regulator of DIOs activity, stimulating the activity of DIO1 while having an opposite effect on DIO2. Hyperthyroidism increases *DIO1* and decreases *DIO2* expression, while the opposite is observed in hypothyroidism, in which the peripheral conversion T4 to T3 is enhanced by the *DIO2* induction[39]. Moreover, T4 decreases the activity of DIO2 through post translational mechanisms, i.e. ubiquitin conjugation, contrary to DIO1 and DIO3 that are not susceptible to these reactions.

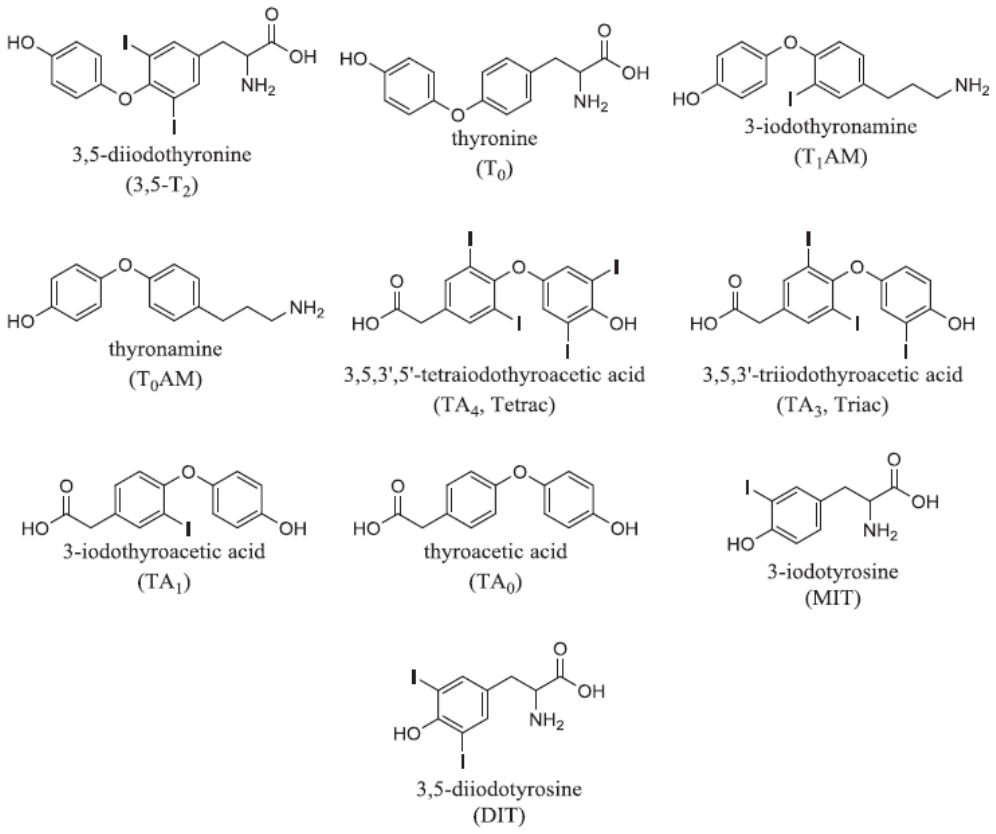

Figure 15. Panel of TH main metabolites (adapted from Borsò M, *et al.* 2022[44]).

T3 and rT3, besides their well-established roles, undergo further deiodination reactions leading to the formation of additional metabolites: 3,5-diiodothyronine (3,5-T2), 3,3'-T2, 3',5'-diiodothyronine (3',5'-T2), and 3-iodo-L-Thyronine (3-T1). While 3,3'-T2 and 3',5'-T2 exhibit no notable activities, 3,5-T2 has garnered significant attention from researchers due to its ability to bind to TR and its multi-faceted effects. The actions of 3,5-T2 extend beyond classical TR interactions, encompassing rapid effects at the cell membrane and mitochondria[104]. In vivo animal experiments have unveiled the diverse impacts of administered 3,5-T2 on canonical T3-regulated genes in various tissues. Notably, in pituitary models, 3,5-T2 has been observed to suppress TSH and stimulate growth hormone (GH)[105]. Animal models have demonstrated that parental administration of 3,5-T2 can modulate energy metabolism, potentially by stimulating liver fatty acid oxidation into mitochondria[106,107]. Furthermore, 3,5-T2 administration has shown promise in preventing body weight gain, liver adiposity, hyperlipidemia, and insulin resistance without inducing signs of thyrotoxicosis[104]. Acute exposure to 3,5-T2 in an isolated rat heart model demonstrated its ability to increase oxidative

metabolism without affecting cardiac contractility[108]. While the physiological relevance of 3,5-T2 and 3,3'-T2 remains to be fully elucidated, their presence in serum has been confirmed through immunoassays and accurate HPLC-MS/MS methods. However, ongoing debates surround their actual serum concentrations, and as of now, no clinical applications based on their detection have been reported[109–111]. DIO enzymes also exhibit the capacity to deiodinate deaminated TH metabolites, namely 3,5,3',5'-tetraiodothyroacetic acid (Tetrac) and 3,5,3'-triiodothyroacetic acid (Triac). Tetrac, resulting from the deamination of T4, has been confirmed in human serum at low nanomolar concentrations. Triac can be generated either by deiodination of Tetrac or by deamination of T3. Despite its importance in cell-specific actions, distorted serum concentrations of Triac have been reported. Both Tetrac and Triac are transported by TTR in serum, acting as thyromimetic compounds that lower TSH concentrations. Tetrac binds to TR through integrin αVβ3, with elevated concentrations observed in Grave's disease patients. Triac, exhibiting potent T3-mimetic activity with high affinity for TRβ, is described as a substrate for the MCT8 transporter[105].

Thyronamines constitute a novel class of endogenous signalling compounds structurally akin to TH, differing mainly in the absence of the carboxylate group on the alanine side chain. Distinguishing themselves by variations in the number and position of iodine atoms, these compounds are designated as TxAM, with nomenclature similar to TH, where 'x' indicates the number of iodine atoms[112]. To date, only two members of this class, thyronamine (T0AM) and 3-iodothyronamine (T1AM), have been identified in human serum through HPLC-MS/MS[113–115]. The discovery of transient hypothermia effects in rats following T1AM administration in 2004 prompted extensive research into this novel class of compounds. Investigators sought to unravel their biosynthetic pathways, mechanisms of action, and potential pathophysiological effects. Pioneering work by Scanlan et al. revealed that the rapid onset of T1AM effects did not align with classical TH nuclear mechanisms but instead suggested involvement with a G-coupled receptor. The trace amine-associated receptor 1 (TAAR-1) was identified as the receptor potentially responsible for T1AM effects, although ongoing debates and uncertainties persist regarding other membrane receptors and intracellular targets that may contribute to the mechanisms of T1AM action. Despite advancements in understanding T1AM's effects, the endogenous biosynthetic mechanism of T1AM remains elusive and is a subject of ongoing investigation[113–115]. The complexity surrounding these novel compounds opens avenues for further exploration into their physiological roles and potential therapeutic applications.

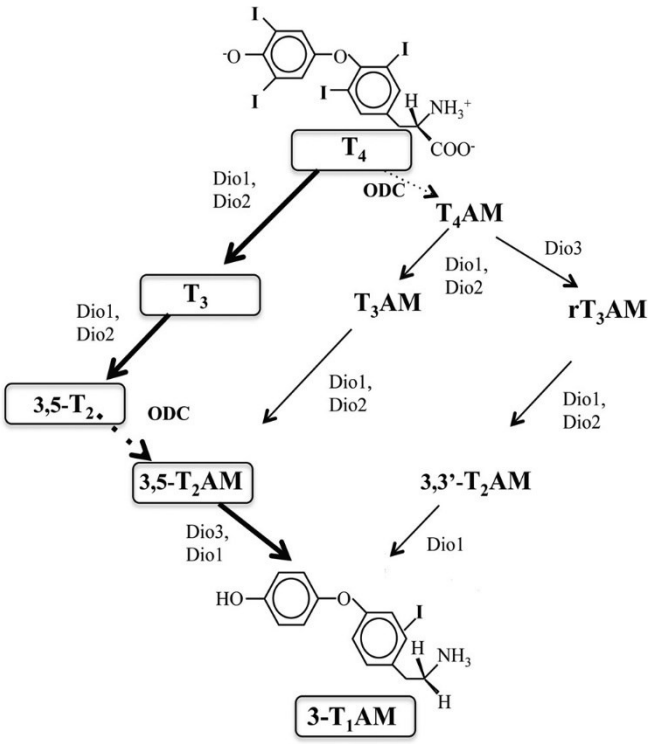

Figure 16. Putative pathway for T1AM formation (adapted from Hoefig CS, *et al.* 2015[116]).

A proposed mechanism involves the deiodination of thyroid hormones T3 or T4, leading to the formation of T2. Subsequently, T2 undergoes decarboxylation to produce di-iodo-thyronamine (T2AM), which is further deiodinated to yield 3-iodothyronamine (T1AM)[117]. Beyond the previously discussed hypothermic effects, both in vivo and in vitro models have demonstrated that administered T1AM can elicit a spectrum of physiological responses. These responses include the reduction of cardiac inotropic and chronotropic effects[118–120], protective effects in ischemia-reperfusion models[121,122], induction of acute metabolic responses with impacts on carbohydrates and lipids[123–126], and potential modulation of the noradrenergic, dopaminergic, and histaminergic systems[127]. Both T1AM and thyronamines can undergo various metabolic reactions, such as sulfonation and glucuronidation, the outcomes of which are still subject to ongoing investigation[128]. In most tissues, the principal metabolites of exogenously administered T1AM and T3AM are the corresponding acidic compounds, specifically, 3-iodo-thyroacetic acid (TA1) and the previously mentioned Triac, respectively. The biosynthetic mechanism for TA1 remains a topic of debate. Lorenzini et al. proposed a putative pathway involving the oxidative deamination of T1AM, resulting in the formation of the corresponding acid, TA1, through an aldehydic intermediate[129]. Despite the advancements, the biological role

of TA1 remains unknown. However, it has been reported to exhibit activity on the histaminergic system, adding another layer of complexity to the intricate interactions within the thyronamines class of compounds. Ongoing research seeks to unravel these metabolic pathways and define the functional significance of these various metabolites, providing valuable insights into the broader physiological roles of thyronamines[130,131].

3. TH in neurogenesis and cognitive disorders

Hypothyroidism is a chronic condition resulting from deficient production of TH or inadequate action of these hormones on target tissues[132]. Primary hypothyroidism is the most common type and occurs when the thyroid gland itself fails to produce enough TH. This can be due to various factors such as autoimmune disorders (Hashimoto's thyroiditis), surgical removal of the thyroid gland, or radiation treatment. Secondary hypothyroidism, on the other hand, is caused by a dysfunction in the pituitary gland or hypothalamus, which are responsible for signalling the thyroid gland to produce hormones. This type is relatively rare and is typically a result of tumours, infections, or trauma to the pituitary gland or hypothalamus. Other types of hypothyroidism include congenital hypothyroidism, acquired hypothyroidism, and subclinical hypothyroidism, each with distinct etiologies and clinical implications[133]. Ongoing research continues to unravel the complexities of thyroid function and its impact on overall health. Cognitive impairment, anxiety, and mood instability are commonly associated with hypothyroidism[134,135]. During the critical period of brain development in mammals, TH deficiency can lead to irreversible morphological defects, causing severe cognitive and neurological impairments.

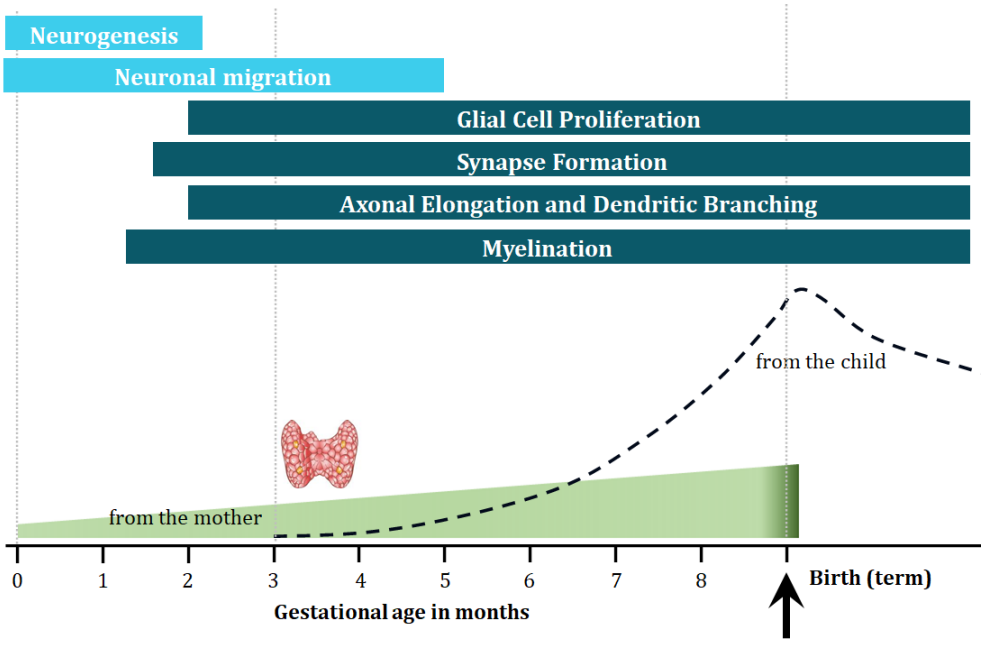

Figure 17. The role of TH in neurodevelopment (created on Biorender.com).

TH plays a crucial role in promoting neurogenesis, neuronal proliferation, migration of post-mitotic neurons, and terminal brain differentiation[136,137]. Notably, TH remains important in adulthood, as adult-onset hypothyroidism is linked to higher depression and anxiety scores and cognitive impairments[138–141]. Animal models of adult-onset hypothyroidism demonstrate cognitive and neuro-psychiatric disturbances[134,135], revealing increased immobility in behavioural tests and impaired performance in spatial learning and memory tasks[142–144]. These impairments are associated with altered hippocampal function and connectivity[145–147]. The hippocampus, crucial for memory and spatial learning, relies on adult hippocampal neurogenesis in the sub-granular zone (SGZ) of the dentate gyrus[148–150]. Disruption of adult neurogenesis is linked to cognitive deficits, neuropsychiatric disorders, dementia, and neurodegenerative diseases. TH signalling is identified as a critical endocrine signal controlling progenitor development within neurogenic niches[151].

TH can access the brain by crossing the BBB, a highly selective permeability barrier separating the bloodstream from the brain extracellular fluids. T4 is considered the primary TH crossing the BBB, subsequently converted into T3 by DIO2 in hypothalamic astrocytes and tanycytes[152]. Specific transporters such as MCT8 or OATP1C1 facilitate TH crossing the BBB, while indirect access occurs via the blood-cerebrospinal fluid barrier. The choroid plexus (CP), a highly vascularized structure in the brain's ventricular part responsible for synthesizing CSF and TTR, serves as the main T4 transporter in the CSF. TTR plays a pivotal role in delivering T4 from plasma into CP and subsequently transporting it into CSF, ensuring optimal exchange for delivering T4 into the brain[153,154].

The standard approach to managing hypothyroidism predominantly relies on levothyroxine (L-T4) monotherapy, a highly effective treatment for the majority of patients[155]. L-T4 supplementation helps restore TH levels and regulate the TSH within the normal range. Despite the success of this therapeutic regimen, a subset of individuals, comprising approximately 10-15% of patients undergoing L-T4 monotherapy, confront persistent symptoms indicative of TH deficiency.

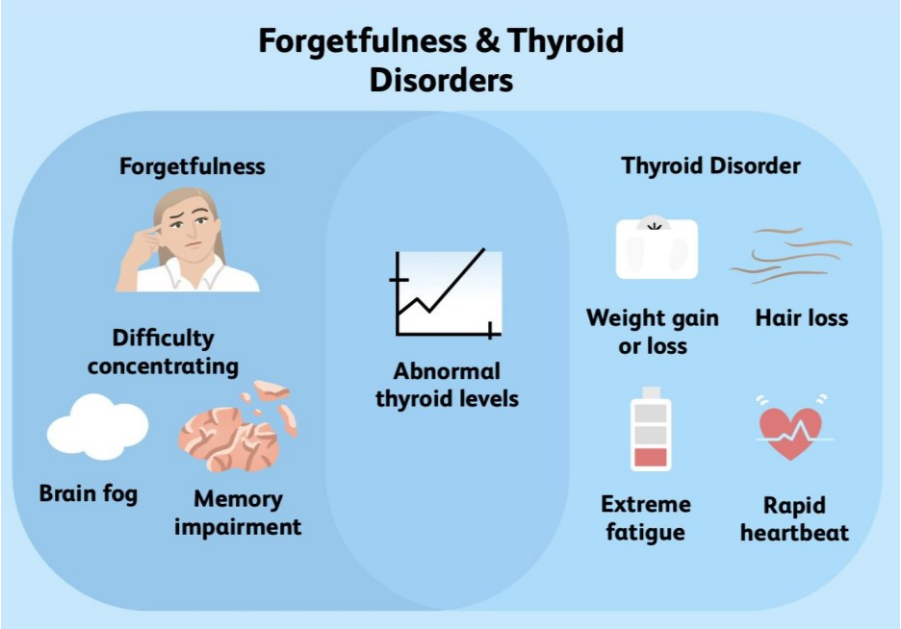

Figure 18. The impact of hypothyroidism on patients' performances (adapted from Heerema E, verywellhealth.com, 2022).

These lingering symptoms may encompass cognitive issues, fatigue, mood swings, and psychomotor performance decline, creating a clinical challenge[156]. Intriguingly, these symptomatic patients often exhibit TSH levels within the expected reference range, highlighting the need for a more nuanced understanding of thyroid function and potentially necessitating alternative therapeutic strategies to address their specific clinical concerns.

Ongoing research aims to elucidate the underlying mechanisms contributing to the persistence of symptoms in this subgroup and explore tailored interventions for improved outcomes. The generation of T3 from thyroxine T4 by deiodinases may not mirror thyroidal secretion of T3, and serum TSH might not reflect tissue intracellular TH levels[38,156]. The hypothesis proposed is that persistent cognitive and neuropsychiatric symptoms in hypothyroidism may be associated with decreased brain levels of downstream TH derivatives, specifically T1AM. Studies in mice treated with methimazole and L-T4 replacement indicate that T1AM biosynthesis requires an intact thyroid gland[157]. T1AM, an endogenous trace amine, modulates various neurotransmitter systems and exhibits neuroprotective actions. T1AM has multiple pharmacological effects, including pro-learning properties[122,124,127,158–161]. As there is evidence that tissue T1AM levels remain low in hypothyroid animals treated with L-T4, a hypothesis suggests that its reduced availability may impact neurocognition and related neurobiological alterations.

4. The homeostatic role of TH in diabetic retinopathy

Diabetic retinopathy (DR) is a common microvascular complication of diabetes mellitus and remains one of the leading causes of blindness worldwide[162]. It is a progressive disease that affects the retina, the light-sensitive tissue at the back of the eye. Chronic high blood sugar levels cause damage to the blood vessels in the retina, leading to various pathological changes. These changes can include the formation of microaneurysms, leakage of blood and fluid into the retina, the growth of abnormal blood vessels, and the development of scar tissue. As the disease progresses, these changes can ultimately lead to vision loss if left untreated. Early detection and timely management are crucial in preserving vision and preventing further deterioration[163–165]. Regular eye examinations, tight glycaemic control, blood pressure management, and other risk factor modifications are key components in the management of DR. Neuronal damage has become a prominent pathophysiological characteristic of DR, prompting the activation of protective mechanisms within the retina to safeguard neurons[166–168].

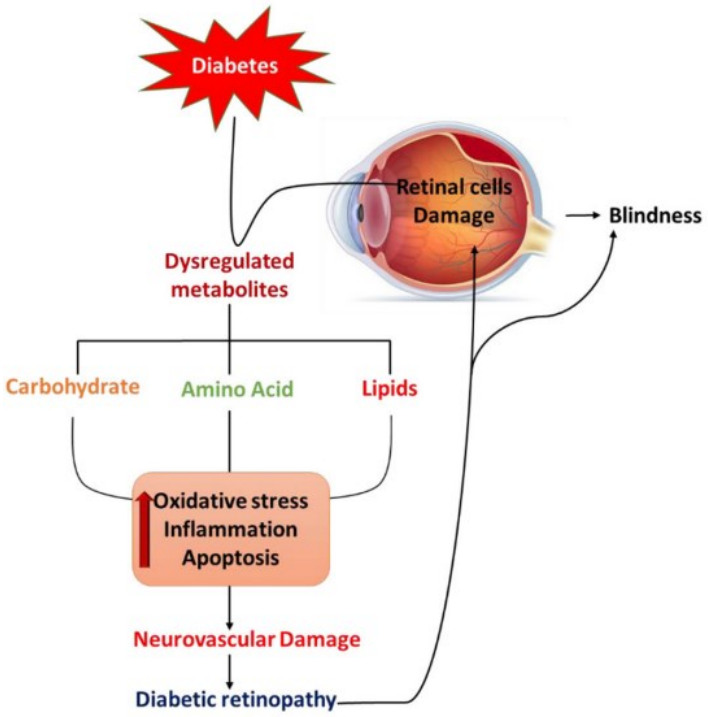

Figure 19. The diabetes-dependent process of retinal damage (adapted from Aldosari DI, *et al.* 2022[162]).

The early upregulation of vascular endothelial growth factor (VEGF), traditionally viewed as a pathological feature in advanced DR stages, may actually be induced as an initial neuroprotective strategy[169,170]. Similarly, the early activation of autophagy could serve as a retinal response to counteract cell death caused by high glucose-induced apoptosis[171]. The reduction of cell metabolism and energy expenditure may represent another protective mechanism adopted by the retina to cope with stress. TH, specifically the biologically active T3 and its precursor T4, are well-established regulators of metabolic homeostasis through their activation of mitochondrial biogenesis, respiration, function, and quality control[172–174]. Therefore, lowering intraretinal TH levels might be a beneficial strategy to mitigate oxidative stress and cell damage under hyperglycaemic conditions.

Although this intriguing hypothesis has not been explored, the presence of TH receptors, the MCT-8, TH-responsive cells, and deiodinase enzymes in the retina suggests the potential for local regulation of the TH system[175–181]. Additionally, anti-TH treatments in experimental models of congenital retinal diseases have demonstrated protection for cone photoreceptors against degeneration[182–184]. Conversely, prolonged systemic or local reduction of T3 levels, known as a low T3 state (LT3S), might become disadvantageous during chronic critical illness[184–187]. Subclinical hypothyroidism, diagnosed when peripheral TH levels are within normal reference laboratory range, but serum TSH levels are mildly elevated, has been associated with DR in diabetic patients. Moreover, reduced T3 and T4 serum levels, even within the euthyroid range, have been negatively correlated with DR in type 2 diabetic patients[188–190]. Generally, LT3S is linked to disease progression and poor long-term prognosis[184,187,191]. In such cases, restoring T3 physiological levels has been observed to be beneficial, as seen in a rat model of cardiac ischemia and reperfusion and in patients with myocardial infarction[192–195]. It remains unknown whether, similar to other pathological conditions, intraretinal TH dyshomeostasis in DR may result from increased activity or expression of DIO3, a fetal gene that converts T4 into the biologically inactive rT3, or a reduction of DIO2, responsible for activating T4 into T3[196–200]. The hypothesis posits that in the retina, as in other organs or tissues, LT3S develops as an adaptive response to protect against diabetes-induced stress and may become detrimental in the chronic stage, contributing to retinal damage progression.

Regarding potential mechanisms by which TH signalling may impact the retina in DR, an intriguing hypothesis suggests that LT3S may affect recently identified T3-dependent microRNA (miRNA)/gene regulatory circuits[194]. For instance, in a rat model of acute

myocardial infarction, the downregulation of miR-133, miR-338, and miR-29, which may also be involved in DR evolution, was rescued by T3 replacement[194]. Additionally, miRNA expression is altered in DR, and some of these miRNAs may be associated with the regulation of retinal TH concentration. While retinal TH signalling may depend on miRNA-regulated mechanisms, the modulation of T3 levels is likely to affect the retina through altered mitochondrial function[201–203]. Given the significant role of mitochondria in the development of DR[204], it is plausible that TH dyshomeostasis may guide the pathophysiology of the disease by interfering with mitochondrial activity.

5. The importance of iodine recycling: DEHAL1

The availability of iodide in the thyroid is pivotal for thyroid functions, and while dietary iodide is primarily obtained from sources like sea salt, milk, meat, and fish, daily intake alone is insufficient. To address this, the enzyme DEHAL1 plays a key role in the enzymatic deiodination of MIT and DIT, generated in excess during TH synthesis[205].

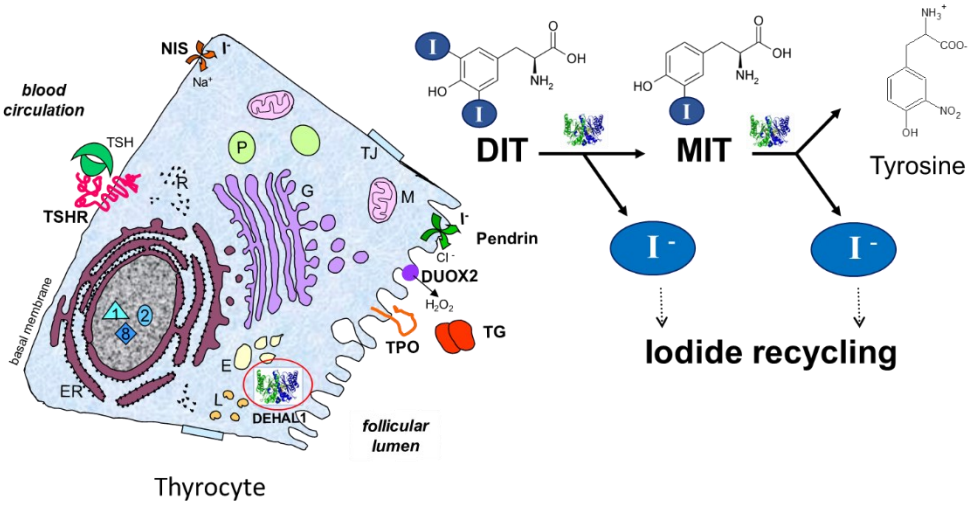

Figure 20. DEHAL1 functioning mechanism (adapted from Alikhani P, *at al.* 2023[206]).

Despite being released more abundantly (six-seven times) than TH during TG proteolysis, MIT and DIT are inactive at the thyroid level. DEHAL1's catalytic activity produces intrathyroidal iodide, which, together with released Tyr molecules, can be recycled and reused for TH synthesis[207]. This gene is primarily present in the thyroid gland, with minor presence in kidneys and liver[208]. Three isoforms of DEHAL1, namely DEHAL1, DEHAL1B, and DEHAL1C, were identified, with only the first exhibiting dehalogenation activity[209]. The crystal structure of DEHAL1, reported by Thomas *et al.* in 2009[210], revealed a transmembrane protein located at the apical membrane of thyrocytes, belonging to the NADH oxidase/flavin reductase superfamily, with flavin mononucleotide (FMN) as a prosthetic group crucial for its catalytic activity. T3 and T4 are not deiodinated by DEHAL1, nor can they bind to the enzyme, lacking the catalytic selenocysteine found in DIOs. DEHAL1 consists of a single transmembrane domain, a short carboxyl terminal domain, and an amino terminal domain housing most of the nitro-reductase activity. The active site residues Glu-153, Tyr 157, and Lys-178 play a vital role in recognizing the zwitterionic forms of MIT and DIT, along with the redox characteristics of

the FMN. Alignment of the larger DIT over the isoalloxazine portion of the FMN is facilitated by minor shifts of Leu-169, Thr-174, and Leu-172.

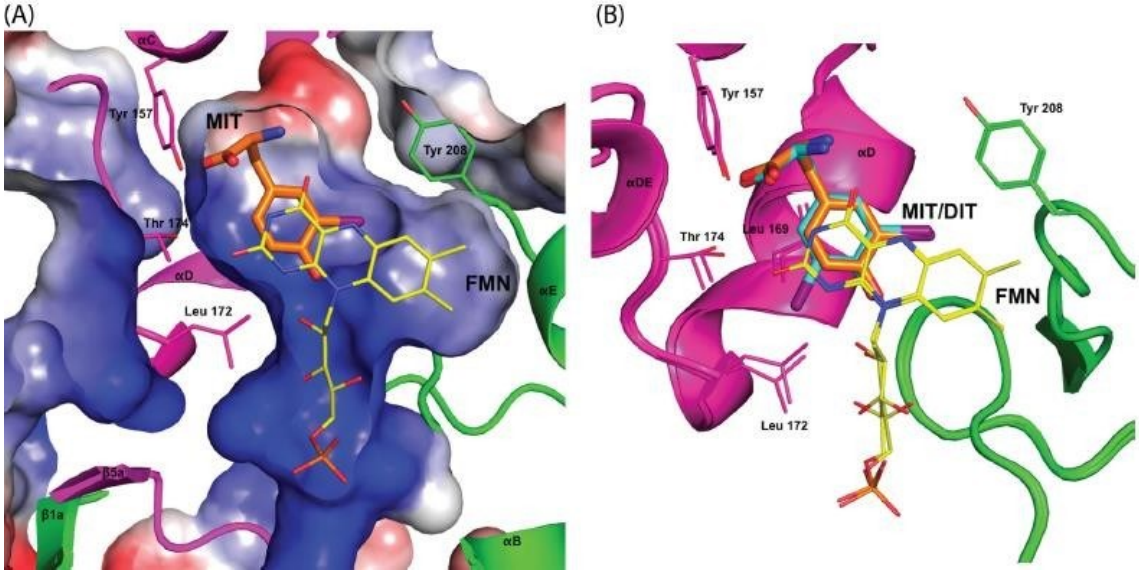

Figure 21. Conformational changes of the DEHAL1 active site to accommodate iodotyrosines. A. MIT-DEHAL1 co-crystal structure showing the surface characteristics: blue indicates positive charges whereas red indicates negative charges; B. Conformational changes required for the alignment of DIT (cyan) to the active site of DEHAL1 equally to MIT (orange) (Adapted from Thomas SR, *et al.* 2009[210]).

The catalysed deiodination reaction happens during TG proteolysis at the apical membrane, close to TG, both before and after TG is endocytosed into the thyrocytes[211]. Even though the previously proposed mechanism of the dehalogenation reaction is still being investigated, recently, a hypothetical process included the biding of the phenolate form of iodotyrosines to DEHAL1 and entails a single electron transfer from the hydroquinone form of FMN.

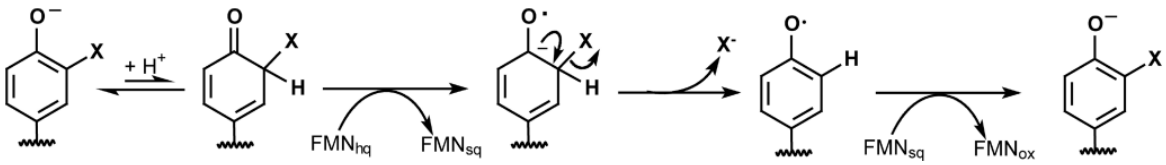

Figure 22. Proposed mechanism of dehalogenation (adapted from Sun Z *et al.* 2017[212]).

The phenolate form facilitates coordination with two hydrogen bond donors, which causes the α-carbon containing halogen to be protonated. A transient semiquinone intermediate is created when the protonated intermediate is subjected to reductive dehalogenation via the electron donation of the hydroquinone form of FMN. By removing the halogen, a stable phenoxy radical is created, which is then able to take an electron from FMN's semiquinone intermediate and regenerate the oxidised form of FMN. Tyr is the reaction's end product, and it can be recycled along with I^- to create TH[212]. DEHAL1 activity was found to be NADPH-dependent and proportional to enzyme concentration *in vitro*. The reported Km for the deiodination of MIT and DIT were $1.35x10^{-6}$ and $2.67x10^{-6}$, respectively, indicating that DEHAL1 has a higher affinity for MIT than DIT. Subsequent research revealed that TSH-stimulated cAMP upregulated *DEHAL1* mRNA in rats, while iodide administration, both acute and long-term, decreased it.[213] Furthermore, hypothyroid rats exhibited increased DEHAL1 activity.

Moreno *et al*. reported the first human *DEHAL1* mutations in 2008[214]. Three distinct mutations were found: an in-frame depletion of Arg101Trp and Ile116Thr, two missense mutations. The patients exhibited a range of pathological phenotypes, which may have been caused by environmental factors like iodine intake or by the timing of the disease's expression. The four patients under analysis were consanguineous, unrelated, and all had severe goitrous hypothyroidism; two of them experienced intellectual deficits as a result of delayed diagnosis and treatment[214]. If proper treatment is not received in the early stages of life, failure of DEHAL1 results in iodotyrosine deiodinase deficiency (ITDD), a known disease that is characterised by goitre, intellectual retardation, psychomotor deficits, and hereditary hypothyroidism. Given that TH is essential for development at the beginning of life and that DEHAL1 expression is absent, the discovery of *DEHAL1* mutations has provided new insights into ITDD. In fact, two of the four patients examined by Moreno et al. underwent neonatal screening for hypothyroidism, and the alarming results indicated that the condition might not exist at birth[215]. Afink et al. (2008)[216] reported the discovery of a second missense homozygous (HO) mutation (Ala220Thr) from a different consanguineous family. Currently, neonatal screening programmes do not include the diagnosis of ITDD, despite reports of negative effects on untreated patients' neurodevelopment[215]. A new homozygous mutation in *DEHAL1* (p.A57SfsX62) was found recently in the progeny of a consanguineous family from Lebanon. An early-stop codon at amino acid 62 of the protein was produced by the frameshift caused by the insertion of an adenosine between positions 168 and 169 of exon 1. This new mutation caused the enzyme to be nearly entirely truncated, which eliminated the functional nitro

reductase domain and reduced DEHAL1 activity[217]. Thanks to new technologies in the genomic field, it is nowadays possible to diagnose new mutations of the *DEHAL1* gene. Therefore, there is an urgent need for diagnostic techniques and biomarkers necessary to monitor these rare and delicate conditions.

6. The use of HPLC-MS/MS for the quantification of TH

Serum and plasma are the common matrices used for the assay of TH. However, more than 90% of circulating TH are bound to serum carrier proteins, making the protein-bound fraction inaccessible to tissues, and considered inactive. To produce their effects, TH must dissociate from carrier proteins and enter cells. Only a small percentage of TH (<1%) is present as the free fraction (fT3 and fT4), which is directly accessible to peripheral tissues and considered biologically active[218]. Quantifying the free fraction is challenging due to its low concentration range, and the assay of the total fraction may not accurately reflect thyroid status when protein concentrations or binding capacities are altered. Clinicians prefer to assess fT3 and fT4 levels routinely[219]. Two main methodologies have been developed for the assay of serum fTH: indirect and direct methods. Indirect methods involve mathematical estimation of the free fraction and are dependent on TH binding protein levels, resulting in an underestimation or overestimation of TH levels. Direct methods are preferred as they measure the free fraction directly, providing more accurate results[220–222]. On the other hand, a number of direct immunoassays have been developed to measure fTH, but they require the physical separation of the unbound fraction before analysis. To achieve this, two primary techniques are employed: Equilibrium dialysis (ED) and Ultrafiltration (UF). However, both methods have their limitations. ED is susceptible to dilution effects and potential interference from buffer components, which can affect the equilibrium between fTH and bound TH[223]. In contrast, UF is not affected by dilution effects and yields a higher measurement of fTH compared to ED[224]. Nevertheless, UF also has its drawbacks, including membrane adsorption, protein leakage, and sensitivity to pH and temperature[223]. Automated immunometric methods have become the norm for determining clinical parameters of the thyroid. Chemiluminescence detection is commonly used in highly sensitive and automated immunoassays, which are considered the gold standard for detecting serum fT3 and fT4[225]. However, the accuracy of immunoassays can be affected by various factors such as pregnancy, genetic variations, medications, and medical conditions that can alter serum-binding protein concentration. Additionally, studies have shown discrepancies in fTH results across different immunoassays, which may be due to the variability in serum binding proteins[218]. Furthermore, the inverse log-linear relationship between fT4 (and fT3) and TSH is poorly correlated when fTH is measured using immunoassays[226,227]. MS can be utilized to overcome some of the weaknesses of immunoassays. HPLC-MS/MS is a highly sensitive and specific technique that can detect hormones at low concentrations. One of the advantages of HPLC-MS/MS is the use of stable isotope-labelled internal standards (ISs) that

can monitor the analytical process and compensate for analytical errors. HPLC-MS/MS is becoming a powerful technique for detecting serum fTH and total TH (TTH), complementing traditional immunoassay methods[218]. Furthermore, specific HPLC-MS/MS methods can be developed to detect TH in matrices other than serum, along with their metabolites and precursors. However, the low throughput of HPLC-MS/MS compared to automated high throughput immunoassay platforms is a technical limitation. During the 1970s, MS was utilized for the quantification of serum TH, and numerous GC-MS methods were created[228–233]. However, these methods were abandoned due to their laborious sample clean-up and time-consuming nature, despite their accuracy. The advent of ESI and APCI interfaces enabled effective coupling with HPLC systems, leading to the development of highly sensitive and accurate HPLC-MS/MS methods capable of detecting serum T3 and T4[233,234]. Most of these methods can quantify the serum total fraction of TH, which requires a protein precipitation step followed by sample purification. These methods paved the way for the development of novel HPLC-MS/MS procedures, with several research groups introducing the more specific solid-phase extraction (SPE) or liquid-liquid extraction (LLE) for a more selective isolation of TH[235–239]. Technological advancements over the years have led to increasingly sensitive MS methods for TTH assay, with some researchers implementing online extraction or a derivatization step to achieve the best sensitivity[240–244]. Clinicians are primarily interested in measuring the free fraction of serum TH, and high-throughput immunoassays are commonly used to detect most thyroid biochemical parameters. However, the assay of serum fTH at low concentrations presents methodological difficulties. Despite this, several HPLC-MS/MS methods have been developed and are now considered gold standards. The first methods proposed involved the use of the ED step to isolate the free fraction, but these were time-consuming and required expensive devices. They have largely been replaced by more rapid UF tandem MS methods, which are more sensitive and versatile[245–252]. HPLC-MS/MS has played a crucial role in quantifying TH and their metabolites, including rT3, 3,5-T2, 3,3'-T2, MIT, DIT and thyronamines, in serum and other human matrices such as urine, saliva, breast milk, and CFS. MS methods have also been used to measure these molecules in cell lysates and various tissues from animal models. The main advantage of this technique is the ability to measure and quantify multiple molecules in a single run with a small amount of sample, as well as the ability to transfer and validate the method to other matrices[44,253].

Aim

HPLC-MS/MS stands as a cornerstone in the field of biochemistry, providing an invaluable tool for the meticulous analysis of compounds within intricate and heterogeneous mixtures. This method's fusion of a liquid chromatography system with a tandem mass spectrometer enables the efficient separation, identification, and quantification of components. The significance of HPLC-MS/MS extends across diverse fields, including pharmaceuticals, environmental analysis, and metabolomics. Its capability to discern and quantify compounds at low concentrations makes it indispensable. In the context of TH and their metabolites, HPLC-MS/MS has garnered substantial attention. Numerous reviews have presented upon its applications, emphasizing the need for adapt techniques to explore novel biochemical insights and detect biomarkers that illuminate previously uncharted facets of thyroid-related diseases. This work delineates the utilization of HPLC-MS/MS as a pivotal instrument in four different topics with implications on the overall thyroid function, employing different pre-analytical approaches and analytical methods to delve into differential matrices.

Unravelling neurocognitive dynamics in adult-onset hypothyroidism

In the realm of brain development, TH acquires a pivotal influence during gestational and perinatal periods, persisting in their contributions to maintaining adult brain health. However, adult-onset hypothyroidism manifests in various cognitive disturbances, necessitating a comprehensive exploration. Leveraging HPLC-MS/MS and other molecular biology techniques, this study explores the intricate interplay between TH deficiency and persisting symptoms, hypothesizing a link to decreased brain levels of T1AM. The experiment employs a rodent pharmacological model, assessing the impact of different replacement strategies (L-T4, T1AM, L-T4 + T1AM) on neurocognitive and neurobiological alterations, with a specific focus on hippocampal neurogenesis. HPLC-MS/MS was here implied to quantify the total fraction of T3 and T4 in the serum samples of the animal hypothyroidism model to confirm the validity of the experimental plan.

Deciphering TH dynamics in diabetic retinopathy

Diabetic retinopathy (DR), characterized by neuronal damage, prompts protective mechanisms in the retina. This venture investigates the role of TH in retinal stress response under hyperglycemic conditions. Delving into the local regulation of the TH system in the retina, the study explores potential mechanisms, including the impact on T3-dependent microRNA/gene regulatory circuits and mitochondrial function. The aims of the present work were to demonstrate the presence of a LT3S in the retina of *db/db* mice (a model of type 2 diabetes) in

concomitance with the presence of typical markers of DR; to investigate, in an *in vitro* model, the possibility of a miRNA-based mechanism for the regulation of retinal T3 levels and to get insights into the possible involvement of a LT3S -induced mitochondrial deregulation in the development of DR. The plasma samples and the retina samples of the *db/db* mouse model were processed using HPLC-MS/MS to detect and quantify the total fraction of T3 and T4.

Unveiling iodine dynamics and the fundamental role of DEHAL1

Addressing the global concern of iodine deficiency, we explored the adverse effects on human health and emphasized the need for efficient markers reflecting individual iodine status. Using a *Dehal1* knockout (*Dehal1*KO) mouse model and HPLC-MS/MS, the study aims to characterize the expression pattern of *DEHAL1* in a mammalian species. By phenotyping mice under controlled diets with varying iodine levels, the project seeks to enhance our understanding of iodine recycling and its consequences. A previously optimized method for the detection of thyroid hormones, using a derivatization process, was adapted to correctly quantify the precursors MIT and DIT in the aforementioned animal model and so monitor the different levels of TH, and their precursors, in different iodine-supplementation conditions.

Investigating DEHAL1 gene mutations in congenital hypothyroidism

The final endeavour centres on congenital hypothyroidism, affecting newborns with significant growth and developmental implications. HPLC-MS/MS is employed to investigate a novel mutation in the *DEHAL1*/*IYD* gene within Sudanese families. Despite the same genetic defect, the project unravels variable phenotypes and underscores the utility of measuring MIT and DIT levels in diagnosing hypothyroidism in iodine-sufficient and borderline areas, more than the actual and usually measured urinary iodine.

In essence, this work outlines the pivotal role of HPLC-MS/MS in driving forward these diverse assignments, each contributing to an enriched understanding of TH and their intricate involvement in physiological and pathological processes.

Materials and Methods

7.1 Mouse model of pharmacologically induced hypothyroidism

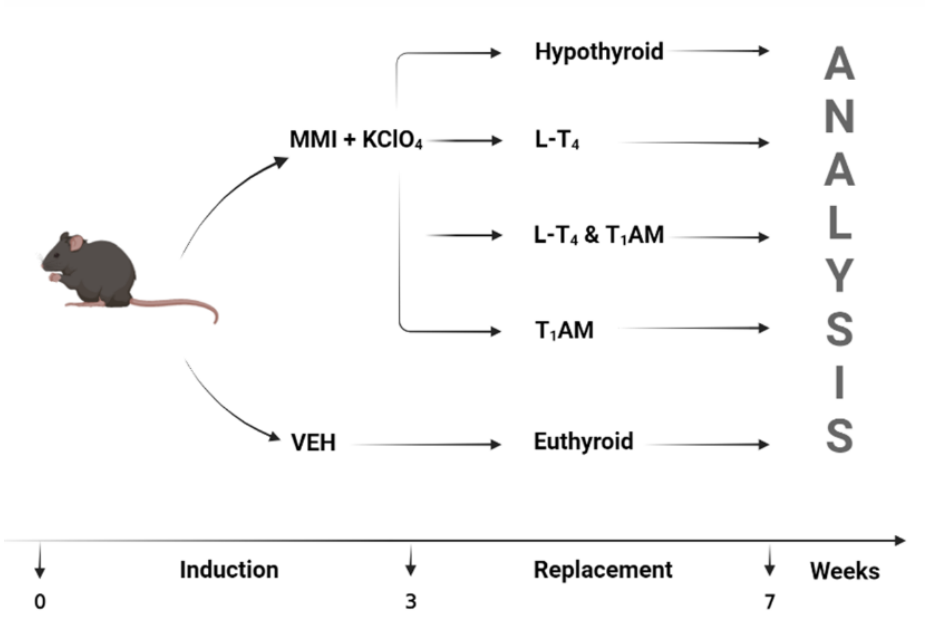

Figure 23. Pharmacological mouse model of hypothyroidism (created on Biorender.com).

Four- to five-week-old C57BL/6J male mice (n=82) were maintained in an air-conditioned animal room with a 12-h light/dark cycle. Mice, up to five per cage, were housed in plastic cages and provided with a pelleted basal diet and tap water *ad libitum*. Six-week-old mice (n=65) were given methimazole (0.20 mg/g/die, Sigma Aldrich-Merck, St. Louis, MO, USA) and potassium perchlorate (0.30 mg/g/die, Sigma Aldrich-Merck, St. Louis, MO, USA) in drinking water for 49 days while the control littermates (n=17) received water. Perchlorate limits active iodine transport into the thyroid and methimazole inhibits intrathyroidal TH production. Body weight (BW), water intake, and food consumption were monitored once per week throughout the hypothyroidism induction period. At day 21, mice were anesthetised with 1.5% isoflurane in 100% oxygen, and implanted with ALZET® subcutaneous osmotic pumps delivering replacement treatments for 28 days (reservoir volume of 100 µL and delivery rate of 0.11 µL/h). Animals were divided in 5 groups: euthyroid (n=17), hypothyroid (n=15), hypothyroid treated with L-T4 (n=18, 0.04 µg L-T4/g BW/die)[254], hypothyroid treated with L-T4 + T1AM (n=17, 0.04 µg L-T4 + 0.004 µg T1AM/g BW/die) and hypothyroid treated with T1AM (n=15, 0.004 µg T1AM/g BW/die)[122,160]. L-T_4 and T1AM were purchased from Sigma Aldrich-Merck (St. Louis, MO, USA). The osmotic pump filling solution was prepared in sterile 1% bovine serum albumin (BSA) in 0.9% saline, NaOH 0.1 M (Sigma Aldrich-Merck,

St. Louis, MO, USA). All parameters, including BW, water intake, and food consumption were monitored once a week throughout the three weeks of induced hypothyroidism. All experiments were conducted in accordance with the principles of animal care and experimentation in the guidelines of the Italian Ministry of Health (Legislative Decree n. 116/92) and the European Community (European Directive 86/609/EEC). The Italian Ministry of Health approved the use of animals in this protocol (65E5B.10, n.734/2017-PR, 10/10/2017).

7.1.1 Serum samples

3,3′,5-Triiodo-L-thyronine (T3) solution and T3-$^{13}C_6$ solution (100 µg/mL in MeOH with 0.1 M NH_3), L-Thyroxine (T4) solution and T4-$^{13}C_6$ solution (100 µg/mL in MeOH with 0.1 M NH_3), water LC-MS grade, methanol (MeOH) LC-MS grade, acetonitrile (ACN) LC-MS grade, 2-propanol LC-MS grade, hexane HPLC grade, dichloromethane HPLC grade, ammonium hydroxide (28% NH_3 in H_2O, ≥99.99% trace metal basis), formic acid LC-MS grade (FA, ≧ 98%), acetone, hydrochloric acid 37% (HCl 37%), potassium acetate ~98% (AcK) were all purchased from Sigma Aldrich-Merck (St. Louis, MO, USA). Bond-Elut Certify 130 mg SPE cartridges were obtained from Agilent Technologies (Santa Clara, CA, USA).

Collected serum samples, before and post replacement treatments, were processed to perform a HPLC-MS/MS quantification of total T3 and T4 based on previously published methods[235,242]. Briefly, 100 µL of serum were placed in a 2 mL Eppendorf ® tube and added with 10 µL of a 200 ng/ml ($^{13}C_6$-T3 and $^{13}C_6$-T4) stable isotope-labelled internal standards mix. Samples were gently vortexed and kept for 30 minutes at room temperature (RT). Then, 300 µL of cold acetone were added and samples were vortexed and kept 30 minutes at 4 °C to allow proteins precipitation. After centrifugation at 22780 x g for 10 minutes, the supernatants were transferred to a new 2 mL Eppendorf ® tube and dried, in a thermostated block set at 40 °C, under a nitrogen stream until reaching ~ 100 µL. Afterwards, samples were added with 400 µL of a 0.1 M potassium acetate buffer (pH=4) and submitted to a Solid Phase Extraction (SPE) using Agilent Bond-Elut Certify 130 mg SPE cartridges. Before samples loading, cartridges were conditioned by consecutive wetting with 2 mL of dichloromethane/2-propanol (75/25 by volume), 2 mL of MeOH and 2 mL of 0.1 M potassium acetate buffer (pH = 4). After four consecutive washing steps using 3.5 mL of water, 2 mL of 0.1 M hydrochloric acid, 7 mL of MeOH and 3.5 mL of dichloromethane/2-propanol (75/25 by volume), samples were eluted with 2 mL of dichloromethane/2-propanol/ammonium hydroxide (70/26.5/3.5 v/v/v). Eluates, warmed up at 40 °C, were dried under a gentle stream of nitrogen, reconstituted with 100 µL

of MeOH/H_2O (30/70, v/v) and 5 µL were injected into the HPLC-MS/MS system. Minor stock solutions of T3 and T4 were prepared at 1 µg/mL concentration in methanol. Calibration curves were prepared by serial dilution with methanol at a concentration ranging from 0.10 to 100 ng/mL as follows:

Concentration (ng/mL)	**Volume from level to level (µL)**	**Volume of MeOH (µL)**	**Total final volume (µL)**
100 (L1)	30 µL from each 1 µg/mL minor stock solution of analyte (T3 and T4), for a total of 60 µL	240	300
50 (L2)	150 of L1	150	300
25 (L3)	150 of L2	150	300
10 (L4)	120 of L3	180	300
5 (L5)	150 of L4	150	300
2.5 (L6)	150 of L5	150	300
1 (L7)	120 of L6	180	300
0.5 (L8)	150 of L7	150	300
0.25 (L9)	150 of L8	150	300
0.10 (L10)	120 of L9	180	300

Table 1. Calibration points for serum T3 and T4 quantification.

100 µL remaining from each point (L1 to L10) were transferred to new 1.5 mL tubes and added with 10 µL of the 200 ng/mL internal standard mixture. Each calibration point was vortexed sit at RT for 15/20 minutes before drying. Eventually, tubes were reconstituted with 100 µL of H_2O:MeOH 70/30 (v/v), vortexed, spun and 5 µL were injected into the HPLC-MS/MS system. At the end of the procedure, both calibration points and samples will have the same nominal concentration of internal standard.

The instrument layout consisted in an Agilent (Santa Clara, CA, USA) 1290 UHPLC system, including a binary pump, a column oven set at 20 °C, and a thermostated autosampler, coupled to a Sciex (Concord, Ontario, Canada) QTRAP 6500+ mass spectrometer working as a triple quadrupole, and equipped with an IonDrive™ Turbo V source performing an ESI ionization. Chromatographic separation was achieved by using a 110 Å, 2x50 mm, 3µm particle size, Gemini C18 column (Phenomenex, Torrance, CA), protected by a C18 Security Guard Cartridge and using (A) MeOH/ACN (20/80 v/v) added with 0.1% FA and (B) water containing 0.1% FA as mobile phases. The integrated 6 ports switching valve was used to discard both head (the first two minutes) and tail (the last four minutes) of the HPLC runs. Gradient elution (400 µL/min flow rate) was performed as follows: 0.1-3 min (A) 5%, 8.5 min (A) 65%, 9.0-

11.0 min (A) 100%, 11.50-13.50 (A) 5%. System control, data acquisition and analyses were performed using a Sciex Analyst® version 1.7.3 software.

A mass spectrometry selected reaction monitoring (SRM) method operated in positive ion mode. For each compound, after the optimization of declustering potential (DP), collision energy (CE) and collision exit potential (CxP), three transitions were considered in the analysis. Based on the highest signal/noise ratios, one of them was used as quantifier (Q) and the other two as qualifiers (q) as reported in Table 2. Further operative parameters were gas source 1 (GS1), 60 arbitrary units; gas source 2 (GS2), 45 arbitrary units; ion spray voltage (ISV), 5.5 kV; source temperature (TEM), 650 °C; entrance potential (EP), 10V; Curtain gas (CUR), 20 arbitrary units; collision gas (CAD) N_2, operative pressure with CAD gas on, 2 mPa.

Analyte	**SRM transitions (Da)**	**Operative Parameters**		
		DP (V)	**CE (V)**	**CXP (V)**
T3	651.8 → 478.9 (q)	76	47.7	13.7
	651.8 → 508.0 (q)		31.2	14.8
	651.8 → 605.9 (Q)		31.3	17.9
$^{13}C_6$-T3	657.8 → 484.9 (q)	76	47.7	13.7
	657.8 → 514.0 (q)		31.2	14.8
	657.8 → 611.9 (Q)		31.3	17.9
T4	777.8 → 604.8 (q)	82	52.8	17.0
	777.8 → 633.9 (q)		36.0	18.6
	777.8 → 731.9 (Q)		34.0	22.0
$^{13}C_6$-T4	783.8 → 610.8 (q)	82	52.8	17.0
	783.8 → 639.9 (q)		36.0	18.6
	783.8 → 737.9 (Q)		34.0	22.0

Table 2. MS parameters for T3 and T4 detection.

7.1.2 Statistical analysis

For this specific study, all data were analysed to check for outliers with the ROUT method with value Q=1%. The D'Agostino & Pearson normality test was used to determine if data were normally distributed. Data were reported as mean ± standard error of the mean (SEM), if normally distributed, or as median and interquartile ranges, if not normally distributed. Data deriving from the one-week monitoring of BW were analysed using two-way ANOVA for repeated measures, followed by Sidak's post hoc tests. Differences between groups in hormonal level, behavioural performances, immunohistochemistry, and gene expression were assessed with one-way ANOVAs, followed by Tukey's post-hoc tests, in case of normal distribution of data, or with the non-parametric Kruskal-Wallis test, in case of non-normally distributed data. As regards the novel object recognition test (ORT), one-sample t-test was used to determine whether the average of the discrimination index (DI) for each group was different from chance (hypothetical value = 0). Statistical significance was set at $*p \leq 0.05$, $**p \leq 0.01$, $***p \leq 0.001$ and $****p \leq 0.0001$. Statistical analyses were conducted using GraphPad Prism v. 6 and v. 8 (GraphPad Software Inc., La Jolla, CA, USA).

7.2 Diabetic retinopathy in db/db mice (a model of type 2 diabetes)

BKS.Cg-+Leprdb/+Leprdb/OlaHsd (*db/db*) male mice (ENVIGO, San Pietro al Natisone, Udine, Italy), which are affected by type 2 diabetes[255–257], were used. C57BL/6J mice were used as controls. In respect of the 3Rs principles for ethical use of animals in scientific research, the retinas analysed in these studies derived from animals (both *db/db* and controls) also used for a study on dermal tissue regeneration without any involvement of the retinas or any other ocular tissues[258]. All the procedures were performed in compliance with the ARVO Statement for the Use of Animals in Ophthalmic and Vision Research, the EU Directive (2010/63/EU), and the Italian guidelines for animal care (DL 26/14; Italian Ministry of Health, decree numbers 905/2018-PR and 132/2019- PR). At the moment of analysis, the mice were sixteen-week-old. Non-fasting glycemia was measured by tail sampling using a OneTouch Ultra glucometer (LifeScan Inc., Milpitas, CA, USA). A total of 34 *db/db* and 15 control mice were used in these studies.

7.2.1 Plasma and retinas of diabetic mice for T3 and T4 quantification

Plasma samples were processed and analysed as the aforementioned serum samples of the previous model and so the pre-analytical procedure will be not further discussed. Retinas processing follows different steps instead, based on a previously validated method[242,259]. Retinas, kept at -80 °C, were quickly transferred to 2 mL homogenizing PRECELLYS® tubes (Bertin Technologies (Montigny-le-Bretonneux, France), weighted and processed as reported in previously validated methods. Each sample was suspended in 1 mL of a solution made of 840 µL of acetonitrile and 150 µL of pure water added with 10 µL of a 10 ng/mL internal standard mixture ($^{13}C_6$-T3 and $^{13}C_6$-T4). After being vortexed, samples were sonicated for 15 minutes and then homogenized using a Precellys®24-Dual Homogenizer (Bertin Technologies, Montigny-le-Bretonneux, France) through three homogenization steps of 45 seconds with 60 seconds pause at 5000 rpm.

Figure 24. Precellys tissue homogenizer for tissue grinding (adapted from Bertin-Technologies.com)

Afterwards, homogenized samples were sonicated again for 15 minutes and then centrifuged for 15 minutes at 22780 x g. Supernatants were transferred to new 2 mL Eppendorf® tubes and washed three times using 1 mL of hexane to remove the phospholipid excess. The lower phase was then dried under a gentle stream of nitrogen, in a thermostated block set at 40 °C. Before injection, samples were eventually reconstituted using 100 µL of H_2O: MeOH 70:30 (v/v), vortexed for 10 minutes to guarantee a full resuspension and centrifuged for 15 minutes at 22780 x g. Volumes were then transferred to a 96-well collection plate and 20 µL were injected in the HPLC-MS/MS system. The quantification of analytes was performed using standard T3 and T4 calibration curves built in methanol from 0.025 ng/mL to 5 ng/mL. Minor stock solutions of T3 and T4 were prepared at 1 µg/mL concentration in methanol. Calibration points were set at: 0.025 – 0.050 – 0.100 – 0.250 – 0.500 – 1 – 2 – 5 ng/mL and prepared as follows:

Concentration (ng/mL)	**Volume from level to level (µL)**	**Volume of MeOH (µL)**	**Total final volume (µL)**
5 (L1)	30 µL of a mixture 50 ng/mL of T3 and T4 combined	270	300
2 (L2)	120 of L1	180	300
1 (L3)	150 of L2	150	300
0.5 (L4)	150 of L3	150	300
0.25 (L5)	150 of L4	150	300
0.1 (L6)	120 of L5	180	300
0.05 (L7)	150 of L6	150	300
0.025 (L8)	150 of L7	150	300

Table 3. Calibration points for tissue T3 and T4 quantification in retinas.

100 µL remaining from each point (L1-L8) were transferred to new 1.5 mL tubes and added with 10 µL of the 10 ng/mL internal standard mixture. Each calibration point was vortexed sit at RT for 15/20 minutes before drying. Eventually, tubes were reconstituted with 100 µL of H_2O:MeOH 70/30 (v/v), vortexed, spun and 5 µL were injected into the HPLC-MS/MS system. At the end of the procedure, both calibration points and samples will have the same nominal concentration of internal standard.

Both plasma and retina samples were analysed with the aforementioned HPLC-MS/MS method that will not be further discussed here.

7.2.2 Statistical analysis

All variables in this study satisfied the criteria for parametric analysis. The data underwent analysis using either Student's t-test for single comparisons or one-way ANOVA followed by Tukey's post-hoc test for multiple comparisons. The results were presented as mean ± SEM of the biological replicates in each experiment (individual data points are depicted in each graph; Prism v. 8; GraphPad software, San Diego, CA, USA). Differences with $p < 0.05$ were deemed statistically significant.

7.3 Iodine deficiency model

Female 5–6-month-old C57BL/6J *Dehal1* WT and KO mice were fed a free iodine pellet diet containing 0.25 g of I/g (TD180914, Envigo, Indianapolis, IN, USA). Mice were divided into three groups, each of which received a different iodine-containing diet. In normal iodine diet (NID), low iodine diet (LID), and very low iodine diet (VLID), drinking water iodine content was 1400 g of I/L, 200 g of I/L, and without any iodine supplementation, respectively. The daily iodine intake of mice was 5.6 g, 1 g, and 0.25 g for NID, LID, and VLID, respectively.

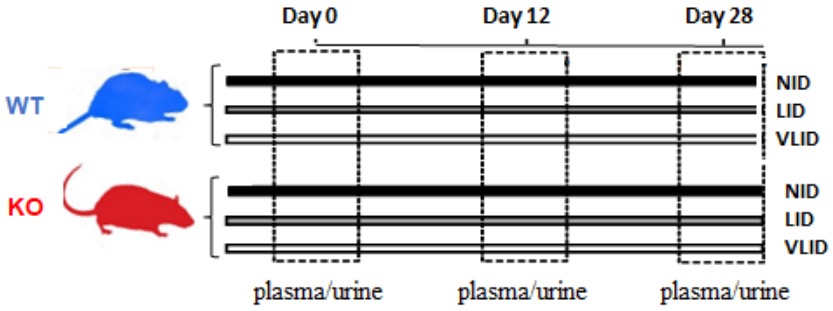

Figure 25. *Dehal1* KO and WT mouse model and the different iodine supplementations (adapted from González-Guerrero G, *et al.* 2023[260]).

Urine was collected on days 0, 12, and 28 using a special hydrophobic sand (Sodispan Research, Madrid, Spain). Before storage, samples were centrifuged at 1230 x g for 5 minutes, and supernatants were collected. Blood was collected from the submandibular vein at the same time points, and plasma was obtained by centrifugation at 1230 x g for 10 minutes. The samples were kept at -80° C until the extraction and then analysed using HPLC-MS/MS. Furthermore, pregnant female C57BL/6J *Dehal1* WT and KO mice were given an NID. Plasma was collected from 10-day old mice (pups) and 1 month old mice (juveniles), along with urine in the latter case. Samples were kept at -80° C until they were extracted and submitted to HPLC-MS/MS analysis. All animal studies adhered to the guidelines established by the European Community and Animal Research Ethical Committee guidelines, following approval from the Autonomous University of Madrid Animal Research Ethical Committee (CEI, Madrid, Spain).

Prof. José Carlos Moreno created the *Dehal1* KO mice, and Dr. Cristian González Guerrero and Pouya Alikhani maintained the colony in the Thyroid Research Laboratory (University Hospital La Paz, Madrid, Spain). The creation of the first *Dehal1* KO extends beyond the scope of my PhD project and will be briefly described. A specific targeting vector containing lacZ as the reporter gene and Neomycin as the selection gene was inserted by homologous recombination between exon 1 and exon 2 of the *Dehal1* WT allele. As a result, the DEHAL1

protein expression was truncated. Crossbred C57BL/6J mice were used to create HO mutants. Genotype analysis on mouse tail genomic DNA was performed to confirm the generation of the KO and to differentiate the three possible genotypes WT, heterozygous (HT), and HO. Electrophoresis gels, molecular studies, and immunohistochemistry analysis all confirmed the absence of the DEHAL1 protein in KO, as opposed to WT, where the protein was expressed constitutively. All details regarding the DEHAL1 model characterization techniques will not be further discussed here and can be retrieved at the referenced article[260] while relative results will be explored in the following chapter.

7.3.1 Plasma and urines samples derivatization process and analysis

The previously utilized method[235,242] for the detection and quantification of T3 and T4 in serum and tissue samples was modified, thanks to the work of Dr. Marco Borsò and prof. Alessandro Saba, to simultaneously analyze T3, T4, MIT and DIT. To do so, since the interaction of MIT and DIT in the chromatographic column was weak and considering the aim of achieving the best sensitivity possible for our analytes, we decided to improve the pre-analytical procedure by adding a derivatization step.

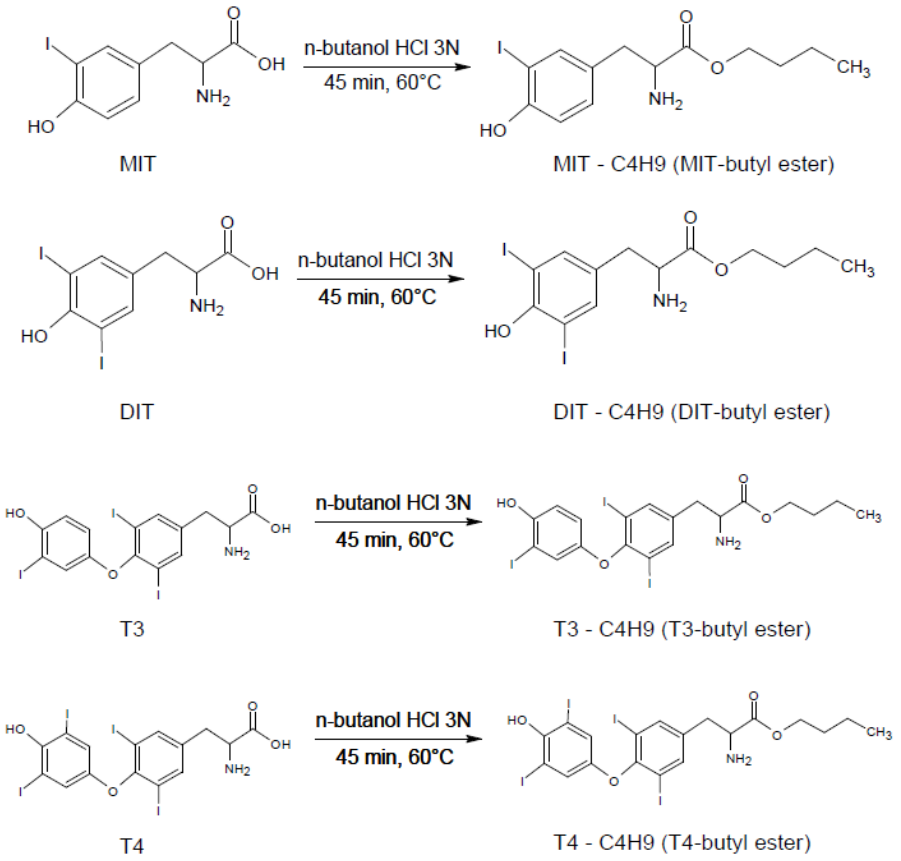

Figure 26. Derivatization reaction of TH to obtain the corresponding butyl ester forms (realized with ADC/Chem Sketch)

Analytical standards of MIT, DIT were also supplied by Sigma-Aldrich. Stable isotope-labelled $^{13}C_9$-MIT and $^{13}C_9$-DIT were kindly provided by Prof. Alireza Mani (University College of London, UK), since they were not commercially available.

Briefly, 100 µL of urine/plasma were placed in a 2mL Eppendorf tube® with an appropriate amount (10 µL of a 100 ng/mL mixture) of stable isotope labelled ISs. Samples were vortexed, equilibrated for 30 minutes at RT, and then 300 µL of cold acetone were added and samples were kept 30 minutes at 4 °C to allow proteins precipitation. The use of organic solvents reduces the hydration of the proteins and leads to their aggregation and precipitation. Consequently, the TH-bound fraction is released and, together with the fTH fraction, can be detected as TTH. After centrifugation at 22780 x g for 10 min, the supernatants were transferred to a new 2 mL Eppendorf tube®, warmed up at 40 °C, and dried under a gentle stream of nitrogen. The concentrated samples were derivatized adding 200 µL of 3.0 N hydrochloric acid in n-butanol and incubated for 45 min at 60 °C. This derivatization step allows the formation of the corresponding butyl esters of tyrosines, TH and their ISs.

Afterwards, samples were dried again as mentioned above and then, reconstituted with 500 µL of 0.1 M potassium acetate buffer (pH=4) prior to loading onto Agilent Bond-Elut Certify 130 mg SPE cartridges. The extraction procedure for derivatized samples is the same as for the un-derivatized ones. Briefly, before loading the samples, cartridges have been previously conditioned by consecutive wetting with 2 mL of dichloromethane/isopropanol (75/25 by volume), 2 mL of MeOH and 2 mL of 0.1 M potassium acetate buffer (pH = 4). After consecutive washes with 3.5 mL of water, 2 mL of 0.1 M hydrochloric acid, 7 mL of MeOH and 3.5 mL of dichloromethane/isopropanol (75/25 by volume), samples were eluted with 2 mL of dichloromethane/isopropanol/ammonium hydroxide (70/26.5/3.5 by volume).

Eluates were dried under nitrogen, reconstituted with 100 µL of ACN / 0.1 M HCl (50/50 by volume) and 2 µL were injected into the HPLC-MS/MS system. Minor stock solutions of MIT, DIT, T3 and T4 were prepared at 1 µg/mL concentration in methanol. Calibration curves were prepared daily as follows:

Concentration (ng/mL)	Volume from level to level (µL)	Volume of MeOH (µL)	Total final volume (µL)
100 (L1)	30 µL from each 1 µg/mL minor stock solution of analyte (T3, T4, MIT and DIT), for a total of 120 µL	180	300
50 (L2)	150 of L1	150	300
25 (L3)	150 of L2	150	300
10 (L4)	120 of L3	180	300
5 (L5)	150 of L4	150	300
2.5 (L6)	150 of L5	150	300
1 (L7)	120 of L6	180	300
0.5 (L8)	150 of L7	150	300
0.25 (L9)	150 of L8	150	300
0.10 (L10)	120 of L9	180	300

Table 4. Calibration points for plasma and urine MIT, DIT, T3 and T4 absolute quantification.

100 µL remaining from each point (L1 - L10) were transferred to new 1.5 mL tubes and added with 10 µL of the 100 ng/mL internal standard mixture. Each calibration point was vortexed sit at RT for 15/20 minutes before drying. The calibration points were then derivatized and treated following the same procedure as for the real samples. At the end of the procedure, both calibration points and samples will have the same nominal concentration of internal standard. The instrumental layout used for the analysis retraces the same as the previous method, as for mass spectrometer, UHPLC system, mobile phases, and chromatographic column. The chromatographic method implied was slightly modified as reported in Table 5.

HPLC Binary pump

Total time (min)	Flow rate (µL/min)	Solvent A (%)	Solvent B (%)
0.1	400	5	95
3.0	400	5	95
8.5	400	65	35
9.0	400	100	0
11.0	400	100	0
11.5	400	5	95
14.0	400	5	95

Table 5. HPLC pump modified gradient. Solvent A: MeOH/ACN (20/80 by volume) + 0.1% FA; Solvent B: water + 0.1% FA.

Mass spectrometry selected reaction monitoring (SRM) method operated in positive ion mode. For each compound, after the optimization of declustering potential (DP), collision energy (CE) and collision exit potential (CxP), three transitions were considered in the analysis. Based on the highest signal/noise ratios, one of them was used as quantifier (Q) and the other two as qualifiers (q) (Table 6). Additional operative parameters were set as follow: Collision gas (CAD) N2; operative pression with CAD gas, 2 mPa; Curtain gas (CUR), 20 arbitrary units; Gas source 1 (GS1), 60 arbitrary units; Gas Source 2 (GS2), 45 arbitrary units; ion spray voltage (ISV), 5.5 kV; Source temperature (TEM), 650 °C; Entrance potential (EP), 10 V.

Analyte	SRM transition (Da)	DP (V)	CE (V)	CxP (V)
MIT-C4H9	363.9 → 135.0 (q)		44.0	10.3
	363.9 → 261.8 (Q)	65.0	25.0	14.1
	363.9 → 291.0 (q)		22.0	16.1
^{13}C9-MIT-C4H9	373.1 → 143.2 (q)		44.0	10.3
	373.1 → 270.1 (Q)	95.0	25.0	14.1
	373.1 → 300.2 (q)		22.0	16.1
DIT-C4H9	489.9 → 260.9 (q)		51.2	7.7
	489.9 → 290.0 (q)	55.0	36.0	8.3
	489.9 → 387.9 (Q)		31.4	11.0
^{13}C9-DIT-C4H9	498.8 → 268.8 (q)		48.0	5.9
	498.8 → 298.9 (q)	64.0	35.0	7.1
	498.8 → 395.8 (Q)		28.0	9.5
T3-C4H9	707.9 → 479.1 (q)		53.5	12.3
	707.9 → 605.9 (Q)	84.0	38.2	17.2
	707.9 → 651.9 (q)		26.7	19.0
^{13}C6-T3-C4H9	713.9 → 485.1 (q)		53.5	12.3
	713.9 → 611.9 (Q)	84.0	38.2	17.2
	713.9 → 657.9 (q)		26.7	19.0
T4-C4H9	833.9 → 605.0 (q)		60.7	15.5
	833.9 → 731.9 (Q)	82.0	43.4	19.5
	833.9 → 777.9 (q)		29.5	22.6
^{13}C6-T4-C4H9	839.9 → 611.0 (q)		60.7	15.5
	839.9 → 737.9 (Q)	82.0	43.4	19.5
	839.9 → 783.8 (q)		29.5	22.6

Table 6. MS parameters for derivatized MIT, DIT, T3 and T4.

The validation of the analytical method encompassed a comprehensive assessment across various parameters to ensure its robustness and reliability[261,262].

Selectivity, a fundamental criterion, was scrutinized to ascertain the method's capacity to discriminate molecules of interest and their respective ISs from other sample components and potential interferents. This involved multiple injections of analytes into the system, monitoring their retention times meticulously.

The linearity of our method was evaluated within the calibration curve range established in the preceding paragraph. Instrumental sensitivity was gauged through the determination of limits of detection (LOD) and limit of quantification (LOQ) for the analytes. Using the specialized tool in Sciex Analyst® software, concentrations yielding a Signal-to-Noise (S/N) ratio close to 3 and 10 were designated as LOD and LOQ, respectively.

Accuracy (%), a pivotal parameter, was calculated by comparing the measured concentration with the nominal concentration spiked into plasma and urine samples. This involved three different concentration levels of analytes (2.5 ng/mL, 10 ng/mL, and 50 ng/mL) subtracted from the endogenous concentration. Intra-day and inter-day precision, expressed as relative Standard Deviation (RSD %), were evaluated. Intra-day precision involved injecting 5 replicates of the aforementioned concentration levels within the same run, while inter-day precision was assessed by injecting the same 3 concentration levels over 5 consecutive days.

Recovery (%) was determined by comparing the peak areas of the IS added before and after the extraction procedure, employing the formula [(peak area of IS added before the extraction/peak area of IS added after the extraction) x 100]. The matrix effect (%) was estimated by comparing the peak area of the IS added to water (A) and matrix (B), both subjected to the extraction process. Matrix effect was then calculated using the formula [(B/A) x 100].

As an integral part of the validation process, the efficacy of our method to quantify MIT, DIT, T3 and T4 in urine and plasma from a pilot experiment involving female 5-6 months C57BL/6J *Dehal1* WT and KO mice subjected to a NID was rigorously tested. Urine and blood samples collected on day 28 were subjected to HPLC-MS/MS analysis to ensure the method's applicability and accuracy under real experimental conditions.

7.3.2 Statistical analysis

Data analysis for method validation utilized Microsoft Excel (Microsoft Office, Redmond, WA), and the outcomes were expressed as mean ± standard deviation (SD). GraphPad Prism v.8® (GraphPad software, San Diego, CA) was employed for processing and statistically analysing data from both mice and human experiments, presenting results as mean ± SEM. In the pilot experiment and the natural early life model, the non-parametric Mann-Whitney's test for two independent samples was applied to assess the statistical difference between WT and KO groups. In the iodine deficiency model, statistical significance between WT and KO was determined using multiple t-tests, and corrections for multiple comparisons were made through the Holm-Sidak method.

7.4 Investigating DEHAL1 gene mutations in congenital hypothyroidism

Findings from two Sudanese families, hailing from diverse regions of the country, exhibiting congenital hypothyroidism (CH) and goiter attributed to a novel mutation in the *DEHAL1* gene will be presented in this present work. The phenotypic manifestations, as discerned through thyroid function tests and goiter examination, showcased variability, spanning from hypothyroid to euthyroid conditions, despite the presence of an identical genetic defect within the two families. All patients were directed to a pediatric endocrinologist at the University of Khartoum, Sudan, either due to the manifestation of hypothyroidism symptoms or as a consequence of a sibling already diagnosed with hypothyroidism. Prior to blood sampling, oral consent was secured from patients, their guardians, and family members, considering literacy constraints. The studies received approval from the University of Miami Institutional Review Board. The initial thyroid testing, encompassing TSH and fT4 assessments, took place in Sudan at the time of diagnosis. Subsequent follow-up visits at local clinics in Sudan led to the collection of blood samples, which were then dispatched to Miami, Florida where testing procedures were executed utilizing the Immulite™ 1000 platform (Siemens, Munich, Germany). Genomic DNA isolation from whole blood, facilitated by the Qiagen QIAamp™ DNA Blood Mini Kit (Hilden, Germany), was carried out at the University of Miami as well. Blood samples were procured from the propositus, siblings, and parents whenever feasible.

For each of the two families, genomic DNA from the proband and one parent underwent whole exome sequencing (WES) using Novogene (Sacramento, CA, USA) and the Agilent (Santa Clara, CA, USA) SureSelect Human All Exon V6 Kit. An evaluation of a compilation of thyroid genes linked to thyroid disorders was conducted, and potential mutations associated with the observed phenotype were identified based on predicted functional scores, allele frequency, and zygosity. Subsequently, genomic DNA from all available family members was subjected to analysis and confirmation through Sanger sequencing (Genewiz, Abi 3730xl DNA Analyzer) to validate the WES results and establish the genotype of all sampled family members. Identified variants underwent further scrutiny through in silico prediction scores.

The measurement of MIT and DIT in serum and urine was executed using the aforementioned pre-analytical procedure and HPLC-MS/MS method, while iodine quantification employed the Sandell–Kolthoff method. All the other aforementioned and miscellaneous tests performed on these samples were executed outside of our laboratory, so further details will not be elucidated here but are available in the dedicated section of the referenced article[263].

7.5 Further investigations on TH-related metabolism with molecular biology techniques

During my PhD, in the exploration of thyroid metabolism, I had the chance to integrate various molecular biology techniques to enhance our understanding of the intricate processes at the molecular level, thereby better corroborating and contextualizing our HPLC-MS/MS results in our studies. By employing methodologies such as polymerase chain reaction (PCR), immunofluorescence, and behavioural tests, we enabled a deeper investigation into the genetic and morphological aspects underlying thyroid function. These techniques provided crucial insights into the expression patterns of genes involved in TH synthesis and regulation. Furthermore, the application of Western blotting allowed for the quantification of specific proteins associated with thyroid metabolism. Integrating these molecular biology techniques with the HPLC-MS/MS analysis of diverse samples facilitated a comprehensive interpretation of the results. This synergistic approach not only broadened the scope of thyroid research but also contributed to a more nuanced comprehension of the molecular mechanisms governing TH dynamics. The techniques personally executed are well described below, while those outside my knowledge field and experience are briefly introduced for the sake of the comprehension of the results' interpretation but can be further explored in the referenced articles[260,263–265].

7.5.1 Immunofluorescence analysis for hippocampal neurogenesis

To assess neurogenesis in the SGZ of the dentate gyrus, immunofluorescence for specific markers was performed: Ki67 for cell proliferation and doublecortin (DCX) for new-born Type 2b and Type 3 neuroblasts. Animals (n=4 for each group) were anesthetized and transcardially perfused with a 4% paraformaldehyde solution. Brains were removed, cryoconserved using 30% sucrose and stored at -80 °C. Coronal sections, 10 μm each, were cut using a cryostat (Leica CM3050 S, Leica Biosystems) at 180 μm intervals across the hippocampus, between -1.28 mm and - 2.92 mm from bregma.

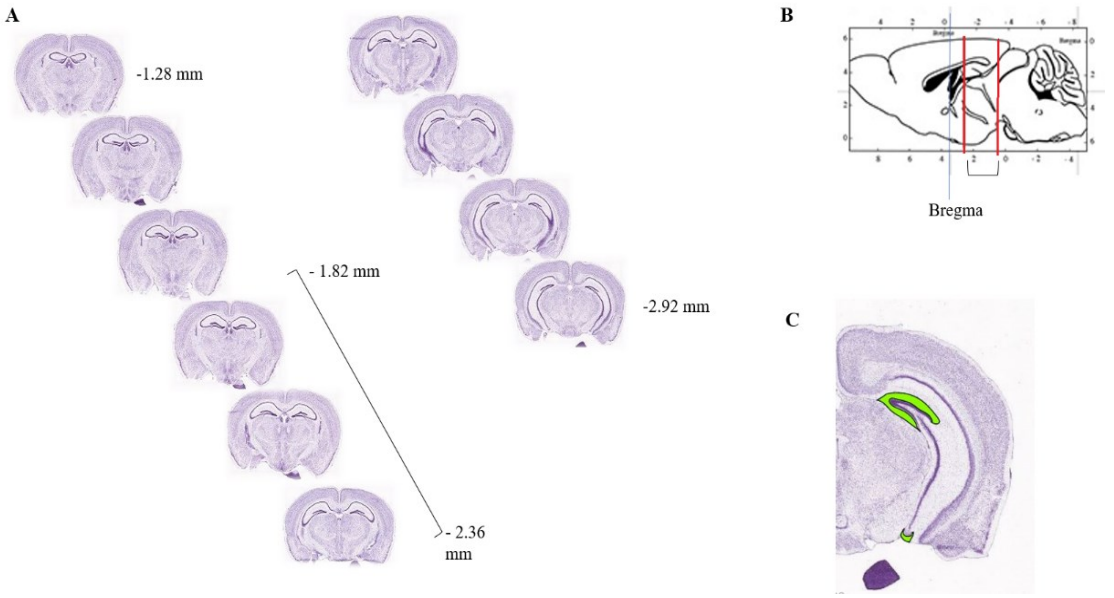

Figure 27. (A) Hippocampal coronal sections (Allen Brain Atlas). (B) Sagittal view of the hippocampus showing Bregma (0 coordinate) and the regions of cut (Paxinos, George, and Keith B.J. Franklin). (C) Coronal view of the dentate gyrus, bright green = dorsal part of the Dentate Gyrus (adapted from Allen Brain Atlas).

Then, hippocampal slices from 4 successive sections (between -1.82 mm and -2.36 mm) were mounted onto polarized slides and processed. Antigen retrieval was obtained through three 1-min immersions in sodium citrate pH 6.0 at 85 °C. Slides were hydrated using a Phosphate Buffer Saline (PBS, Sigma Aldrich-Merck, St. Louis, MO, USA) for 20 min at RT and washed twice using 0.3% Triton™ X-100 (Sigma Aldrich-Merck, St. Louis, MO, USA) in PBS. Following a one-hour blocking step using 5% BSA and 0,5% Triton™ X-100 solution in PBS, at RT, and two more washing steps, hippocampal slices were incubated with anti-Ki67 (Rat monoclonal, Invitrogen, USA, #14569880) (1:500) and anti-DCX (Rabbit, Abcam, UK, #Ab18723) (1:800) primary antibodies (dissolved in 0.1% BSA, 0.1% Triton™ X-100 in PBS solution) at 4 °C overnight.

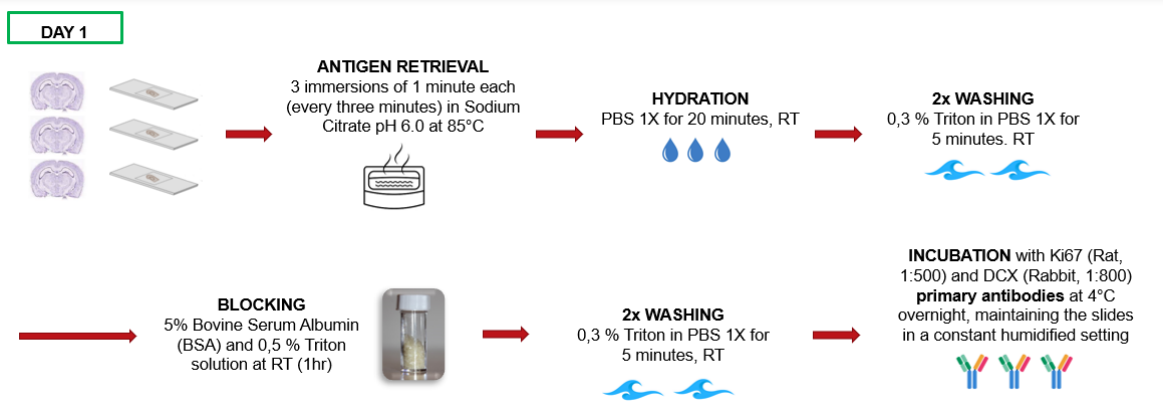

Figure 28. Graphical representation of the immunofluorescence staining procedure (day1) for the analysis of neurogenetic markers in SGZ (created on Biorender.com).

After washing, slides were incubated for 2 h at RT, in the dark, with the corresponding Goat anti-rat Alexa 488-conjugated (1:1000, Invitrogen, USA, #A11006) and Donkey anti-rabbit Alexa 647-conjugated (1:1000, Abcam, UK, #Ab150075) secondary antibodies (dissolved in 1% BSA and 0.1% Triton™ X-100 in PBS). Two last washing steps were performed before mounting the slices with a Fluoroshield™ mounting medium containing DAPI (Abcam, UK, #Ab104139) for staining nuclei. Images were captured using a Leica TCS SP8 Laser Scanning Confocal Microscope (Leica Microsystems, Mannheim, Germany) and analysis was performed using Fiji software v. 2.9.0. The number of DCX+ cells obtained from 4 coronal sections (-1.82 mm to -2.36 mm from bregma) have been added to obtain a single estimate per mouse.

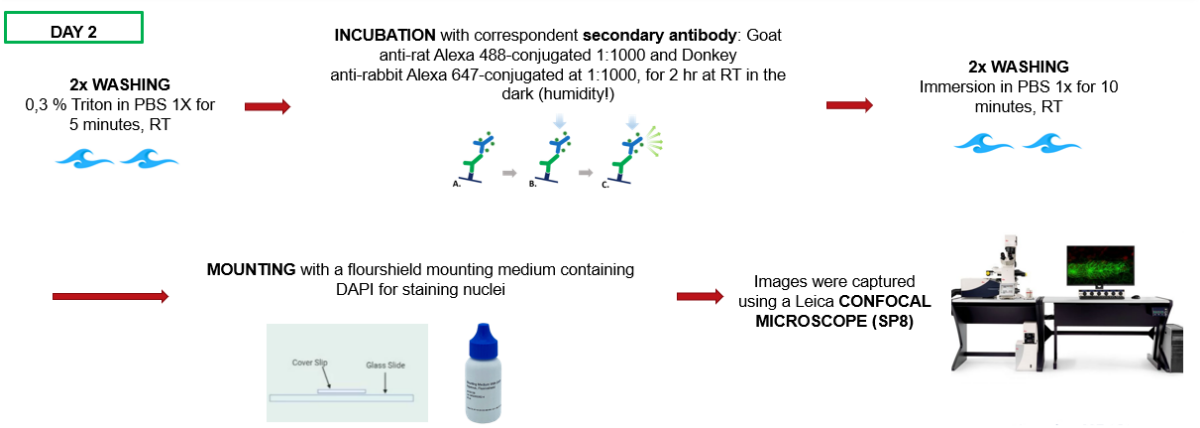

Figure 29. Graphical representation of the immunofluorescence staining procedure (day2) for the analysis of neurogenetic markers in SGZ (created on Biorender.com).

7.5.2 Gene expression analysis of neurogenetic markers

Hippocampi were dissected (n=4 for euthyroid and L-T_4 group, n=5 for hypothyroid group, n=6 for T_1AM group and n=7 for L-T_4 + T_1AM group) and homogenized in 1 mL TRIzol™ Reagent (ThermoFisher Scientific, USA) using a rotor-stator homogenizer (TissueRuptor II, QIAGEN, Germany). RNA was isolated according to the manufacturer's instructions. RNA yield was determined with the Qubit™ RNA BR (Broad-Range) Assay Kit in the Qubit Fluorometer (ThermoFisher Scientific, USA). RNA samples (ng) were used for DNase digestion and retrotranscription, using the iScript Clear cDNA Synthesis kit (Bio-Rad, USA). qPCR analysis was performed using PrimePCR™ "Neurogenesis Tier 1 M96" collection panel (Bio-Rad, USA), a predesigned 96-well PCR plate containing primer sets for 88 gene targets involved in neurogenesis pathway for use with SYBR® Green on a CFX Connect Real Time System (Bio-Rad, USA).

	1	2	3	4	5	6	7	8	9	10	11	12
A	*Akt1*	*Bmp2*	*Ctnnb1*	*Epo*	*Gdnf*	*Igf1r*	*Mapk8*	*Nfkb1*	*Ntrk2*	*Rein*	*Sox2*	*Tbp*
B	*Akt2*	*Bmp4*	*Cxcl12*	*Esr1*	*Gfap*	*Jak2*	*Mapt*	*Ngf*	*Ntrk3*	*Rest*	*Src*	*Gapdh*
C	*Akt3*	*Casp3*	*Cxcr4*	*Esr2*	*Gsk3b*	*Kdr*	*Met*	*Ngfr*	*Pax6*	*Ret*	*Stat3*	*Hprt*
D	*Apoe*	*Cd44*	*Dcx*	*Fgf2*	*Hes1*	*Kit*	*Ncam1*	*Notch1*	*Pdgfra*	*Rhoa*	*Tgfb1*	gDNA
E	*App*	*Cdk5*	*Dll1*	*Fgfr1*	*Hif1a*	*L1cam*	*Nes*	*Nr3c1*	*Prom1*	*S100b*	*Th*	PCR
F	*Ascl1*	*Cnr1*	*Egf*	*Fgfr2*	*Hras1*	*Lep*	*Neurod1*	*Nrg1*	*Psen1*	*Shh*	*Trp53*	RQ1
G	*Bcl2*	*Cntf*	*Egfr*	*Foxg1*	*Ifng*	*Mapk1*	*Neurog1*	*Ntf3*	*Pten*	*Smad4*	*Vegfa*	RQ2
H	*Bdnf*	*Creb1*	*Ephb2*	*Gap43*	*Igf1*	*Mapk3*	*Neurog2*	*Ntrk1*	*Rb1*	*Sod1*	*Wnt1*	RT

Figure 30. Predesigned 96-well PrimePCR™ "Neurogenesis Tier 1 M96" collection panel (Bio-Rad, USA) containing primer sets for 88 gene targets involved in neurogenesis pathway (created on Microsoft Word 365).

Ct values > 35 were considered as no expression. Fold change calculation by ΔΔCt method[266] was performed with the CFX Maestro™ Software (Bio-Rad, USA), using all the three reference genes of the panel for normalization: TATA-binding protein (*Tbp*), glyceraldehyde-3-phosphate dehydrogenase (*Gadph*) and Hypoxanthine-guanine phosphoribosyltransferase (*Hprt1*). The normalized expression for each target gene was scaled by dividing the expression level of each sample by the geometric mean level of expression of all the samples. The expression of each sample per experimental group was averaged together to determine the weighted average of each group.

7.5.3 Behavioural tests for hypothyroidism effects investigation

Performances at memory, locomotion, anxiety-, and depression-related tasks in response to different replacement strategies were monitored using the following behavioural tests: Elevated Plus Maze (EPM, for primary and secondary anxiety), Open Field Test (OF, locomotor activity and associated anxiety), ORT (hippocampus-dependent memory), Tail Suspension Test (TST, depression). Before testing, mice were daily habituated to experimental handling for 10 min. Over the last 3 consecutive days before the experiment, mice were individually habituated for one hour to the testing room. Behavioural tests were performed at the end of the replacement treatment with ALZET® osmotic pumps. After each session, the behavioural test area was cleaned thoroughly with ethanol 5% and left to dry completely. Mouse behaviour was monitored and recorded through a camera positioned above the apparatus.

Since the behavioural tests were not personally conducted for this project, additional details regarding the dynamics of the test apparatus for each experiment will not be discussed here. Any other relevant information can be found in the referenced article[264].

7.5.4 Electroretinography and Immunofluorescence analysis in db/db mice

The mice underwent an electroretinogram (ERG) recording protocol, encompassing an examination of the rod pathway through scotopic ERG (scERG), an assessment of the cone pathway using photopic ERG (phERG), and an evaluation of retinal ganglion cell (RGC) activity via pattern ERG (PERG). Glial activation was appraised by analysing glial fibrillary acidic protein (GFAP) immunofluorescence in Müller cells, a phenomenon known as reactive gliosis, commonly associated with certain chronic conditions like DR[267]. Comprehensive details for both techniques can be found in the referenced article[265].

7.5.5 MIO-M1 cell culture, mRNA and miRNA genetic analysis and oxidative stress tests in the diabetic retinopathy context

In vitro experiments utilized MIO-M1 cells, generously supplied by Dr. Gloria Astrid Limb from the Division of Ocular Biology and Therapeutics at the UCL Institute of Ophthalmology in London, UK. MIO-M1 represents a spontaneously immortalized human Müller cell line, preserving the morphological characteristics, marker expression, and electrophysiological responses akin to primary isolated Müller cells in a cultured environment. Both cells extracts and retinas were used for RNA/miRNA extraction and analysis, as well as for oxidative stress tests evaluating oxygen reactive species (ROS) by flow cytometry. Again, since these tests and techniques fall outside the scope of my professional expertise, they will not be discussed in detail within this chapter. However, all details can be found in the referenced article[265], while the results will be further discussed in the next chapter of this thesis.

Results

8.1 *Generation of a pharmacologically induced model of hypothyroidism*

Hypothyroidism was induced in a cohort of 65 male C57BL/6J mice aged six weeks. The alterations in BW over the experimental period are illustrated in Figure 31. Control euthyroid mice initiated the study with an average BW of 21.38 ± 0.45 g on day 0, experiencing an increase to 25.88 ± 0.46 g over the subsequent 3 weeks. In contrast, hypothyroid mice exhibited a less pronounced change in BW, transitioning from 22.48 ± 0.18 g to 23.89 ± 0.18 g. A two-way ANOVA analysis revealed a significant interaction between treatment and time on BW. Hypothyroid mice treated with L-T4 (final BW: 26.46 ± 0.42 g) and L-T4 + T1AM (final BW: 26.79 ± 0.45 g) partially regained BW, while T1AM-treated (final BW: 25.58 ± 0.45 g) and untreated hypothyroid mice (final BW: 26.0 ± 0.49 g) maintained significantly lower BW compared to euthyroid mice (final BW: 27.79 ± 0.46 g). Post-hoc tests using Tukey's method revealed that, starting from week 5 (corresponding to the second week of replacement treatment), euthyroid and T1AM-treated mice exhibited significant differences in BW and remained significantly different throughout weeks 6 and 7. Significant differences in BWs between euthyroid and hypothyroid mice appeared at week 6.

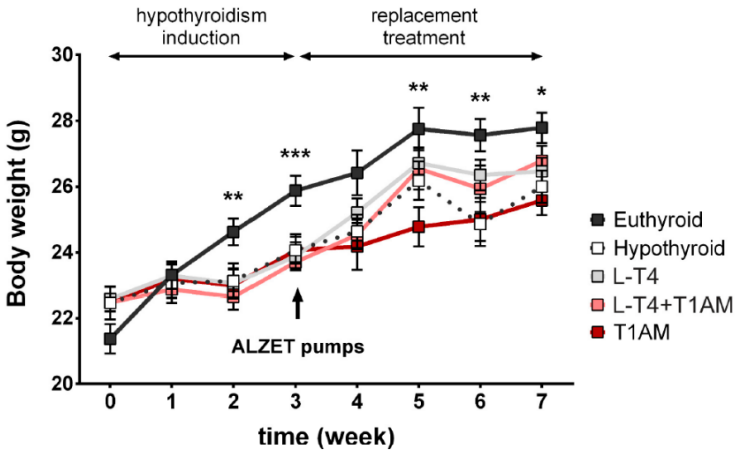

Figure 31. Body weight changes throughout the induction period of hypothyroidism. Two-way ANOVA testing the effect of treatment, time and their interaction and Tukey's post-hoc comparison were used to test differences between the groups (* $p < 0.05$, ** $p < 0.01$, *** $p < 0.001$) (adapted from Rutigliano G, *at al.* 2023[264]).

8.1.1 T3 and T4 serum quantification

Hypothyroid mice displayed significantly lower T4 levels compared to euthyroid conditions (2.53 ± 0.12 ng/mL and 32.77 ± 1.48 ng/mL, Figure 32). Treatment with L-T4 and the combination of L-T4 + T1AM significantly restored T4 serum levels to the euthyroid state (38.92 ± 10.49 ng/mL and 38.88 ± 6.13 ng/mL). However, animals treated with T1AM showed

serum T4 levels overlapping with hypothyroid mice (3.40 ± 1.01 ng/mL). No significant differences in T3 levels were observed among the treatment groups.

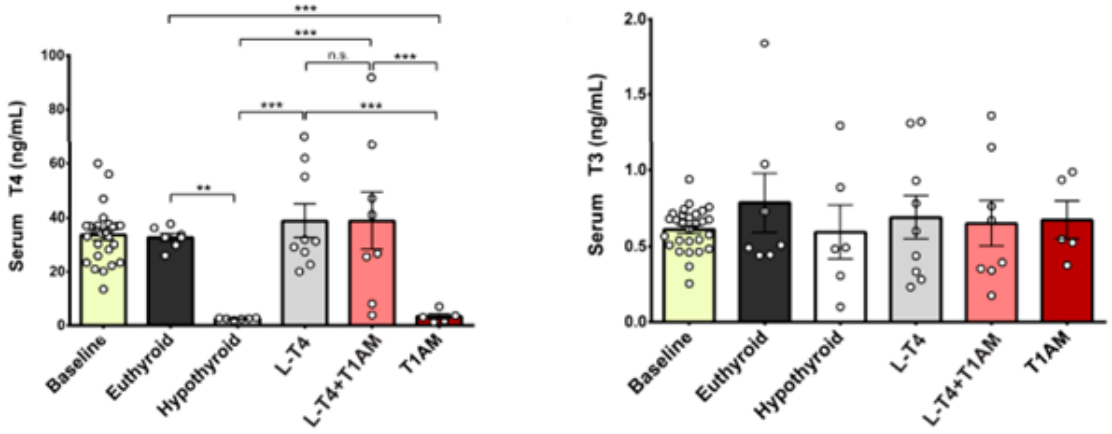

Figure 32. Serum T3 and T4 levels in the five treatment groups. ANOVA and Tukey's multiple comparison were used to test differences between the groups (** $p < 0.01$, *** $p < 0.001$, n.s. not significant) (adapted from Rutigliano G, *at al.* 2023[264]).

8.1.2 Behavioural tests results

Regarding behavioural tests, conducted by Dr. Grazia Rutigliano, unpaired t-tests (in the EPM) indicated a significantly lower number of stretch-attend postures (SAP)[268–270] in hypothyroid mice compared to euthyroid mice, indicating reduced risk-assessment behaviours in the hypothyroid condition (Figure 33).

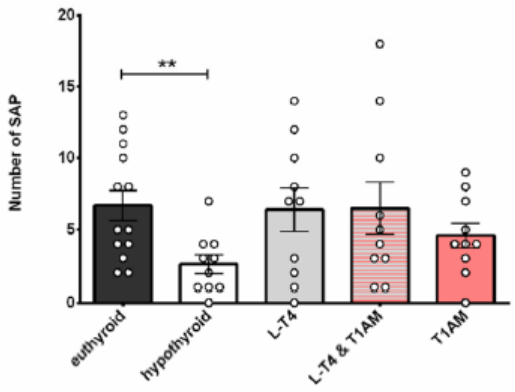

Figure 33. Risk-assessment and decision-making behaviours. ANOVA and Tukey's multiple comparison test were used to evidence eventual significant differences between the different groups (** $p < 0.01$) (adapted from Rutigliano G, *at al.* 2023[264]).

A significant reduction in the number of entries into closed arms, a measure of spontaneous locomotion, was also observed in hypothyroid relative to euthyroid mice, although this did not survive Bonferroni correction. One-way ANOVAs did not reveal significant differences in primary anxiety-related behaviours, secondary anxiety-related behaviours, or decision-making and risk-assessment measures between treatment conditions. Visual inspection of the plot suggested that the number of SAP returned to normal in mice treated with L-T4, either alone or in combination with T1AM, while intermediate average values were recorded in mice receiving T1AM only. No significant differences in spontaneous locomotor activity and thigmotaxis among the experimental groups were observed. Measures of % immobility time, indicative of depression-related behaviour, did not significantly differ across the five groups. However, hypothyroid mice exhibited impaired hippocampus-dependent memory compared to euthyroid mice, as evidenced by significantly lower discrimination indices (DIs) in the ORT (DI: hypothyroid: 0.02 ± 0.09; euthyroid: 0.29 ± 0.06) (Figure 34). One-way ANOVA showed a globally significant effect among the five experimental groups. Post-hoc tests identified a significant difference between hypothyroid mice and those treated with L-T4+T1AM (mean diff.=-0.31). Visual inspection of the DI suggested a nearly complete recovery of hippocampus-dependent memory in L-T4-treated mice relative to hypothyroid mice. The DI overlapped with the hypothyroid condition in T1AM-treated mice (DI: - 0.01 ± 0.10). One-sample t-tests comparing DIs of the five groups to a hypothetical value of 0 (no discrimination of the novel vs. familiar object) revealed significant divergence from 0 in euthyroid ($t = 4.82$, $p < 0.001$), L-T4-treated ($t = 3.53$, $p < 0.01$), and L-T4 + T1AM-treated ($t = 4.04$, $p < 0.01$) mice, confirming preserved memory in these groups.

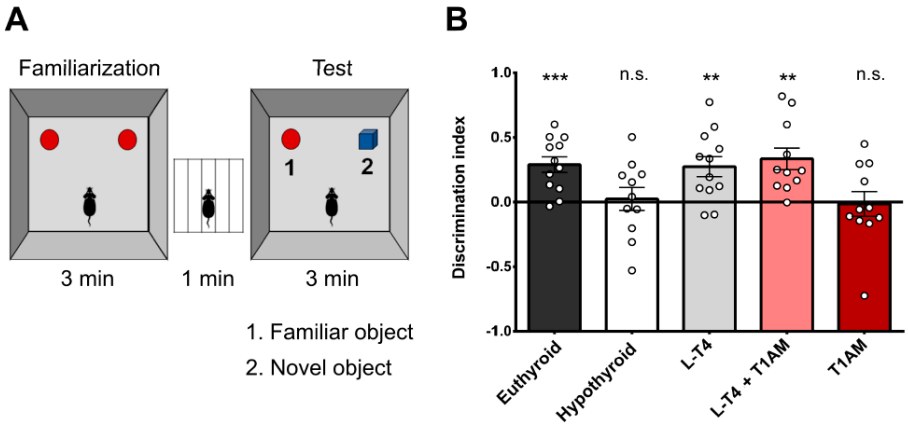

Figure 34. Effect of hypothyroidism and different replacement treatments on memory. (A) Graphical representation of the apparatus used for the novel object recognition test (ORT). (B) One sample t-test comparing Dis in the five treatment groups. A t-test comparing DIs of the five experimental groups was performed (** $p < 0.01$, *** $p < 0.001$, n.s. not significant) (adapted from Rutigliano G, *at al.* 2023[264]).

8.1.3 The impact of different replacement therapies on neurogenesis and neurogenetic pathways

In our adult-onset hypothyroidism model lasting 49 days, there was a 20% reduction in the number of DCX+ newly generated cells (mean diff=-53.50±23.81). One-way ANOVA revealed a trend toward a globally significant effect of treatment (Figure 35). Pairwise comparisons with Bonferroni correction demonstrated that L-T4 treatment increased the number of cells by 45.58% (mean diff = 106.9±21.40), while L-T4 + T1AM treatment produced a 60.44% increase (mean diff=141.6±31.91), corresponding to a 30.61% rebound relative to euthyroidism (mean diff=88.13±36.99). Replacement treatments with T1AM showed no significant effect per se (mean diff=72.13±58.84). These results confirm the crucial role of L-T4 as an endocrine signal controlling progenitor development within neurogenic niches, while T1AM exhibited no significant effects on adult hippocampal neurogenesis modulation.

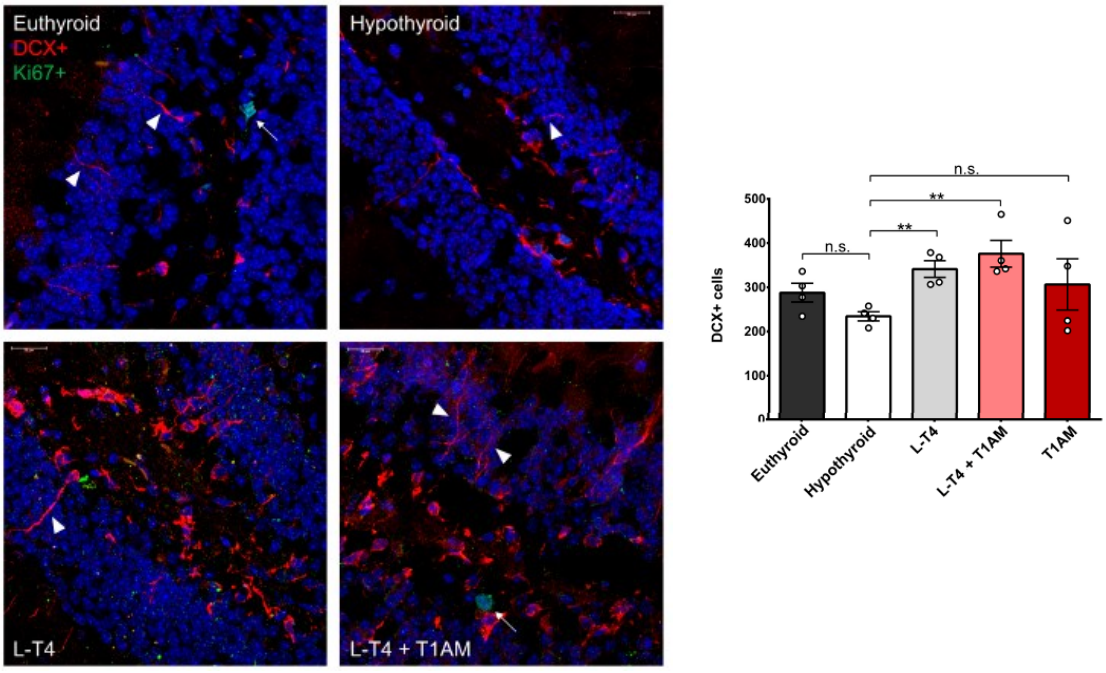

Figure 35. The effect of different replacement treatments on hippocampal neurogenesis. (left) Representative confocal microscopy images of sections illustrating immunofluorescence of DCX+ (red) and Ki67+ (green). DAPI was used to counterstain nuclei (blue). The arrows point at proliferating cells, and the arrowheads point at some neuroblast neurites. Scale bars 20 µm. DCX+ cell count (right). Each point represents the sum of DCX+ cells from four coronal sections taken across the hippocampus of a single mouse. t-test pair-wise comparisons were performed to test the differences between L-T4+T1AM and either L-T4 or T1AM (** $p < 0.01$, n.s. not significant) (adapted from Rutigliano G, *at al.* 2023[264]).

In the qPCR analysis, we observed differentially expressed genes in neurogenetic pathways (Figure 36). One-way ANOVA revealed a significant effect of treatment on the expression of *Kdr*, *L1cam* , *Mapk3* , and *Neurog2*. A trend towards an effect of treatment was observed for *Ngf*, *Kit*, and *Ntf3*. Pairwise comparisons with Bonferroni correction showed that *Mapk3* and *Neurog2* were significantly upregulated in L-T4+T1AM-treated relative to L-T4-treated mice, with non-significant differences between L-T4+T1AM and T1AM, suggesting that changes in gene expression could be induced by T1AM on its own.

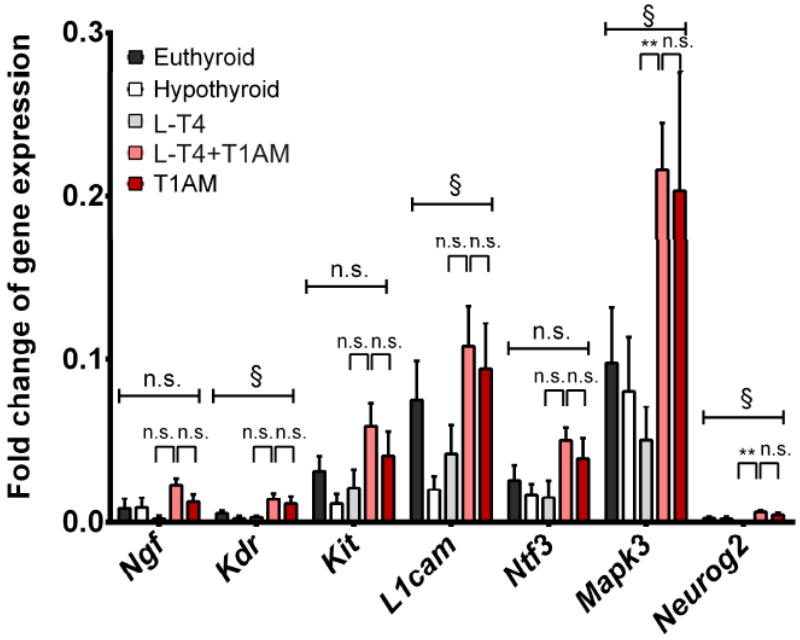

Figure 36. Analysis of expression of genes involved in neurogenetic pathways. One-way ANOVA showed significant between-treatment differences in gene expression (§ $p < 0.05$). t-test pair-wise comparisons were performed to test the differences between L-T4+T1AM and either L-T4 or T1AM (** $p < 0.01$, n.s. not significant) (adapted from Rutigliano G, *at al.* 2023[264])..

8.2 Visually impaired db/db mice does not show alteration in plasma TH

The glycaemic alteration found in *db/db* mice, displaying blood sugar concentration levels of around 500 mg/mL, did not show a correlation with fluctuations in circulating TH levels. Specifically, neither plasma T3 nor T4 levels were significantly affected in *db/db* mice (Figure 37).

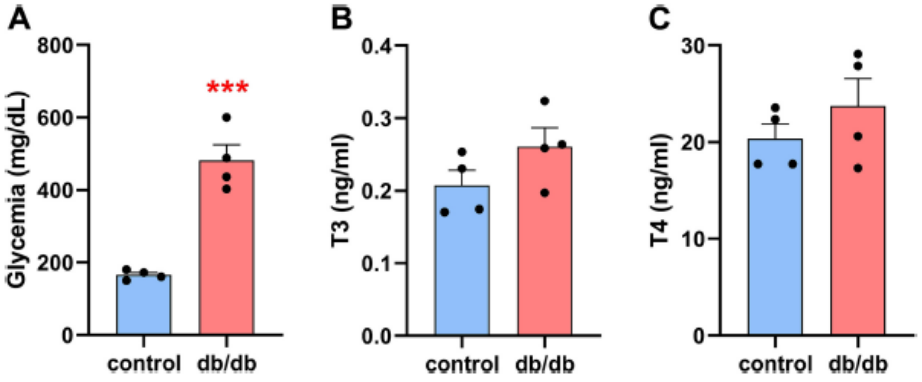

Figure 37. Blood glucose levels (A) and plasma concentrations of T3 (B) and of T4 (C) evaluated with mass spectrometry in *db/db* mice in respect control mice. ***p < 0.001 vs. control (adapted from Forini F. *et al.* 2023[265])

The electroretinographic routine, conducted by our colleagues at the National Research Council and the Department of Biology of the University of Pisa, aimed to assess retinal function, covering dark- and light-adapted activities of photoreceptors, post-receptor retina, and retinal ganglion cells (RGCs). The analysis of dark-adapted scERG showed a notable reduction in *db/db* mice compared to controls, affecting both photoreceptor-related a-wave amplitude and dark-adapted post-receptor b-wave amplitude. Beyond dark-adapted changes, *db/db* mice exhibited altered light-adapted phERG responses related to cone-mediated retinal activity, showing significant decreases in post-receptor phERG b-wave and RGC-related PhNR amplitudes compared to controls. These changes in receptor and post-receptor activities in *db/db* mice were reflected in impaired RGC activity, as assessed by PERG, with significant alterations in both n35-p50 and p50-n95 components compared to controls (data not shown, see referenced article[265]).

In addition to changes in retinal function, Forini and her team members highlighted a distinct pattern of GFAP immunofluorescence in the retinas of control and *db/db* mice. GFAP immunofluorescence in control retinas was limited to astrocytes within the ganglion cell layer, while in *db/db* mouse retinas, it labelled the processes of numerous Müller cells, which typically extended throughout the retinal thickness. (Figure 38.D-E) The levels of two major

markers of oxidative stress and inflammation, Nrf2 and NF-kB, were investigated. Nrf2 is a redox-sensitive transcription factor that, in response to increased free radicals, enters the cell nucleus, and promotes the transcription of antioxidant genes[271]. On the other hand, NF-kB is an oxidant-sensitive transcription factor that regulates the expression of genes involved in inflammatory responses[272], and the ratio of phosphorylated NF-kB (pNF-kB) to NF-kB levels can serve as an index of pro-inflammatory activity. Nrf2 protein levels were significantly elevated in *db/db* mouse retinas compared to controls, indicating high levels of oxidative stress. Simultaneously, *db/db* mouse retinas exhibited a higher pNF-kB/NF-kB ratio than control retinas, indicating increased pro-inflammatory activity (Figure 38.A-B). The increased levels of oxidative stress and inflammatory markers in *db/db* retinas were associated with characteristic features of DR, such as overproduction of *VEGF* and damage to the blood-retinal barrier (BRB). qPCR (Figure 38.C) data revealed significantly higher expression of *VEGF* mRNA and lower expression of zona occludens 1 (*ZO1*), a protein of the tight junction expressed in the BRB, in *db/db* retinas compared to control retinas.

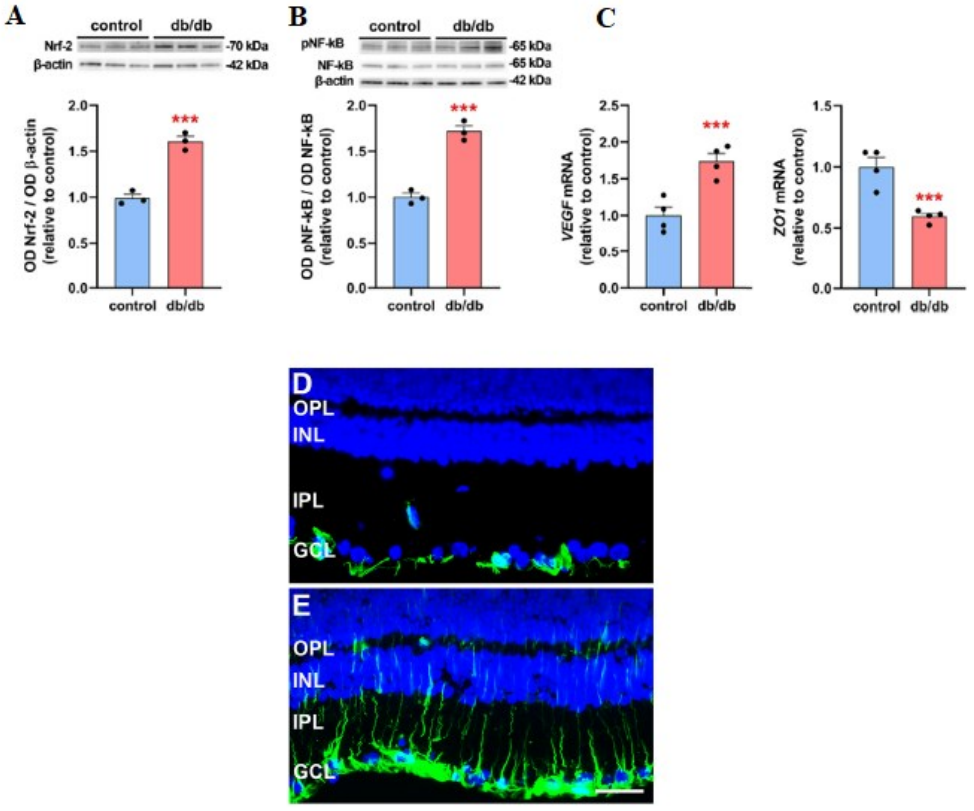

Figure 38. (A) and (B) show the immunoreactive bands and the protein levels, relative to control, of Nrf2 and of pNF-kB/NF-kB, respectively. β-Actin was used as an internal standard. (C) shows the mRNA levels, relative to control, of *VEGF* and of zona occludens 1 (*ZO1*) mRNA, respectively. (D-E) GFAP immunostaining patterns in control and *db/db* retinas, respectively (scale bar, 50 μm). GCL, ganglion cell layer; INL, inner nuclear layer; IPL, inner plexiform layer; OPL, outer plexiform layer.***$p < 0.001$ vs control (adapted from Forini F. *et al.* 2023[265]).

8.2.1 Diabetes leads to notable alterations in TH levels and markers associated with TH signalling in the retina

The concentrations of TH measured in the retina revealed significant reductions in *db/db* retinas compared to control retinas. The levels of T3 were 3.04 ± 0.39 pmol/g, whereas they were 4.43 ± 0.52 pmol/g in control retinas. Similarly, T4 levels in *db/db* retinas were 2.88 ± 0.30 pmol/g, significantly lower than the 11.45 ± 1.18 pmol/g observed in control retinas (Figure 39.A-B). These substantial alterations in T3 and T4 concentrations in *db/db* retinas were likely influenced by changes in the expression of deiodinase enzymes, specifically *DIO2* and *DIO3*. As it was predictable from the investigations of my peers, relative qPCR analysis (Figure 39.C-E) indicated a dramatic reduction in *DIO2* mRNA expression and a significant increase in *DIO3* mRNA expression in *db/db* retinas compared to controls. Consequently, the *DIO3/DIO2* mRNA ratio was also increased. At the protein level, DIO2 showed a significant decrease in *db/db* retinas, although to a lesser extent than observed at the mRNA level. Conversely, DIO3 protein levels and the DIO3/DIO2 protein ratio were significantly increased (Figure 40.F-H).

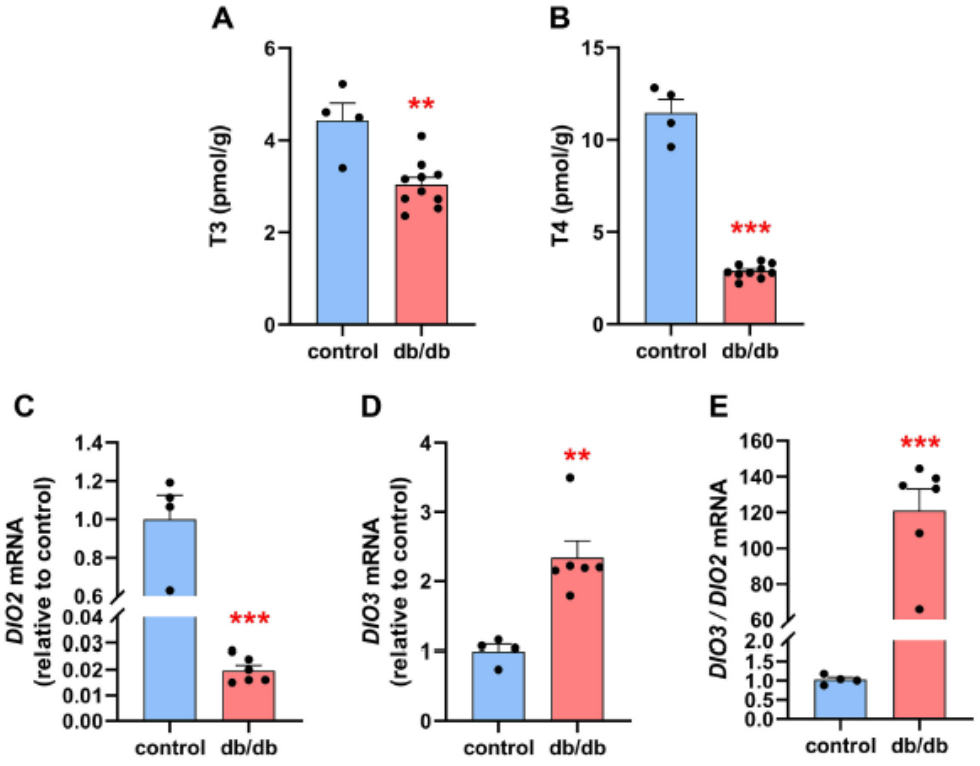

Figure 39. TH levels and deiodinase enzyme expression in retinas. **p < 0.01, ***p < 0.001 vs control (adapted from Forini F. *et al.* 2023[265]).

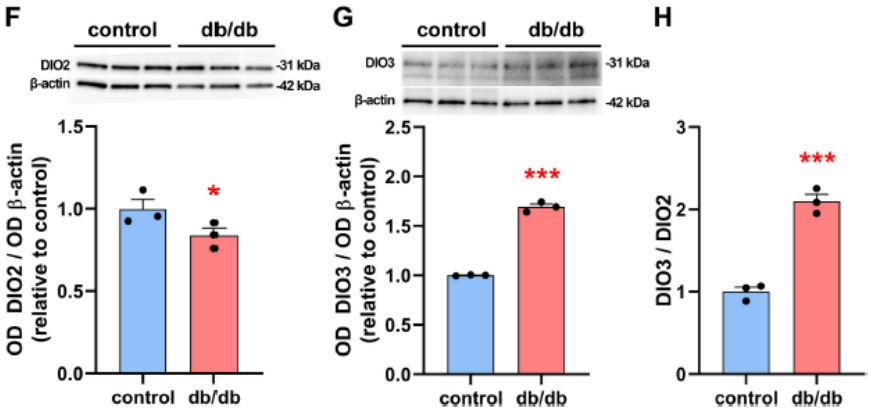

Figure 40. Western blots showing immunoreactive bands and protein levels of DIO2 and DIO3 are in (F) and (G), respectively, while the ratio DIO3/DIO2 protein is shown in (H). *p < 0.05, ***p < 0.001 vs control (adapted from Forini F. *et al.* 2023[265]).

Receptors *THRα1* and *THRβ2* exhibited significant decreases in expression in *db/db* retinas compared to control retinas, both at the mRNA and protein levels. However, the ratios of *THRα1/THRβ2* mRNA and THRα1/THRβ2 protein were not significantly different between control and *db/db* retinas (Figure 41).

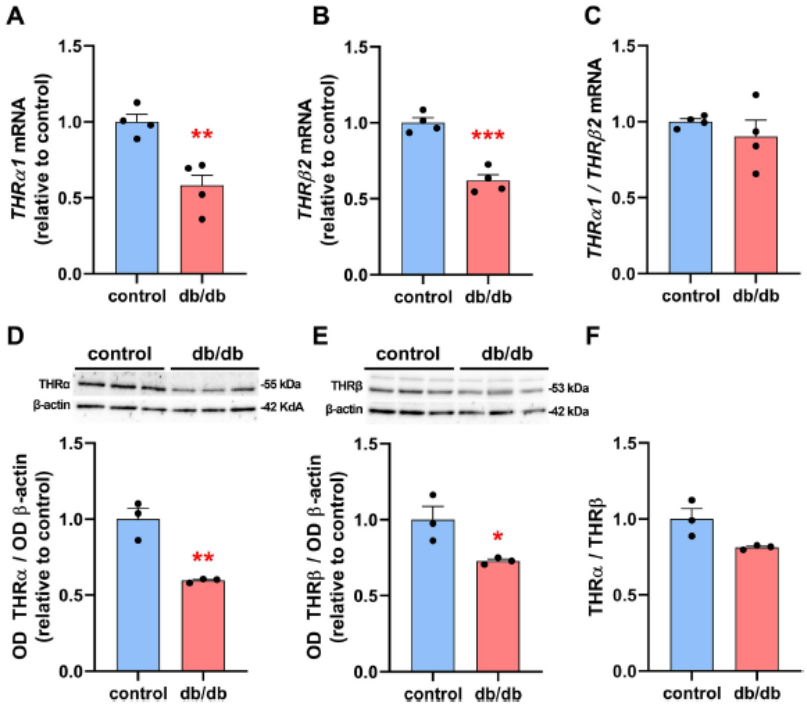

Figure 41. (A-C) *THR* expression in retinas of *db/db* mice compared wild type mice (control). (D-E) Western blots analysis of THRα and THRβ. *p < 0.05, **p < 0.01, ***p < 0.001 vs control (adapted from Forini F. *et al.* 2023[265]).

8.2.2 Genetic and functional insights of db/db mice

Our collaborators further analysed the expression of *miR-133a*, *miR-338*, and *miR-29c* in the retinas of *db/db* mice, as these microRNAs are influenced by TH and are known to respond to stress and T3 replacement[195]. All three miRNAs were noticeably decreased in *db/db* mouse retinas compared to controls. Additionally, markers related to TH activity and mitochondrial function as *PGC-1α*, a key regulator of mitochondrial biogenesis and metabolic balance, *CPT2*, an enzyme crucial for fatty acid oxidation in mitochondria, and *MFN2*, a GTPase involved in mitochondrial dynamics and quality control, along with *MFN1* and *OPA1*[273–275], showed significantly reduced transcripts in *db/db* retinas compared to controls (Figure 42).

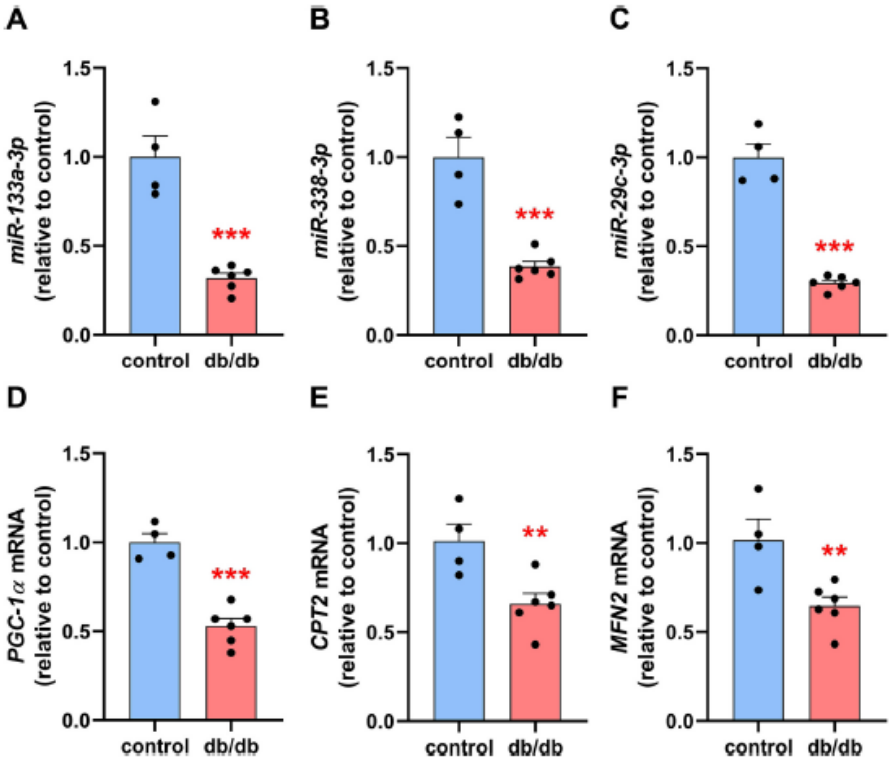

Figure 42. (A-C) Expression of miRNAs and of markers of mitochondrial function in retinas. **p < 0.01, ***p < 0.001 vs control (adapted from Forini F. *et al.* 2023[265]).

In order to examine the potential mechanisms associated with TH signalling in both the normal and diseased retina, *in vitro* experiments were conducted by our co-partners in this study using MIO-M1 cells as the experimental model. The objective was to validate our in vivo findings by confirming the impact of high glucose (HG) exposure on triggering a stress response and influencing DIO enzymes. The investigation involved assessing the levels of oxidative stress, *VEGF* expression, and DIO2 and DIO3 levels in cells exposed to HG. As anticipated, a 24-

hour HG treatment resulted in heightened production of ROS and increased *VEGF* levels in MIO-M1 cells (data not shown, see referenced article[265]). Consistent with the findings from the in vivo study, both 24 and 72 hours of HG exposure led to a significant reduction in *DIO2* expression and an elevation in *DIO3*, at both the genetic and protein levels. Previous research conducted on non-retinal tissues suggests that *DIO3* may be upregulated through a HIF-1α-dependent pathway under stressful conditions[276]. Furthermore, experimental evidence indicates that oxidative stress may activate HIF-1α via Nrf2, potentially involving the expression of heme oxygenase-1 (HO-1)[170]. To investigate this signalling cascade in MIO-M1 cells, an examination was carried out to determine whether inhibiting HIF-1α or Nrf2 could prevent the upregulation of *DIO3* induced by HG exposure for 24 hours. The results demonstrate that co-treatment with either the HIF-1 inhibitor ACF or the Nrf2 inhibitor K67 effectively prevented the HG-induced increase in *DIO3* expression (Figure 43).

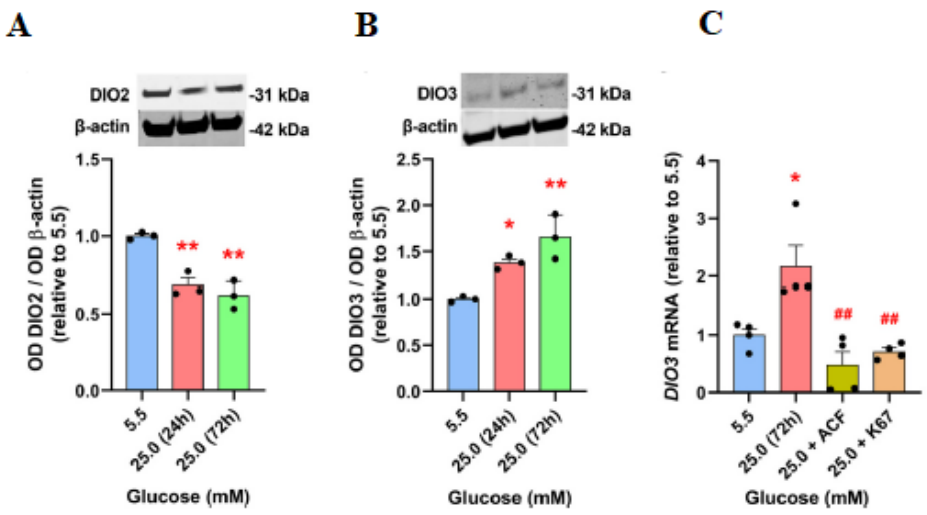

Figure 43. (A-B) Immunoreactive bands and protein levels of DIO2 and DIO3 evaluated with Western blotting in MIO-M1 cells incubated in normal (5.5 mM) or high (25.0 mM) glucose for 24 or for 72 h. (C) *DIO3* mRNA expression in MIO-M1 cells incubated for 24 h in normal (5.5 mM) or high (25.0 mM) glucose with or without 5 μM ACF, a HIF inhibitor, or 5 μM K67, a Nrf2 inhibitor. *p < 0.05, **p < 0.01 vs 5.5 mM glucose; ##p < 0.01 vs 25.0 mM glucose (adapted from Forini F. *et al.* 2023[265]).

Eventually, to explore the relationship between T3-dependent miRNAs (*miR-133a, miR-338, miR-29c*) and *DIO3* expression in *db/db* mice, additional *in silico* and *in vitro* experiments were conducted outside our laboratory. The *in-silico* analysis predicted *miR-338* as a potential inhibitor of DIO3 mRNA, and *miR-133a* was previously confirmed to regulate DIO3 expression through a *3'UTR*-dependent mechanism[277]. In MIO-M1 cells, *miR-133a* mimic

decreased *DIO3* expression, while *miR-338* had no effect in luciferase reporter assays. Furthermore, *miR-133a* mimic reduced *DIO3* transcript levels, and its inhibition increased them, showing a role in T3-induced *DIO3* downregulation. T3 treatment also decreased *DIO3* mRNA, partially prevented by co-administration with *miR-133a* decoy. In an experiment mimicking early diabetic retinopathy, stress markers (*Nrf2* and *VEGF*) increased in HG + T3, normalized in HG-T3, and rose again in HG-T3 + T3. Mitochondrial markers (*PGC-1α* and *CPT2*) followed a similar pattern. The experimental groups included a control, hyperglycaemia with T3 (HG + T3), early LT3S (HG-T3), and T3 replacement (HG-T3 + T3). This scenario replicates early diabetic retinopathy and MIO-M1 responses to T3 correction. More images and graphical data regarding the latter aforementioned experiments can be retrieved in the referenced article[265] and, since the fall out of the personal knowledge, will be not further discussed here.

8.3 Characterization of Dehal1 KO mice

The *Dehal1* KO mouse, generated using gene-trap technology, produces a recombinant protein (trDehal1-βG) consisting of a truncated DEHAL1 protein and the β-galactosidase enzyme under the control of the endogenous *DEHAL1* promoter. Both heterozygous and homozygous *Dehal1* KO mice were successfully bred. Homozygous mice lacked wild-type *Dehal1* RNA and protein in their thyroids. The endogenous promoter driving trDehal1-β-Gal expression was examined in the developing thyroid, kidney, and liver, with X-Gal labelling revealing activity in these tissues[278,279]. Immunoreactivity for β-Gal was observed in thyrocytes, kidney tubules, liver hepatocytes, and choroid plexus cells in adult *Dehal1* KO mice. *Dehal1* RNA exhibited the highest expression in the thyroid, suggesting potential additional functions. In response to iodine deficiency, *Dehal1* mRNA levels increased 2- and 3.5-fold in the thyroid under mild and severe iodine-restricted diets, respectively, while no significant changes were observed in the kidneys or liver. These findings emphasize the primary role of DEHAL1 in maintaining iodine homeostasis in the thyroid. Further detailed information is available at the referenced article[260].

8.3.1 HPLC-MS/MS method validation and application

HPLC-MS/MS techniques are commonly utilized for the analysis of TH in diverse sample matrices. However, these methods often fall short in allowing the simultaneous quantification of TH and their precursors, MIT, and DIT. The scrutiny of iodotyrosines, especially in urine and plasma, has been the subject of extensive discourse. In 2008, Afink *et al.* introduced a distinctive HPLC-MS/MS method capable of exclusively detecting MIT and DIT in urine[216,280]. In our proposed methodology, samples undergo derivatization using a butanolic HCl solution, leading to the formation of corresponding butyl esters. This widely employed derivatization technique in TH analysis contributes to an augmented S/N ratio by enhancing in-source ionization efficiency and fostering interaction with the C18 reverse-phase column[44,242]. An inherent limitation of Afink et al.'s method is its reliance on 3-chloro-L-tyrosine as IS for quantifying MIT and DIT, given the unavailability of stable isotope-labelled IS for these compounds. In our approach, we overcame this limitation by utilizing stable isotope-labelled MIT and DIT molecules ($^{13}C_9$-MIT and $^{13}C_9$-DIT) graciously provided by Prof. Alireza Mani. The inclusion of a suitable IS for each compound, co-eluting with the analytes, proves beneficial for signal normalization and effectively mitigating matrix effects. In the analysis of urine, our exclusive focus was on MIT and DIT due to the comparatively low or nearly absent levels of T3 and T4 in this biofluid.

Representative traces and specific retention times of T3, T4, MIT and DIT from standard solutions were achieved and are illustrated in Figure 44. Each compound exhibited three traces, each corresponding to a specific multiple reaction monitoring transition (MRM) in Table 6 in the Materials and Methods section: the one possessing the higher signal to noise ratio was used for quantification (quantifier, Q, as shown in Figure 44) of the analyte, while the others, which are representative of the specific analyte structure, confirmed its identity (qualifier, q). Retention time further confirmed the peak correspondence.

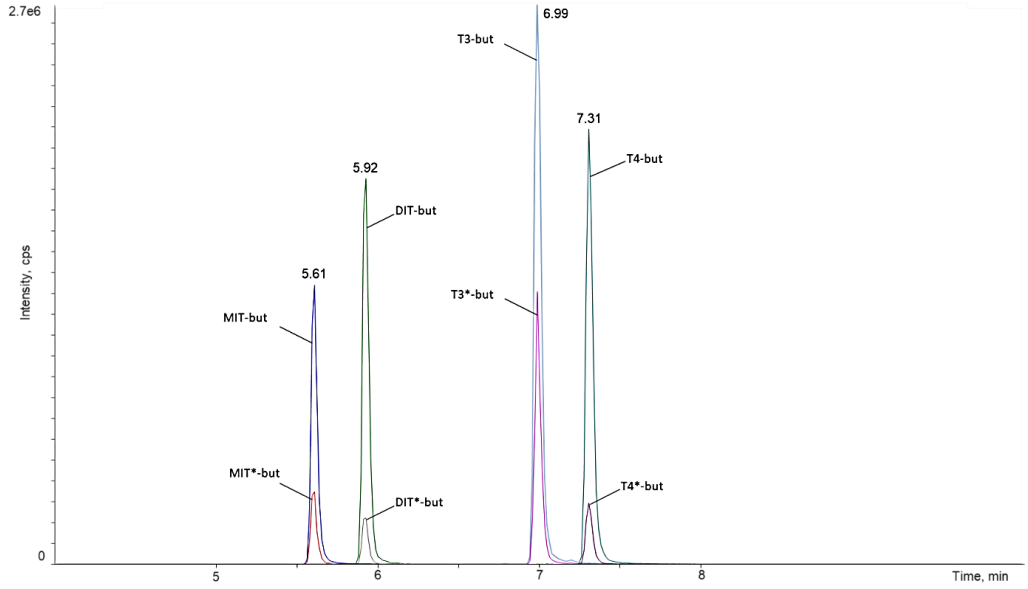

Figure 44. Representative chromatogram of derivatized MIT, DIT, T3 and T4. For each analyte the illustrated trace is the one considered for quantification as it possesses the highest S/N ratio (extracted and obtained from Sciex Analyst software v. 1.7.3).

These features demonstrated excellent specificity and sensitivity (LOD and LOQ values) of the HPLC-MS/MS method for the quantification of TH and their precursors.

	LOD		LOQ	
Analyte	ng/mL	nM	ng/mL	nM
MIT-C_4H_9	0.05	0.14	0.10	0.28
DIT-C_4H_9	0.02	0.04	0.10	0.20
T_3-C_4H_9	0.01	0.01	0.02	0.03
T_4-C_4H_9	0.01	0.02	0.05	0.06

Table 7. LOQ and LOD of the analytical method.

Linearity resulted > 0.998 for each analyte. Recovery, matrix effect, and methodological inter-day and intra-day accuracy was in the optimal range of 85–115%, which is following the European Medicines Agency guidelines[262] (Table 8). Precision for all the injected concentration levels demonstrated values in the range of 3.68-11.30 % and 2.85-10.36 %, respectively. Re-analysis of samples after storage showed no degradation of analytes or their relative internal standards, thus confirming the stability of our protocol.

	Plasma		Urine	
Analyte	Recovery (%)	Matrix effect (%)	Recovery (%)	Matrix effect (%)
$^{13}C_9$-MIT-C_4H_9	84.4	78.9	84.6	105.0
$^{13}C_9$-DIT-C_4H_9	94.1	112.2	87.2	107.3
$^{13}C_6$-T3-C_4H_9	76.2	99.6		
$^{13}C_6$-T4-C_4H_9	63.8	81.0		

	Plasma			Urine		
Analyte	Spiked (ng/mL)	Assayed (ng/mL)	Accuracy (%)	Spiked (ng/mL)	Assayed (ng/mL)	Accuracy (%)
MIT-C_4H_9	2.50	2.77	110.8	2.50	2.18	87.3
	10.00	10.18	101.8	10.00	10.83	108.3
	50.00	49.16	98.3	50.00	53.93	107.8
DIT-C_4H_9	2.50	2.30	92.2	2.50	2.65	106.1
	10.00	9.81	98.1	10.00	11.19	111.9
	50.00	48.56	97.1	50.00	62.50	124.9
T3-C_4H_9	2.50	2.28	91.2			
	10.00	9.78	97.8			
	50.00	52.28	104.6			
T4-C_4H_9	2.50	2.60	104.0			
	10.00	10.35	103.5			
	50.00	46.50	93.0			

Table 8. Recovery, matrix effect and accuracies of the analytical method. For accuracies, The assayed concentration was obtained by subtracting the endogenous concentration to the spiked concentration.

Before analyzing the whole set of samples, the method has been tested and used for the quantification of MIT, DIT and TH in plasma and urines from a pilot experiment. The findings presented in Figure 45 are indicative of impaired DEHAL1 activity, as evidenced by a general elevation in MIT and DIT levels in the plasma and urine of KO mice compared to WT. In KO samples, the inability of DEHAL1 to remove iodine from MIT and DIT led to an accumulation of these molecules in plasma, coupled with an increased excretion of both through urine. Conversely, under normal dietary iodine conditions, the thyroid maintained the synthesis of TH, resulting in no statistically significant differences in their levels between WT and KO mice (data not shown).

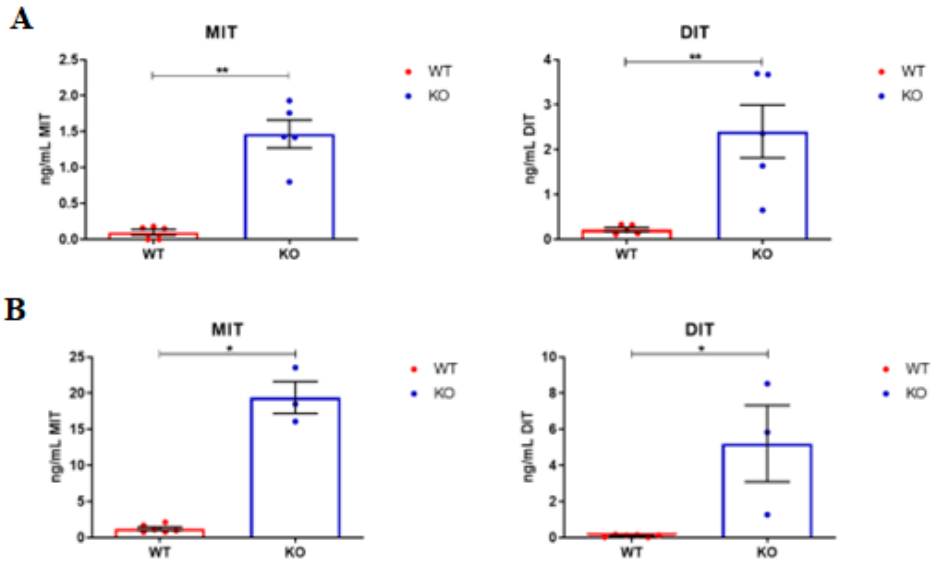

Figure 45. MIT, DIT levels in mice plasma (A) and urine (B) samples from the pilot experiment (WT n=5, KO n=3) (created using Graph Pad Prism v.8).

The method yielded favourable outcomes in terms of robustness, accuracy, and selectivity, proving to be successful and usable in our research projects.

8.3.2 Dehal1 KO mice experience an adverse iodine balance caused by the urinary loss of iodotyrosines

In adult *Dehal1* KO mice fed an iodine-sufficient diet (NID), normal plasma concentrations of TSH, T4, and T3 were observed (Figure 46). A striking finding emerged as they exhibited a ten-fold increase in plasma levels of MIT and DIT compared to their WT counterparts. The elevation in urinary MIT and DIT was even more pronounced, reaching a thirty-fold increase

in KO mice compared to WT (Figure 46). This significant disparity in both plasma and urine iodotyrosines levels highlights their potential as highly discriminatory indicators to unveil DEHAL1 defects in rodents. Additionally, *Dehal1* KO mice demonstrated nearly double the amount of iodine excretion in urine, as determined by the Sandell-Kolthoff (S-K) method, compared to WT mice (Figure 46).

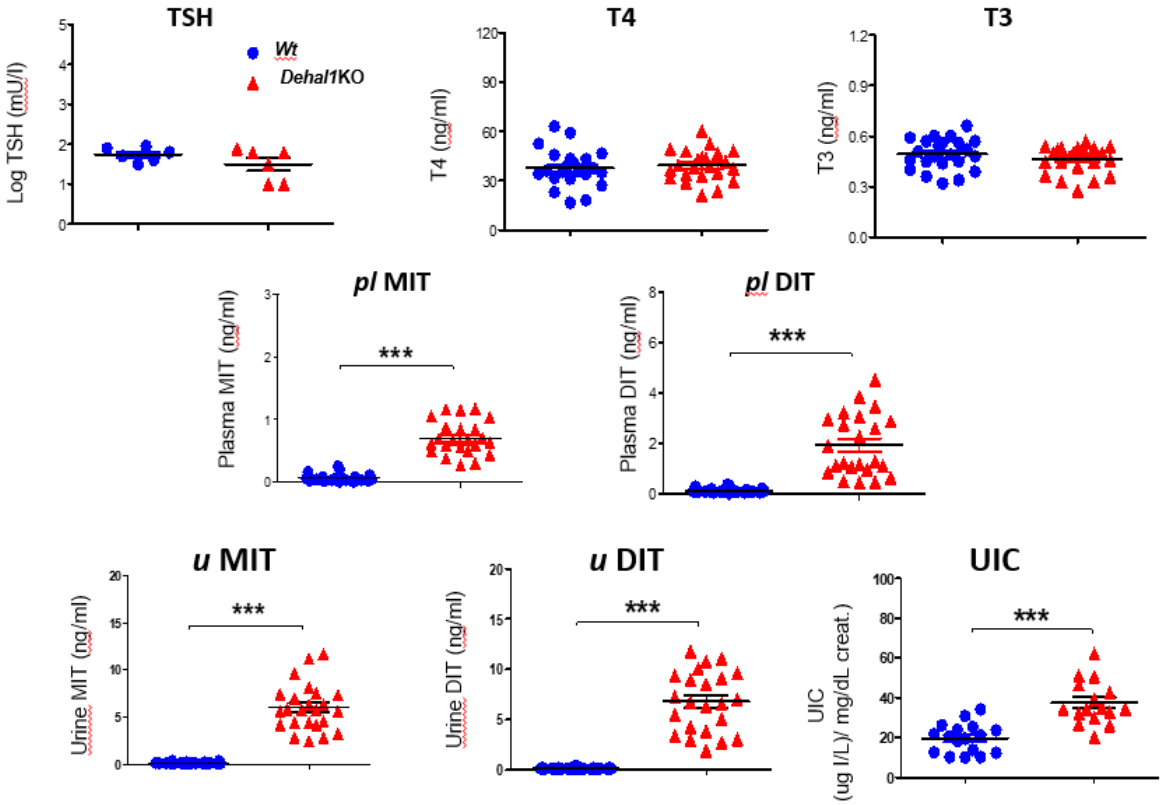

Figure 46. Plasma (pl) TSH, T3, T4, MIT and DIT and urinary (u) concentrations of MIT, DIT, and iodine (UIC) in WT vs KO were determined using radioimmunoassay, HPLC-MS/MS and Sandell-Kolthoff reaction, respectively. Results are in mean±SEM (* p<0,05;** p<0,01; *** p<0,005) (adapted from González-Guerrero G, *et al.* 2023[260]).

Despite both genotypes being provided the same iodine intake, this result suggests that *Dehal1* KO mice experience a negative iodine balance due to chronic urinary loss of MIT and DIT, and consequently implies how the S-K method, traditionally assumed to measure only inorganic (dietary) iodine content in urine, appears to capture the organic iodide present in iodotyrosines. (for further information see the Supplementary materials of the referenced article[260]). Under conditions of sufficient iodine supply, *Dehal1* KO mice can maintain euthyroidism despite having a negative iodine balance. This susceptibility makes them particularly vulnerable to iodine shortages. Furthermore, this discovery underscores that elevated levels of plasma or

urinary iodotyrosines serve as reliable markers of iodotyrosines deiodinase deficiency, even in the presence of iodine sufficiency.

8.3.3 Iodotyrosines exhibit elevated levels from an early age in Dehal1 KO mice

To investigate the concentrations of iodotyrosines in early postnatal life, the levels of MIT and in the plasma and urine of *Dehal1* KO mice at various developmental stages were meticulously investigated (Figure 47). The results revealed that, despite both *Dehal1* KO and WT mice exhibiting comparable levels of plasma TSH, T3 and T4 during the neonatal, juvenile, and young adult stages (data not shown, see referenced article[260]), only the *Dehal1* KO mice demonstrated a substantial increase in plasma MIT and DIT. This augmentation in iodotyrosines levels was particularly prominent in the neonatal stage, with *Dehal1* KO pups exhibiting a more than 10-fold increase compared to their WT counterparts. Furthermore, urine samples from juvenile and young adult *Dehal1* KO mice displayed a five-fold increase in iodotyrosines levels compared to WT mice. Of note, the UIC only demonstrated elevation in *Dehal1* KO mice upon reaching the adult stage. This phenomenon could be attributed to the functional immaturity of the kidneys in juvenile and neonatal mice, providing iodotyrosines with a unique advantage in identifying postnatal diseases in a timely manner. These findings suggest that, even under normal iodine intake, the detection of significantly increased iodotyrosines in plasma and urine samples from 10-day-old *Dehal1* KO pups, corresponding to the time of birth in humans, could potentially facilitate early diagnosis of the disorder.

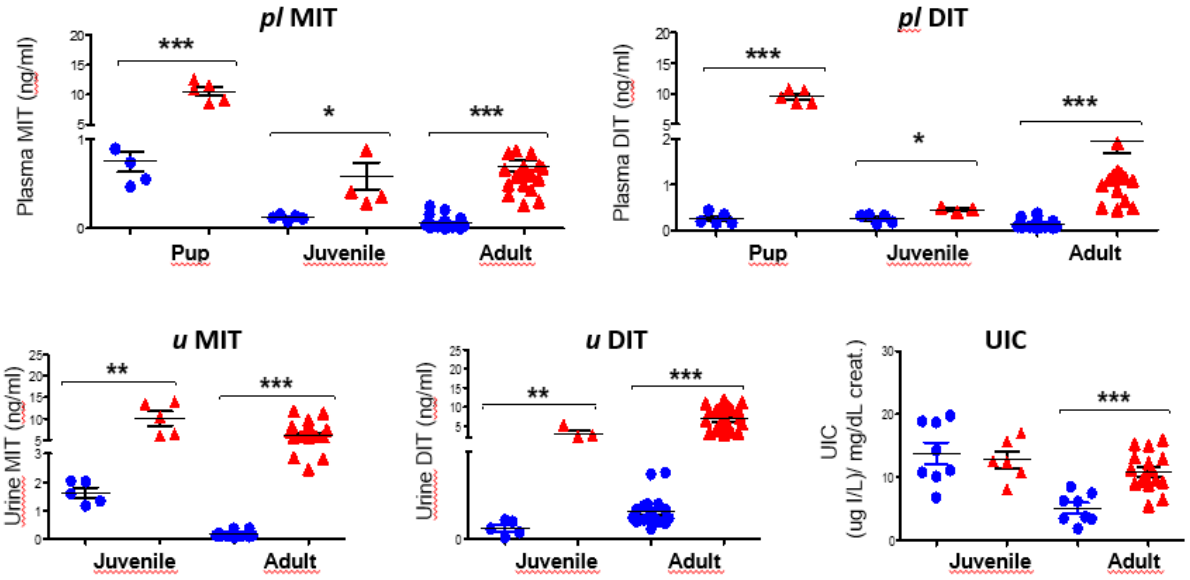

Figure 47. Plasma (pl) MIT and DIT and urinary (u) concentrations of MIT, DIT, and iodine (UIC), at various developmental stages, were determined using HPLC-MS/MS and S-K reaction, respectively. Results are in mean±SEM (* p<0,05;** p<0,01; *** p<0,005) (adapted from González-Guerrero G, *et al.* 2023[260]).

8.3.4 Insufficient iodine promptly induces hypothyroidism in Dehal1KO mice

The influence of DEHAL1 on thyroid function in conditions of regulated iodine availability was examined conducting a study involving adult WT and *Dehal1* KO mice exposed to normal (NID), low (LID), and very low iodine (VLID) diets over a 28-day duration (Figure 48-50). The daily iodine intake of mice was 5.6 g, 1 g, and 0.25 g for NID, LID, and VLID, respectively. Throughout the investigation, multiple parameters were evaluated, including plasma levels TSH, T3 and T4 along with plasma and urinary iodotyrosines, and urinary UIC at various time points (day 0, day 1, day 28). The results revealed that under normal and low iodine diets, both WT and KO mice displayed comparable levels of TSH, T4, and T3. However, *Dehal1* KO mice exposed to the very low iodine diet exhibited a notable increase in TSH levels and a decline in T4 and T3 levels, culminating in the development of severe hypothyroidism by day 28. In contrast, WT mice maintained euthyroid status throughout the study. Notably, the onset of hypothyroidism in *Dehal1* KO mice was observed as early as day 12. Additionally, there was a transient surge in T3 levels at day 12 in KO mice, possibly due to preferential T3 synthesis under iodine-deficient conditions[281]. Subsequently, *Dehal1* KO mice experienced a complete failure of thyroid hormone synthesis, while WT mice sustained normal thyroid function.

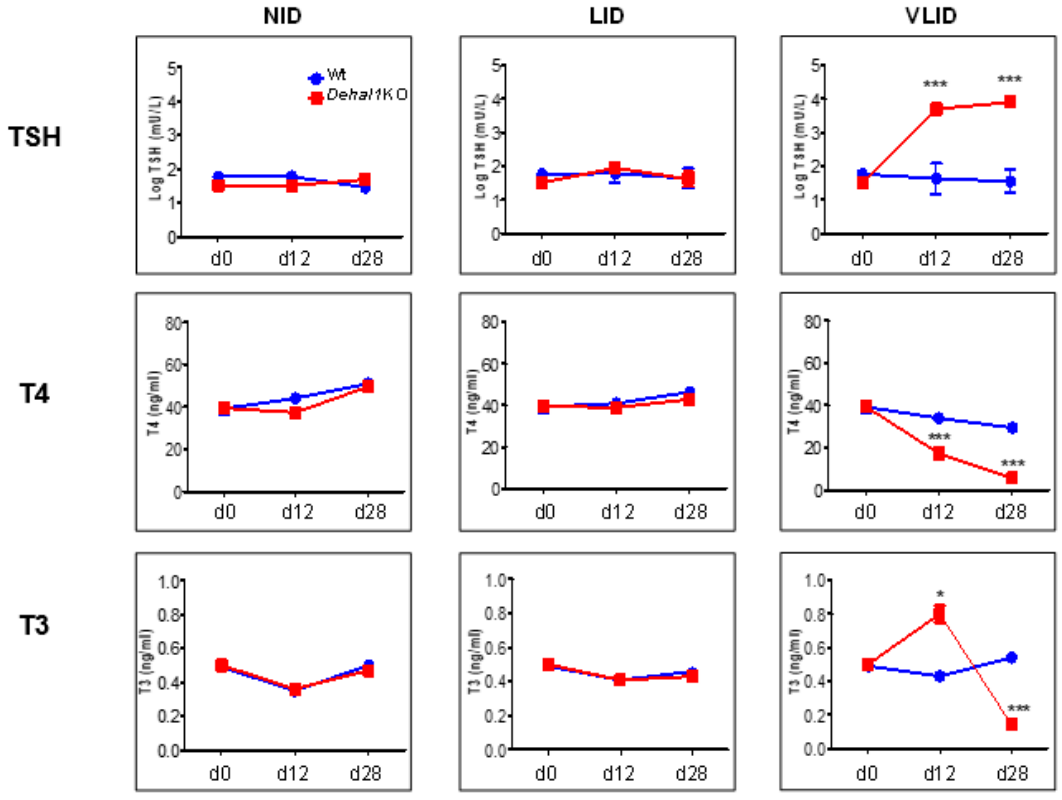

Figure 48. Plasma TSH, T3 and T4 were determined, over a 28-day duration, using radioimmunoassay and HPLC-MS/MS, respectively. Results are in mean±SEM (* p<0,05;; *** p<0,005) (adapted from González-Guerrero G, *et al.* 2023[260]).

Furthermore, plasma and urinary iodotyrosines levels (Figure 49-50), indicative of iodine metabolism, were significantly elevated in *Dehal1* KO mice on the NID compared to WT mice. On the LID, iodotyrosines levels gradually declined in *Dehal1* KO mice but remained higher than those in WT mice. However, with the VLID, a sharp decrease in iodotyrosines was observed in *Dehal1* KO mice, resulting in no detectable differences between the genotypes by the study's conclusion. These results emphasize the critical function of DEHAL1 in safeguarding thyroid function and overseeing iodine metabolism, especially in situations of pronounced iodine insufficiency. The findings highlight the indispensable contribution of DEHAL1 in maintaining the intricate balance of thyroid hormones and iodine homeostasis, particularly in the face of severe iodine scarcity.

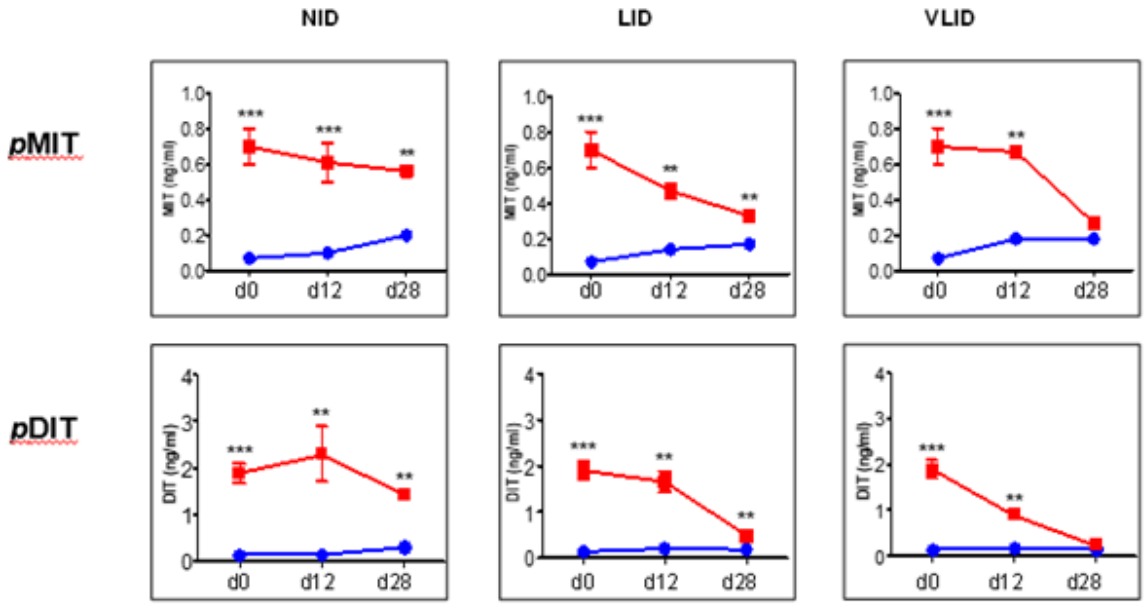

Figure 49. Plasma (p) MIT and DIT were determined, over a 28-day duration, using HPLC-MS/MS. Results are in mean±SEM (** p<0,01; *** p<0,005) (adapted from González-Guerrero G, *et al.* 2023[260]).

The concentrations of iodotyrosines in urine (Figure 50) were found to mirror the changes observed in plasma, as depicted in Figure 49. However, despite a decreasing trend under iodine restriction, the levels of MIT/DIT remained significantly higher in *Dehal1* KO mice throughout the experiment. Interestingly, DIT, which requires two iodine atoms, exhibited a steeper decrease compared to MIT in *Dehal1* KO mice under very low iodine diets, possibly indicating the depletion of iodine reserves. Moreover, the UIC was significantly higher in *Dehal1* KO mice compared to WT mice only under normal iodine diets and low iodine diets, with no detectable difference between genotypes under very low iodine diets (Figure 50). In conclusion, our findings demonstrate that DEHAL1-deficient mice are highly sensitive to iodine

deficiency, leading to the development of severe hypothyroidism in a surprisingly short period of time. Importantly, the elevated levels of iodotyrosines in the plasma and urine of *Dehal1* KO mice, even when they are still euthyroid, serve as reliable biomarkers for latent iodotyrosines dehalogenase deficiency. These biomarkers can anticipate the risk of rapid progression to severe hypothyroidism in the event of a shortage of external iodine supplies.

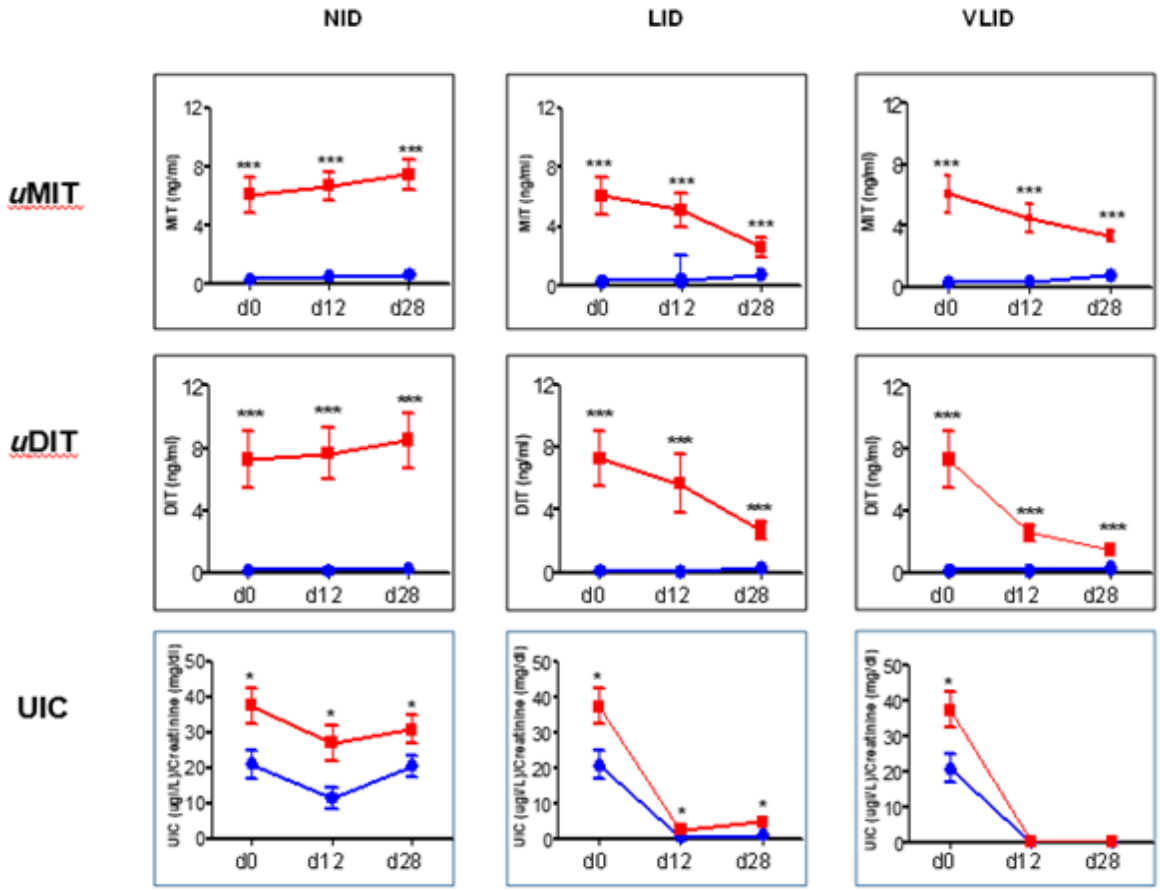

Figure 50. Urinary (u) concentrations of MIT, DIT, and iodine (UIC) were determined, over a 28-day duration, using HPLC-MS/MS and S-K reaction, respectively. Results are in mean±SEM (* p<0,05; *** p<0,005) (adapted from González-Guerrero G, *et al.* 2023[260]).

8.4 Sudanese families pedigrees and description

Family 1: The first family, originating from Western Sudan and depicted in Figure 51, came to attention in 2017 when the propositus, born to consanguineous parents (first cousins), presented at the age of 7 years with impaired cognitive function, goiter, elevated TSH, and low serum T4. Initiation of L-T4 therapy prompted the evaluation of younger siblings, aged 8 and 3 years, both exhibiting cognitive impairment and goiter. Thyroid function tests confirmed a hypothyroid state, with classic facial features indicative of hypothyroidism. Serum collected after 7 days of L-T4 treatment normalized thyroid function tests for the propositus and his brother, while the younger sister achieved normalization after 6 months. WES on the propositus and mother identified a mutation in exon 5 (c.835C>T; R279C) of the *DEHAL1* gene. Sanger sequencing confirmed homozygosity for the mutation in all three siblings and heterozygosity in the parents. Subsequent to the discovery of the *DEHAL1* (also referred as *IYD*) gene mutation, L-T4 supplementation was replaced with Lugol's iodine, to support iodine intake, for 4 weeks, ensuring the maintenance of euthyroidism. Upon encountering difficulty in obtaining Lugol's iodine, the patients were switched back to L-T4, with continued maintenance of normal thyroid tests. Spot urine iodine was obtained after restarting L-T4.

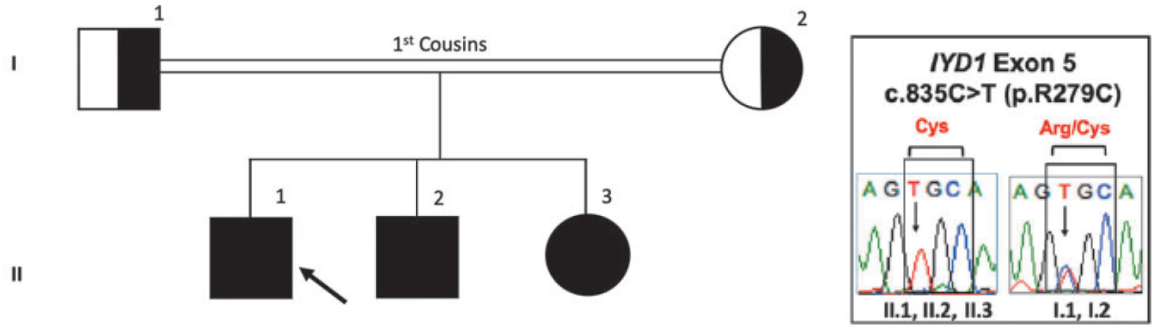

Figure 51. Family 1 pedigree and *IYD* mutation pattern (adapted from Shareef R. *at al*. 2023[263]).

Family 2: The second family, originating from northern Sudan and illustrated in Figure 52, came to attention in 2018 when the propositus (II-1), born to consanguineous parents (first cousins), presented at age 7 and was initiated on L-T4. Incomplete medical notes were available, but at age 13, he self-discontinued L-T4, experienced well-being with normal thyroid function tests, and did not resume L-T4 treatment. Siblings II-2 and II-3 exhibited goiter and were not treated with L-T4, while II-4, lacking goiter, experienced some lethargy and was

briefly treated with L-T4. WES conducted on DNA from the propositus, and mother revealed the same *IYD* mutation as Family 1 (exon 5; c.835C>T; R279C), with subjects II-1, II-3, and II-4 being homozygous, and the mother (I-2) and a sibling (II-2) heterozygous. Spot urine iodine was obtained. Blood and urine were collected on two different occasions and sent to Miami for analysis, revealing consistent normal values for all thyroid function tests and urine iodine. The identification of an identical mutation in these two families from different parts of Sudan prompted haplotyping of the gene locus, demonstrating a minimally shared genetic interval surrounding the mutation of 2.7 megabases.

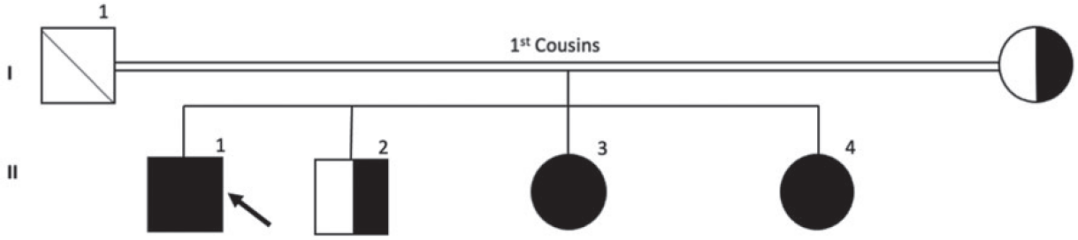

Figure 52. Family 2 pedigree (adapted from Shareef R. *at al*. 2023[263]).

8.4.1 Concentrations of TH and iodothyronines in blood and urine

Serum samples from individuals belonging to Family 1 (Table 9) were subjected to iodothyronines and iodotyrosines measurements, while both urine and serum samples from individuals of Family 2 (Table 10) were analysed. The results revealed significantly elevated levels of serum MIT and DIT in all homozygous individuals compared to the heterozygous father (I-1), along with slightly higher concentrations of T3 and T4 in the affected subjects. In Family 2, the affected individuals exhibited markedly elevated levels of serum and urinary MIT and DIT, but no significant changes were observed in T3 and T4 concentrations. Other parameters, including TG, TSH, UIC and anti-TG antibodies were recorded and are reported in the aforementioned tables. It wasn't easy to have uniform samples and data because patients were being monitored in Khartoum, and due to the political conditions in Sudan, achieving optimal patient monitoring has been challenging.

	I-1	II-1		II-2		II-3		I-2	
Age (at diagnosis)	30	10	11	8	9	3	4	25	26
Treatment	-	L-T4	L-T4	L-T4	L-T4	L-T4	L-T4	-	-
Goiter	-	+	-	+	-	+	-	-	-
TT4 µg/dL (4.5-12.5)	9.82	14.6	9.14	17.3	7.94	12.8	10.8	9.95	-
TT3 ng/dL (81-178)	82.5	272	123	408	105	529	125	97.8	-
fT4 ng/dL (0.89-1.76)	1.37	2.29	1.53	2.96	1.84	2.18	1.51	1.52	-
TSH µUI/mL (0.4-4)	3.66	2.07	<0.004	1.78	0.021	18.8	0.576	3.98	-
TBG µg/mL (14-31)	24.9	41.9	25.5	21.8	15.5	35.4	29.7	22.2	-
TG ng/mL (1.7-55.6)	10.6	849	6.70	5.88	59.9	944	18.7	9.09	-
s MIT ng/mL (0.08-80)	0.075	2.8	-	6	-	35	-	0.35	-
s DIT ng/mL (<0.3)	0.2	0.95	-	8	-	7.5	-	0.6	-
UIC µg I/L (34-523)	-	-	319	-	86	-	65	-	59

Table 9. Family 1 thyroid function tests, and urine iodine values. Values in red are above the limit of normal and values in blue are below the limit of normal (adapted from Shareef R. *at al*. 2023[263]).

	II-1	II-2			II-3			II-4			I-2		
Age (at diagnosis)	22	41		19	15		16	13		14	41		42
Treatment	-	-	-	-	-	-	-	-	-	-	-	-	-
Goiter	-	+	+	+	+	+	+	-	-	-	-	-	-
TT4 µg/dL	7.69	8.31	5.73		6.55	6.41		8.19	6.57		9.03	8.01	
TT3 ng/dL	106	156	109		126	109		139	124		83.0	96.6	
fT4 ng/dL	1.93	1.02	1.09		1.88	1.39		1.2	1.17		2.5	1.23	
TSH µUI/mL	2.23	1.22	1.30		1.94	1.85		2.22	1.86		1.81	1.53	
TBG µg/mL	12.6	28.3	26.3		13.8	18.6		25.4	19.8		10.6	22	
TG ng/mL	40.8	19.0	13.6		0.477	1.21		27.6	20.2		12.4	11.7	
Tg Ab IU/mL	<20	<20	<20		>3000	>3000		<20	<20		<20	<20	
s MIT ng/mL	2	3			10			08			1.8		
s DIT ng/mL	1.5	1.5			1.5			5			0.4		
uMIT/uDIT (0.8-1.2/0.2-0.5)		7/5			70/110			50/55					
UIC µg I/L				143			91			125			170

Table 10. Family 2 thyroid function tests, and urine iodine values. Values in red are above the limit of normal and values in blue are below the limit of normal (adapted from Shareef R. *at al*. 2023[263]).

8.4.2 New interesting insights coming from a third Sudanese family

Recently, our laboratory initiated the analysis of new samples from three individuals belonging to a new Sudanese family residing in the Al Jazeera state. Specifically, we examined urine and serum samples from a mother and her two children. Following genetic analysis and DNA sequencing, it was discovered that these children share the same mutation (c.835C>T; R279C) in exon 5 of the *DEHAL1* gene as the two Sudanese families previously described. Their serum and urine iodotyrosine levels were found to be outside the reference range. Unfortunately, the family's medical history is incomplete, as are the details provided by our American colleagues who sent us the samples. Due to the political situation in Sudan, information is fragmented and partial, making the monitoring of these subjects extremely challenging.

From the limited information available, it appears that the HT mother does not exhibit thyroid stress. One of the three children of the mother died at the age of 9 months due to a presumed respiratory infection, although earlier symptoms suggested hypothyroidism. The two HO children show goiter and are expected to undergo therapy with L-T4. The only other information about the family suggests possible thyroid disorders in the mother's brother, although this has not been confirmed. No detailed information is available about the family’s father.

Discussion

9.1 Effects of a combined L-T4 and T1AM supplementation on memory and adult hippocampal neurogenesis in a mouse model of hypothyroidism

In this study, it was found that using L-T4 monotherapy alone was both necessary and sufficient for restoring memory deficits and adult hippocampal neurogenesis in individuals with adult-onset hypothyroidism. Interestingly, the addition of T1AM to L-T4 did not result in any further improvements in neurocognitive and neurobiological impairments. Furthermore, contrary to previous clinical observations and studies, there were no changes in locomotion, anxiety, or depression-related behavioural measures[142,282–284]. The hypothyroidism induction protocol effectively lowered serum T4 levels, indicating moderate hypothyroidism, while serum T3 levels remained unchanged. This suggests that there may be some residual thyroperoxidase activity contributing to sufficient T3 production, which in turn prevents alterations in measures of depression or anxiety. However, cognitive impairments were still evident, highlighting the vulnerability of cognitive functions to TH deficiency[140–145,285].

There was a significant decrease of 20% in the population of newly generated neuroblasts in the SGZ of the dentate gyrus, indicating a reduction in neurogenesis. However, the administration of L-T4 for a duration of 4 weeks proved to be both necessary and sufficient for the restoration of memory function and the number of neuroblasts. These results are consistent with previous studies that have demonstrated the beneficial effects of L-T4 in reversing various alterations induced by hypothyroidism, including behavioural, electrophysiological, morphological, and molecular changes[142,144,285,286]. Although the importance of TH in the survival of adult dentate granule cell progenitors has been emphasized, it remains unclear whether the decline in survival is due to a delay or block in neuronal differentiation or if these cells are specifically targeted for cell death. The susceptibility of cognitive functions and neurogenesis to moderate changes in TH levels highlights the connection between TH and neurodegenerative diseases, such as Alzheimer's disease, which have been observed in clinical populations[287–289], including those with subclinical hypothyroidism[139]. Interestingly, our findings indicate that the combination of L-T4 monotherapy and L-T4+T1AM did not result in any significant differences in terms of memory function and the number of DCX+ cells, suggesting that T1AM did not exert any independent effects. This study focused on T1AM because we hypothesized that certain neurocognitive symptoms commonly associated with TH deficiency in hypothyroidism may be caused, at least in part, by a decrease in the availability of downstream metabolites. Previous research has shown that T1AM cannot be detected in the tissues of animals that have undergone pharmacological TH depletion, even after their fT4 and

fT3 levels have fully recovered[157]. Additionally, there is a growing body of evidence supporting the role of T1AM in the CNS. T1AM has been identified as a regulator of noradrenergic, dopaminergic, and histaminergic transmission[128]. Its effects on various aspects, such as sleep[159] regulation, exploratory behaviour, and the acquisition and retention of memory[290], have been documented. Furthermore, T1AM has demonstrated neuroprotective effects in different models, including excitotoxic damage related to seizures, altered autophagy, amyloidosis, ischemia-reperfusion injury, and neuroinflammation[122,160,161,290,291]. It is worth noting that these studies involved the administration of T1AM through perfusion on ex vivo brain acute/organotypic slices or intracerebral microinjection, while our study utilized systemic administration.

Our investigation has uncovered changes in the expression of multiple genes, such as *Ngf*, *Kdr*, *Kit, L1cam*, *Ntf3*, *Mapk3*, and *Neurog2*, in response to replacement treatment. Specifically, mice treated with L-T4+T1AM showed an increase in the expression of *Mapk3* and *Neurog2* compared to mice treated with L-T4 alone. However, there were no significant differences in the expression of *Mapk3* and *Neurog2* between mice treated with L-T4+T1AM and T1AM alone, suggesting that T1AM may independently induce changes in gene expression. These genes play crucial roles in neurogenic mechanisms, including the promotion of increased proliferation of DCX+ cells in the hippocampus, initiation and progression through the G1 phase of the cell cycle, determination of neuronal cell fate, and suppression of glial fate that promotes neurogenesis[292–294]. TH regulate gene transcription through TR, which are expressed at various stages of granule cell progenitors[286]. Importantly, T1AM does not bind to TR but interacts with different molecular targets, including TAAR 1, alpha2 adrenergic receptors, transient receptor potential channels, and ApoB-100[295].

Further investigations are essential to unravel the intricate connection between the unique target profile of the treatment and gene expression. One potential avenue worth exploring is the role of TAAR1, given the growing body of evidence implicating its involvement in neuropsychiatric disorders[296,297], and the documented neuroprotective effects of T1AM in models of amyloidosis and ischemia–reperfusion injury[122,161]. TAAR1 engages in distinct signalling pathways based on its subcellular localization. When situated on the plasma membrane, TAAR1 activation leads to increased intracellular cAMP levels and the activation of protein kinase A by coupling to G proteins and activating adenylyl cyclase[298–300]. Intracellular activation of TAAR1 involves coupling with G proteins to activate the GTPase RhoA. Additionally, TAAR1 activation is

linked to G protein-coupled inwardly rectifying potassium channels and G-protein-independent inhibition of glycogen synthase kinase 3β[301–304].

Despite the insights gained from this study, it is crucial to acknowledge certain limitations. Firstly, the findings do not establish a causal relationship between replacement treatments and the memory improvements mediated by alterations in hippocampal neurogenesis. Future investigations should delve into whether blocking neurogenesis during L-T4 and/or L-T4+T1AM treatment impedes memory rescue. Secondly, in some comparisons, the sample size may have been insufficient to attain adequate statistical power. This could be attributed to our protocol inducing moderate hypothyroidism (compensated T3 levels), potentially resulting in behavioural changes of small-to-moderate effect size. Our statistical analysis, however, was designed to detect larger effect sizes based on previous findings in thyroidectomized or transgenic rodents. Finally, our attempt to measure brain T1AM in different treatments, as part of our hypothesis that T1AM deficiency contributes to hypothyroidism-induced cognitive impairments, faced challenges. In alignment with findings from other studies, we encountered difficulties in detecting a clear endogenous signal of T1AM (below the detection limit) in the majority of our pilot samples due to technical reasons. Consequently, we made the decision to discontinue this particular aspect of our investigation[305]. Surely, the possibility of achieving a correct quantification of TH and their derivatives in tissues, with a specific interest in T1AM, could highlight intrinsic mechanistic effects achieved locally and not peripherally. In fact, local TH regulation may differ from systemic evidence, as dysregulations of local metabolisms are not always reflected in circulating markers and hormones, as we will further discuss in the next chapters.

9.2 Local modulation of TH signalling in the retina affects the development of DR

In the realm of DR, the impact of HG levels on neuronal damage is a crucial aspect. The resulting metabolic imbalance induces cellular distress, particularly affecting neural cell types with high energy demands, such as RGCs. Early stages of DR witness significant alterations in RGCs as they strive to adapt and bolster their resilience. However, these adaptive responses can evolve into pathological factors as the disease progresses. Hyperglycaemia-induced stress triggers various cellular responses, including the overexpression of *VEGF*, autophagy induction, and reorganization of RGC dendritic arborizations[166,169,306]. This study proposes that the regulation of the retinal local TH system acts as an additional adaptive mechanism, aiming to conserve cellular energy and alleviate metabolic challenges following early exposure to HG. Our findings highlight reduced TH levels in diabetic retinas, linked to decreased expression of *DIO2* and increased expression of *DIO3*. Additionally, diminished expression of TR contributes to the establishment of a LT3S. Further insights from our data reveal altered expression of specific microRNAs in diabetic retinas, indicating potential regulatory mechanisms in deiodinase expression. Changes in mitochondrial markers hint at potential consequences of TH alterations on mitochondrial function. *In vitro* experiments using MIO-M1 cell cultures replicate these alterations under HG conditions, unveiling a feedback regulatory mechanism involving *miR133*a. This mechanism leads to upregulation of *DIO3* through a pathway dependent on nuclear factor erythroid 2-related factor 2 (Nrf2) and hypoxia-inducible factor 1 (HIF-1). Notably, in an experimental setup mimicking early DR conditions, the removal of T3 (mimicking LT3S) reduces retinal stress induced by HG, while T3 replacement increases this stress.

Clinical investigations have reported an inverse relationship between circulating TH levels and the risk of DR [188–190,307]. However, conflicting reports exist, suggesting no association between thyroid dysfunction and diabetic complications, including DR[308]. To explore potential connections between the TH system and DR progression, a comprehensive examination of the correlation between plasma and retinal TH levels and key DR indicators in the *db/db* mouse model of type 2 diabetes mellitus was conducted. The *db/db* mouse, widely employed as a DR model, provided diverse data for characterizing the retinas of these mice. This study introduces innovative findings indicating the presence of a LT3S in the retinas of *db/db* mice. Importantly, the manifestation of DR characteristics in these mice appears unrelated to alterations in plasma levels of T3 or T4. Instead, a distinct LT3S within the retina itself is marked by significant

reductions in both T3 and T4 concentrations, implying crucial TH-mediated mechanisms unfolding within the retina, influencing DR development independently of systemic TH levels.

The concept of local control of TH signalling in the retina aligns with various existing observations. Recent research has highlighted the pivotal role played by the regulation of TH signalling among different retinal cell types in light/dark adaptation[309]. Moreover, evidence suggests that deiodinases can modulate intracellular TH levels independently of systemic TH, observed in both animals and humans[69]. Deiodinases, specifically DIO1, DIO2, and DIO3, play distinct roles, offering tissue-specific regulation of TH signalling. Consistent with our current findings, the localized LT3S in *db/db* retinas is associated with upregulated *DIO3* expression and downregulated *DIO2* expression, indicating a reprogramming of the retinal TH system. This reprogramming shifts the balance away from T4 conversion into T3 and towards an increase in inactive forms, namely rT3 and T2, resulting in an overall reduction of TH signalling[103]. Further exploration of *DIO2* in *db/db* retinas revealed a more pronounced reduction in mRNA expression compared to protein levels, suggesting intricate post-transcriptional regulation[310]. The diminished T3 signalling in the diabetic retina is likely influenced not only by increased *DIO3* expression but also by the downregulation of TRs. Our data demonstrate significant decreases in both *THRα1* and *THRβ2* expression, suggesting a unique response of the TR system to stress in the retinas of *db/db* mice, consistent with previous findings in a model of brain ischemia[192,311]. Previous studies had already highlighted the presence of a local TH dysmetabolism not necessarily reflected into systemic evidence. Weltman *et al*. reported the presence of local reduction of T3 and T4 levels in cardiac tissues of a diabetic rat model. Even in this case, no significant changes in serum fT3 and fT4 levels were appreciated[311b]. Interestingly, alterations of *DIOs* mRNA levels, with an increase of *DIO3* expression and a decreased *DIO2* expression, were also observed in the diabetic hearts showing cardiomyopathy.

The findings presented in this study strongly suggest that DIO3 is the primary driver behind the establishment of a LT3S in the diabetic retina, aligning with similar observations in the ischemic heart[276,277]. In the context of cardiac ischemia, a metabolic regulation mechanism has been elucidated during hypoxic-ischemic injury, wherein the induction of *DIO3* and the subsequent reduction of local TH signalling are orchestrated by HIF-1[276]. A similar relation pattern was also evidenced in a rat model of diabetes showing cardiomyopathy[311b]. Given the pivotal role of HIF-1 in DR[170,312], we posit that the observed decrease in T3 levels in *db/db* retinas is linked to HIF-1-mediated upregulation of *DIO3* expression. To test this hypothesis,

an *in vitro* model involving MIO-M1 cells exposed to HG was employed, exhibiting alterations in oxidative balance and *VEGF* expression, along with a substantial increase in DIO3, closely resembling the in vivo condition. Importantly, inhibition of HIF-1 prevented the HG-induced elevation of *DIO*3 mRNA expression, affirming the role of HIF-1 in the upregulation of *DIO3*.

Furthermore, our earlier observations indicated that HIF-1α stabilization, a prerequisite for HIF-1 formation, can be induced by various factors, including Nrf2 activation[170]. The existence of an intracellular Nrf2-HIF-1 pathway governing *DIO3* expression aligns with our current findings, as demonstrated by the abolition of *DIO3* mRNA overexpression in MIO-M1 cells cultured in HG when subjected to Nrf2 blockade. In summary, the data from the present study, considered in conjunction with insights from preceding investigations, propose a comprehensive mechanistic illustration (Figure 53). According to this model, HG-induced oxidative stress activates Nrf2, which, potentially through an increase in *HO-1* expression, facilitates HIF-1α stabilization, leading to elevated *DIO3* expression and the establishment of LT3S within the diabetic retina[170].

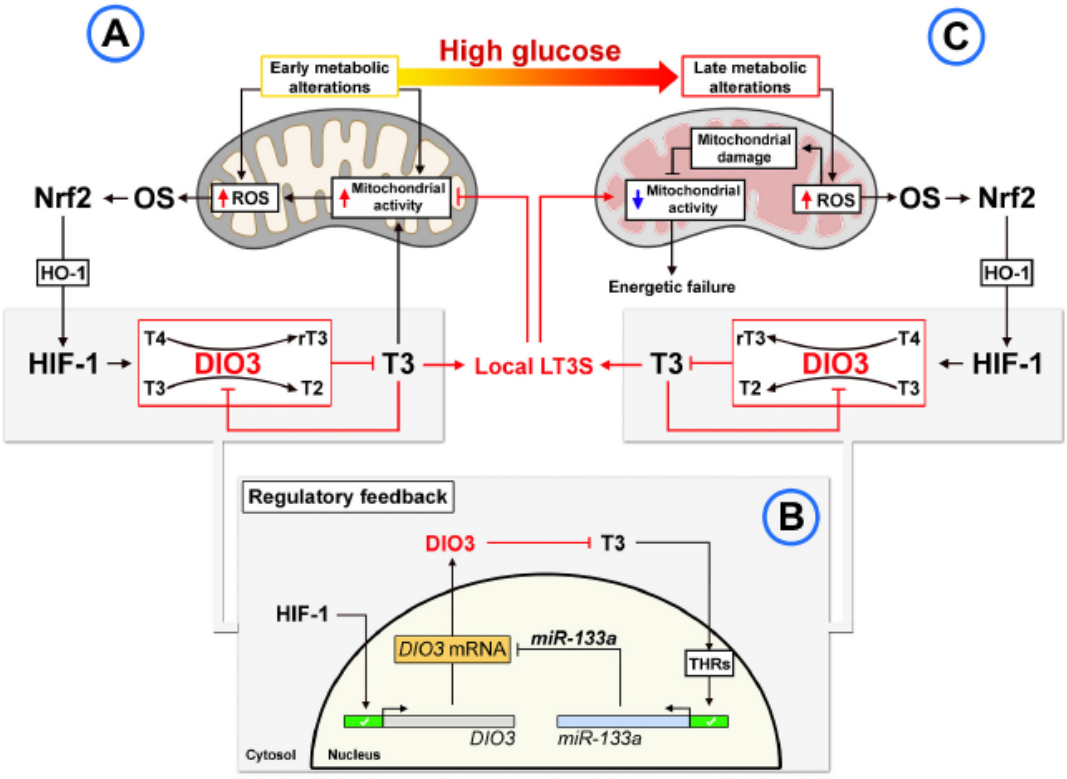

Figure 53. Graphical representation of the proposed mechanisms for TH system modulation in retinal cells under diabetic conditions and its relevance for metabolic stress (adapted from Forini F. *et al.* 2023[265]).

9.3 Iodotyrosines are biomarkers for preclinical stages of iodine-deficient hypothyroidism in Dehal1 KO mice

Iodine deficiency (ID) remains a pervasive environmental concern with global implications for populations worldwide. While extensive research has illuminated the adverse effects of hypothyroidism induced by ID on brain development in both animal models and humans, it is remarkable that individual diagnosis for this critical condition is still unavailable[313–316]. Presently, the diagnosis of ID is confined to predefined populations and lacks a personalized approach that considers individual genetic factors for preventive or therapeutic interventions. This deviation from the principles of personalized medicine underscores the urgent need for biomarkers capable of accurately reflecting the iodine status of individuals. Recent studies have shown that the variability in UIC across populations over time cannot be fully explained by dietary iodine intake alone, implicating genetic factors in iodine metabolism[317,318].

Addressing this need for precise biomarkers, our study delved into the first mammalian model of dehalogenase deficiency, a key player in iodine metabolism. Our findings illuminated that mice lacking the *DEHAL1* gene exhibit a negative iodide balance compared to their normal counterparts, even in the presence of sufficient iodine. This imbalance results from the excessive excretion of iodotyrosines in their plasma and urine. Notably, the aberrant iodine excretion patterns challenge the reliability of the S-K technique, which measures both inorganic and organic iodine, in accurately detecting "low iodine intakes" in urine samples containing iodotyrosines. This raises questions about the precision of the S-K technique in assessing iodine status in individuals.

Moreover, our investigation revealed that *Dehal1* KO mice, when subjected to iodine restriction, undergo a rapid decline in thyroid function compared to normal mice. This rapid decline suggests that KO mice lack sufficient iodine reserves in their thyroids to compensate for even brief periods of iodine deficiency. This underscores the pivotal role of DEHAL1 in iodine storage during times of sufficiency. Further exploration is warranted to unravel the mechanisms through which DEHAL1 influences iodine storage in the thyroid.

The clinical implications of these findings are substantial. In humans, the measurement of MIT and DIT levels could serve as a valuable diagnostic tool for identifying DEHAL1 defects before the onset of hypothyroidism. This is particularly relevant for newborns, as our mouse model demonstrated that affected infants may not manifest signs of hypothyroidism at birth but consistently exhibit elevated iodotyrosines levels. Early detection holds the potential to identify

the risk of hypothyroidism during critical stages of brain development, offering a preventive measure against mental retardation[205,214]. Additionally, the diagnosis of iodine recycling-storage defects in individuals with normal thyroid function could prove crucial for women planning to conceive. The heightened iodine requirements during pregnancy could mirror the effects of iodine restriction in early pregnancy. KO mouse model provides a valuable platform for studying the dynamics of iodine conservation in pregnant DEHAL1 -deficient mice and its implications for offspring[319].

Furthermore, the intriguing expression of *DEHAL1* in tissues beyond the thyroid, particularly in the choroid plexus, prompts further exploration. Apart from its role in iodotyrosines conversion, DEHAL1 demonstrates the ability to remove bromine and chlorine from tyrosines[320,321]. Recent studies have shed light on the essential roles of bromide and chloride in the brain[322,323], leading to a compelling investigation into whether DEHAL1 contributes to maintaining halogen homeostasis in specific tissues. In summary, DEHAL1 emerges as a pivotal player in iodine metabolism within the thyroid gland. During iodine deficiency, it facilitates the recycling of iodine for hormone synthesis from iodotyrosines. Conversely, in the presence of sufficient iodine, it ensures optimal iodine storage in the thyroid gland. The presented model of dehalogenase deficiency supports the proposition that genetic factors mediate the intricate relationship between iodine nutrition and iodine reserves. One intriguing area to further explore would be the levels of iodotyrosines and thyronines at the local thyroid level. Understanding local and peripheral metabolic regulation could enhance comprehension of DEHAL1 defects impact on iodine storage. Preliminary data from thyroid samples[206], both deficient and non-deficient in iodine, have shown reductions in tyrosines and a significant decrease in T4 levels at the thyroid. This reduction appears linked to decreased thyroglobulin presence within and around the thyroid. Despite sufficient iodine intake, *Dehal1* KO mice seems to exhibit signs of iodine deficiency, possibly due to dysregulated TG homeostasis hindering effective iodine accumulation. Therefore, local TH and thyroglobulin measurements (both iodinated and not iodinated forms) could provide insights into the relationship between DEHAL1 defects and iodine storage. While elevated levels of iodotyrosines hold promise as biomarkers for assessing individual risk and vulnerability to iodine-deficient hypothyroidism, further validation in clinical settings is imperative.

9.4 Congenital hypothyroidism in two Sudanese families harboring a novel iodotyrosine deiodinase mutation

In this study, a novel mutation (c.835C>T; R279C) in the *DEHAL1/IYD* gene was identified in two Sudanese families with autosomal recessive inheritance, originating from distinct regions of Sudan. This finding aligns with the first documented case of a dehalogenase defect reported in 1955[324], where the confirmation of altered iodotyrosines metabolism marked a significant milestone. The patient exhibited goiter at birth in a region with a high prevalence of goiter, and treatment with 'thyroid powder' at nine months led to goiter reduction. Intriguingly, the patient's untreated younger brother experienced persistent goiter and cognitive delays. Rigorous experiments involving intravenous administration of ^{131}I-labeled *dl*-DIT and *dl*-MIT, with subsequent minimal changes in urinary excretion, substantiated the presence of a dehalogenase defect[325]. Although previous cases hinted at dehalogenase defects, it took five decades for the sequencing and characterization of DEHAL1. Four distinct *DEHAL1* mutations had been previously reported in nine individuals, showcasing considerable clinical variation even among those with identical mutations in different families[70,214,216,280,326].

Patient	1	2	3	4	5	6	7		8	(9)
Mutation	p.R101W	p.F105-I106L		p.I116L	p.A220T					
	Homo	Homo	Homo	Homo	Homo	Homo	Hetero		Homo	Homo
Diagnosis	1.5y	infancy	infancy	8y	5y	infancy	(9y)	14y	15.9y	(6y)
L-T4 at TFTs	-	-	-	-	+	+	-	-	-	-
TSH	390	-	-	139	1.2	0.6	0.5	>100	1400	2.2
TT3 ug/dL	70	-	-	-	192	124	146	-	-	-
FT3 pg/mL	-	-	-	1.4	-	-	2.25	2.6	2.9	4.2
TT4 ug/dL	1.4	-	-	-	7.4	10.1	9.7	-	-	-
FT4 ng/dL	-	-	-	<0.2	0.5	1.2	1.1	<0.3	<0.5	1.4
TG	-	-	-	-	1040	<20	110	-	6800	11.7
U-DIT, MIT	-	-	-	-	high	normal	high	-	-	high
S-DIT	high	-	-	high	-	-	-	-	-	-
Goiter	+	+	+	+	+	+	None	+	+	None
Reference	(Moreno J.C et al., NEJM, 2008)[18]				(Afink G. et al., JCEM, 2008)[16]				(Burniat A. et al., JCEM, 2012)[17]	

Figure 54. Comparison of phenotype and genotype in other families with *DEHAL1* gene mutations. Values in red are above the limit of normal and values in blue are below the limit of normal (adapted from Shareef R. at al. 2023[263]).

The current study unveiled a novel fifth unique *DEHAL1* mutation, underscoring the genetic heterogeneity in dehalogenase-related disorders. Elevated TSH levels were observed to varying degrees in three individuals (Patients 1, 4, and 8, Table 9 in the Results section) prior to initiating L-T4 treatment, and in one individual (Patient 7, Figure 54), TSH levels became elevated five years after the initial diagnosis. Consistently elevated levels of MIT and DIT were noted, emphasizing the role of iodotyrosines in the pathophysiology. The urinary excretion of iodotyrosines contributed to a reduction in available iodine for recirculation, resulting in iodine deficiency. Limited environmental iodine availability further decreased the threshold for hypothyroidism.

Lastly, the latest information regarding the third Sudanese family, whose samples were recently analysed in our laboratory, and the newly discovered mutation by Moreno from the Lebanese family, suggests that mutations in the *DEHAL1* may likely exhibit geographical adherence and dependence. Further investigations and the discovery of new mutations will need to either refute or confirm this hypothesis.

Conclusions

HPLC-MS/MS affirms to be a highly sensitive analytical tool, allowing the detection of compounds at exceptionally low concentrations. Its outstanding selectivity further facilitates the precise identification and quantification of specific analytes within complex mixtures. HPLC-MS/MS serves as a robust platform for quantitative analysis, delivering accurate and precise measurements of analyte concentrations. The integration of ISs enhances accuracy in these quantitative assessments. This method's versatility is underscored by its wide dynamic range, instrument-dependent, enabling the comprehensive analysis of compounds across a broad concentration spectrum, spanning from trace levels to high concentrations. MS/MS further amplifies the analytical capabilities by facilitating the fragmentation of ions. This not only provides additional structural insights but also enhances specificity in the identification of compounds. The adaptability of MS is evident in its ability to operate with multiple ionization interfaces, such as ESI and APCI, thereby expanding its applicability to different types of compounds. One notable advantage of MS is its reduced susceptibility to interference from co-eluting compounds or matrix effects, setting it apart from some other detectors. This characteristic ensures cleaner chromatograms and, consequently, more accurate results.

High-resolution mass spectrometers, a subset of this analytical technique, demonstrate the ability to distinguish between ions with similar m/z ratios. This capability significantly enhances the resolution and identification of closely related compounds. The versatility of mass spectrometers extends across a wide range of compound analyses, including small organic molecules, peptides, proteins, and large biomolecules. The application of MS as a detector in HPLC systems offers a plethora of advantages, making it a powerful tool for analytical investigations across diverse scientific domains.

This thesis explores the multifaceted benefits of HPLC-MS/MS and delves into its applications in TH detection and quantification, showcasing its versatility and precision. The application of HPLC-MS/MS, particularly utilizing the Sciex Qtrap 6500 mass spectrometer, in our case operating as a triple quadrupole, is explored for the TH analysis across different pursuits.

The utilization of HPLC-MS/MS firstly aimed to measure serum levels of TH in a mouse pharmacological model of hypothyroidism to explore the possible benefits of alternative replacement therapies for the treatment of adult on set hypothyroidism and their impact on neurogenesis and neurobiological alterations. The significance of moderate TH changes in inducing notable impairments in memory and neurogenesis was underscored. Through meticulous analysis, it was revealed that L-T4 alone was both necessary and sufficient to

restore memory and neuroprogenitors levels to the euthyroid state. Despite the hypothetical impact of T1AM on neurogenic pathways, no evidence supporting the involvement of non-canonical TH signalling was found. This prompts the need for further exploration in subsequent studies to fully comprehend the intricate mechanisms at play.

Subsequently, the use of HPLC-MS/MS and other molecular biology techniques, facilitated and demonstrated the existence of a local LT3S in the diabetic retina. The focus on the biological significance of local T3 lowering in the retina, coupled with the concurrent decrement in local T4 levels, shed a light on the TH-dependent response to HG-induced stress. The intricate feedback mechanism involving *DIO3* expression, regulated by T3 levels through mediation of *miR-133a*, was revealed. This mechanism, altered by hyperglycaemia, oxidative stress, and HIF-1α stabilization, led to LT3S, offering early-phase protection against HG-induced stress. However, a T3 replacement strategy in this phase might negate the beneficial effect of LT3S. Interestingly, in the chronic phase, LT3S was no longer associated with retinal protection, suggesting a complex temporal dynamic that influences retinal responses in DR.

Thanks also to the development of a new optimized HPLC-MS/MS method for the contemporary detection of T3, T4, MIT and DIT, the enzyme DEHAL1 was revealed as a key factor in iodine metabolism within the thyroid gland. The research elucidated its role in iodine reuse during deficiency and optimal iodine storage in sufficiency. The model of animal dehalogenase deficiency presented in the study supports the proposed paradigm that genetic factors mediate the relationship between iodine nutrition and status. Elevated iodotyrosines were identified as biomarkers for the risk of iodine-deficient hypothyroidism, offering translational insights awaiting validation in clinical settings.

Eventually, the measurement of serum and urine DIT and MIT candidate them as sensitive indicators of iodotyrosines deiodination defects and the presence of *DEHAL1/IYD* mutations. This approach surpassed traditional urine iodine levels and thyroid function tests, providing valuable diagnostic and management insights into dehalogenase-related disorders. The findings underscored the importance of personalized and nuanced approaches in addressing the clinical heterogeneity observed in affected individuals.

In conclusion, the diverse projects underscore the instrumental role of HPLC-MS/MS in advancing our understanding of TH dynamics across various physiological and pathological contexts. The precision and versatility of this technique have yielded invaluable insights, paving the way for future research endeavours and potential clinical applications.

Embarking on the journey of mastering the HPLC-MS/MS technique at the Mass Spectrometry Centre of the Department of Pathology at the University of Pisa, and other molecular biology techniques, has been an exquisite experience, contributing immeasurably to the depth of my scientific understanding. The privilege of learning under the guidance of exceptional professionals and scientists, notably my supervisor Prof. Alessandro Saba, whose mentorship has been invaluable, and the esteemed Prof. Riccardo Zucchi, has been truly enriching. Moreover. I would like to extend my heartfelt gratitude to CISUP (The Center for Instrument Sharing of the University of Pisa) for their invaluable support in enabling the acquisition of the Sciex 6500+ Qtrap instrument, which significantly contributed to the results discussed in my PhD thesis. Collaborating with these remarkable individuals not only enhanced my technical proficiency but also fostered a collaborative spirit that transcends disciplines. The knowledge gained has propelled me to engage with numerous national and international scientific professionals, enabling me to contribute to the scientific community with groundbreaking works. This journey has not only expanded my scientific horizons but has also left an indelible mark, and I am immensely grateful for the opportunity to have been part of this transformative experience. Thank you.

Referenced articles treated in this thesis:

- Shareef R, Furman A, Watanabe Y, Bruellman R, Abdullah MA, Dumitresu AM, Refetoff S, **Bertolini A**, Borsò M, Saba A, Zucchi R, Weiss RE. Congenital Hypothyroidism in Two Sudanese Families Harboring a Novel Iodotyrosine Deiodinase Mutation (IYD R279C). Thyroid. 2023 Feb;33(2):261-266. doi: 10.1089/thy.2022.0492.
- González-Guerrero C, Borsò M, Alikhani P, Alcaina Y, Salas-Lucia F, Liao XH, García-Giménez J, **Bertolini A**, Martin D, Moratilla A, Mora R, Buño-Soto A, Mani AR, Bernal J, Saba A, de Miguel MP, Refetoff S, Zucchi R, Moreno JC. Iodotyrosines Are Biomarkers for Preclinical Stages of Iodine-Deficient Hypothyroidism in Dehal1-Knockout Mice. Thyroid. 2023 Jun;33(6):752-761. doi: 10.1089/thy.2022.0537.
- Rutigliano, G.; **Bertolini, A**.; Grittani, N.; Frascarelli, S.; Carnicelli, V.; Ippolito, C.; Moscato, S.; Mattii, L.; Kusmic, C.; Saba, A.; et al. Effect of Combined Levothyroxine (L-T_4) and 3-Iodothyronamine (T_1AM) Supplementation on Memory and Adult Hippocampal Neurogenesis in a Mouse Model of Hypothyroidism. *Int. J. Mol. Sci.* 2023, *24*, 13845. https://doi.org/10.3390/ijms241813845.
- Forini F, Nicolini G, Amato R, Balzan S, Saba A, **Bertolini A**, Andreucci E, Marracci S, Melecchi A, Terlizzi D, Zucchi R, Iervasi G, Lulli M, Casini G. Local modulation of thyroid hormone signaling in the retina affects the development of diabetic retinopathy. Biochim Biophys Acta Mol Basis Dis. 2023 Sep 25;1870(1):166892. doi: 10.1016/j.bbadis.2023.166892.

References

1. Ashraf, S. A., Nazir, S., Adnan, M. & Azad, Z. R. A. A. UPLC-MS: An Emerging Novel Technology and Its Application in Food Safety. in (ed. Srivastva, A. N.) Ch. 2 (IntechOpen, 2020)..

2. Cuatrecasas, P., Wilchek, M. & Anfinsen, C. B. Selective enzyme purification by affinity chromatography. *Proc. Natl. Acad. Sci. U. S. A.* **61**, 636–643 (1968).

3. Porath, J. From gel filtration to adsorptive size exclusion. *J. Protein Chem.* **16**, 463–468 (1997).

4. Harris, D. C. *Exploring Chemical Analysis*. (W. H. Freeman, 2005).

5. Gerberding, S. J. & Byers, C. H. Preparative ion-exchange chromatography of proteins from dairy whey. *J. Chromatogr. A* **808**, 141–151 (1998).

6. Donald PL, Lampman GM, Kritz GS, E. R. Introduction to Organic Laboratory Techniques (4th Ed.)Title. *Thomson Brooks/Cole* 797–817 (2006).

7. Harwood, L. M. & Moody, C. J. *Experimental Organic Chemistry: Principles and Practice*. (Blackwell Scientific Publications, 1989).

8. Hoffmann, E. de; Stroobant, V. Mass Spectrometry: Principles and Applications, 3rd ed. *J. Wiley Chichester, West Sussex, Engl. ; Hoboken, NJ* (2007).

9. Alpert, A. J. Hydrophilic-interaction chromatography for the separation of peptides, nucleic acids and other polar compounds. *J. Chromatogr.* **499**, 177–196 (1990).

10. Hemström, P. & Irgum, K. Hydrophilic interaction chromatography. *J. Sep. Sci.* **29**, 1784–1821 (2006).

11. Oyler, A. R. *et al.* Hydrophilic interaction chromatography on amino-silica phases complements reversed-phase high-performance liquid chromatography and capillary electrophoresis for peptide analysis. *J. Chromatogr. A* **724**, 378–383 (1996).

12. Garbis, S. D., Melse-Boonstra, A., West, C. E. & van Breemen, R. B. Determination of folates in human plasma using hydrophilic interaction chromatography-tandem mass spectrometry. *Anal. Chem.* **73**, 5358–5364 (2001).

13. Olsen, B. A. Hydrophilic interaction chromatography using amino and silica columns

for the determination of polar pharmaceuticals and impurities. *J. Chromatogr. A* **913**, 113–122 (2001).

14. Li, R. & Huang, J. Chromatographic behavior of epirubicin and its analogues on high-purity silica in hydrophilic interaction chromatography. *J. Chromatogr. A* **1041**, 163–169 (2004).

15. Guo, Y. & Gaiki, S. Retention behavior of small polar compounds on polar stationary phases in hydrophilic interaction chromatography. *J. Chromatogr. A* **1074**, 71–80 (2005).

16. Cubbon, S., Bradbury, T., Wilson, J. & Thomas-Oates, J. Hydrophilic interaction chromatography for mass spectrometric metabonomic studies of urine. *Anal. Chem.* **79**, 8911–8918 (2007).

17. Leonora. Types of detectors used in HPLC. *b-ac-co.uk* (2022).

18. Gross, J. . Mass Spectrometry. *Springer Int. Publ. Cham* (2017).

19. Fenn, J. B., Mann, M., Meng, C. K., Wong, S. F. & Whitehouse, C. M. Electrospray ionization for mass spectrometry of large biomolecules. *Science* **246**, 64–71 (1989).

20. Bruins, A. P. Mechanistic aspects of electrospray ionization. *J. Chromatogr. A* **794**, 345–357 (1998).

21. Banerjee, S. & Mazumdar, S. Electrospray ionization mass spectrometry: a technique to access the information beyond the molecular weight of the analyte. *Int. J. Anal. Chem.* **2012**, 282574 (2012).

22. Kebarle, P. & Verkerk, U. H. Electrospray: from ions in solution to ions in the gas phase, what we know now. *Mass Spectrom. Rev.* **28**, 898–917 (2009).

23. Byrdwell, W. C. Atmospheric pressure chemical ionization mass spectrometry for analysis of lipids. *Lipids* **36**, 327–346 (2001).

24. Rosenberg, E. The potential of organic (electrospray- and atmospheric pressure chemical ionisation) mass spectrometric techniques coupled to liquid-phase separation for speciation analysis. *J. Chromatogr. A* **1000**, 841–889 (2003).

25. Pitt, J. J. Principles and applications of liquid chromatography-mass spectrometry in clinical biochemistry. *Clin. Biochem. Rev.* **30**, 19–34 (2009).

26. Carvalho, V. M., Nakamura, O. H. & Vieira, J. G. H. Simultaneous quantitation of seven endogenous C-21 adrenal steroids by liquid chromatography tandem mass spectrometry in human serum. *J. Chromatogr. B, Anal. Technol. Biomed. life Sci.* **872**, 154–161 (2008).

27. Nelson, R. E., Grebe, S. K., OKane, D. J. & Singh, R. J. Liquid chromatography-tandem mass spectrometry assay for simultaneous measurement of estradiol and estrone in human plasma. *Clin. Chem.* **50**, 373–384 (2004).

28. Rauh, M., Gröschl, M., Rascher, W. & Dörr, H. G. Automated, fast and sensitive quantification of 17 alpha-hydroxy-progesterone, androstenedione and testosterone by tandem mass spectrometry with on-line extraction. *Steroids* **71**, 450–458 (2006).

29. McMaster, M. C. LC/MS: A Practical User's Guide. *John Wiley, Hoboken, N.J* (2005).

30. Payne, A. H. & Glish, G. L. Tandem mass spectrometry in quadrupole ion trap and ion cyclotron resonance mass spectrometers. *Methods Enzymol.* **402**, 109–148 (2005).

31. Tozuka, Z. *et al.* Strategy for structural elucidation of drugs and drug metabolites using (MS)n fragmentation in an electrospray ion trap. *J. Mass Spectrom.* **38**, 793–808 (2003).

32. Williamson, L. N. & Bartlett, M. G. Quantitative liquid chromatography/time-of-flight mass spectrometry. *Biomed. Chromatogr.* **21**, 567–576 (2007).

33. Bristow, A. W. T. Accurate mass measurement for the determination of elemental formula--a tutorial. *Mass Spectrom. Rev.* **25**, 99–111 (2006).

34. Chernushevich, I. V, Loboda, A. V & Thomson, B. A. An introduction to quadrupole-time-of-flight mass spectrometry. *J. Mass Spectrom.* **36**, 849–865 (2001).

35. Ens, W. & Standing, K. G. Hybrid quadrupole/time-of-flight mass spectrometers for analysis of biomolecules. *Methods Enzymol.* **402**, 49–78 (2005).

36. Hopfgartner, G. *et al.* Triple quadrupole linear ion trap mass spectrometer for the analysis of small molecules and macromolecules. *J. Mass Spectrom.* **39**, 845–855 (2004).

37. Gandhi, K. *et al. Advanced Analytical Techniques in Dairy Chemistry*. (Springer US, 2022).

38. Gereben, B., McAninch, E. A., Ribeiro, M. O. & Bianco, A. C. Scope and limitations of

iodothyronine deiodinases in hypothyroidism. *Nat. Rev. Endocrinol.* **11**, 642–652 (2015).

39. Luongo, C., Dentice, M. & Salvatore, D. Deiodinases and their intricate role in thyroid hormone homeostasis. *Nat. Rev. Endocrinol.* **15**, 479–488 (2019).

40. Burgus, R., Dunn, T. F., Desiderio, D. & Guillemin, R. [Molecular structure of the hypothalamic hypophysiotropic TRF factor of ovine origin: mass spectrometry demonstration of the PCA-His-Pro-NH2 sequence]. *Comptes rendus Hebd. des seances l'Academie des Sci. Ser. D Sci. Nat.* **269**, 1870–1873 (1969).

41. Fekete, C. & Lechan, R. M. Central regulation of hypothalamic-pituitary-thyroid axis under physiological and pathophysiological conditions. *Endocr. Rev.* **35**, 159–194 (2014).

42. Estrada, J. M., Soldin, D., Buckey, T. M., Burman, K. D. & Soldin, O. P. Thyrotropin isoforms: implications for thyrotropin analysis and clinical practice. *Thyroid* **24**, 411–423 (2014).

43. Canadian Society of Clinical Chemists position paper: standardization of selected polypeptide hormone measurements. *Clin. Biochem.* **25**, 415–424 (1992).

44. Borsò, M., Agretti, P., Zucchi, R. & Saba, A. Mass spectrometry in the diagnosis of thyroid disease and in the study of thyroid hormone metabolism. *Mass Spectrom. Rev.* **41**, 443–468 (2022).

45. Thienpont, L. M. *et al.* A Progress Report of the IFCC Committee for Standardization of Thyroid Function Tests. *Eur. Thyroid J.* **3**, 109–116 (2014).

46. Owen, W. E., Gantzer, M. Lou, Lyons, J. M., Rockwood, A. L. & Roberts, W. L. Functional sensitivity of seven automated thyroid stimulating hormone immunoassays. *Clin. Chim. Acta.* **412**, 2336–2339 (2011).

47. Spencer, C. A. *et al.* Applications of a new chemiluminometric thyrotropin assay to subnormal measurement. *J. Clin. Endocrinol. Metab.* **70**, 453–460 (1990).

48. Carvalho, D. P. & Dupuy, C. Thyroid hormone biosynthesis and release. *Mol. Cell. Endocrinol.* **458**, 6–15 (2017).

49. Citterio, C. E., Targovnik, H. M. & Arvan, P. The role of thyroglobulin in thyroid

hormonogenesis. *Nat. Rev. Endocrinol.* **15**, 323–338 (2019).

50. Wright, E. M. & Turk, E. The sodium/glucose cotransport family SLC5. *Pflugers Arch.* **447**, 510–518 (2004).

51. De La Vieja, A., Dohan, O., Levy, O. & Carrasco, N. Molecular analysis of the sodium/iodide symporter: impact on thyroid and extrathyroid pathophysiology. *Physiol. Rev.* **80**, 1083–1105 (2000).

52. Kogai, T. *et al.* Regulation by thyroid-stimulating hormone of sodium/iodide symporter gene expression and protein levels in FRTL-5 cells. *Endocrinology* **138**, 2227–2232 (1997).

53. Ohno, M., Zannini, M., Levy, O., Carrasco, N. & di Lauro, R. The paired-domain transcription factor Pax8 binds to the upstream enhancer of the rat sodium/iodide symporter gene and participates in both thyroid-specific and cyclic-AMP-dependent transcription. *Mol. Cell. Biol.* **19**, 2051–2060 (1999).

54. WOLFF, J. & CHAIKOFF, I. L. Plasma inorganic iodide as a homeostatic regulator of thyroid function. *J. Biol. Chem.* **174**, 555–564 (1948).

55. Eng, P. H. *et al.* Escape from the acute Wolff-Chaikoff effect is associated with a decrease in thyroid sodium/iodide symporter messenger ribonucleic acid and protein. *Endocrinology* **140**, 3404–3410 (1999).

56. WOLFF, J. & CHAIKOFF, I. L. The temporary nature of the inhibitory action of excess iodine on organic iodine synthesis in the normal thyroid. *Endocrinology* **45**, 504–13, illust (1949).

57. Gillam, M. P. *et al.* Functional characterization of pendrin in a polarized cell system. Evidence for pendrin-mediated apical iodide efflux. *J. Biol. Chem.* **279**, 13004–13010 (2004).

58. Portulano, C., Paroder-Belenitsky, M. & Carrasco, N. The Na+/I- symporter (NIS): mechanism and medical impact. *Endocr. Rev.* **35**, 106–149 (2014).

59. Pesce, L. *et al.* TSH regulates pendrin membrane abundance and enhances iodide efflux in thyroid cells. *Endocrinology* **153**, 512–521 (2012).

60. Iosco, C. *et al.* Anoctamin 1 is apically expressed on thyroid follicular cells and

contributes to ATP- and calcium-activated iodide efflux. *Cell. Physiol. Biochem. Int. J. Exp. Cell. Physiol. Biochem. Pharmacol.* **34**, 966–980 (2014).

61. van den Hove, M.-F. *et al.* The loss of the chloride channel, ClC-5, delays apical iodide efflux and induces a euthyroid goiter in the mouse thyroid gland. *Endocrinology* **147**, 1287–1296 (2006).

62. Yokoyama, N. & Taurog, A. Porcine thyroid peroxidase: relationship between the native enzyme and an active, highly purified tryptic fragment. *Mol. Endocrinol.* **2**, 838–844 (1988).

63. Godlewska, M. *et al.* A redundant role of human thyroid peroxidase propeptide for cellular, enzymatic, and immunological activity. *Thyroid* **24**, 371–382 (2014).

64. Belforte, F. S. *et al.* Kinetic characterization of human thyroperoxidase. Normal and pathological enzyme expression in Baculovirus system: a molecular model of functional expression. *Mol. Cell. Endocrinol.* **404**, 9–15 (2015).

65. Ameziane-El-Hassani, R. *et al.* Dual oxidase-2 has an intrinsic Ca2+-dependent H2O2-generating activity. *J. Biol. Chem.* **280**, 30046–30054 (2005).

66. Carvalho, D. P. & Dupuy, C. Role of the NADPH Oxidases DUOX and NOX4 in Thyroid Oxidative Stress. *Eur. Thyroid J.* **2**, 160–167 (2013).

67. Dunn, J. T. & Dunn, A. D. The importance of thyroglobulin structure for thyroid hormone biosynthesis. *Biochimie* **81**, 505–509 (1999).

68. Mondal, S., Raja, K., Schweizer, U. & Mugesh, G. Chemistry and Biology in the Biosynthesis and Action of Thyroid Hormones. *Angew. Chem. Int. Ed. Engl.* **55**, 7606–7630 (2016).

69. Bianco, A. C. & Kim, B. W. Deiodinases: implications of the local control of thyroid hormone action. *J. Clin. Invest.* **116**, 2571–2579 (2006).

70. Gnidehou, S. *et al.* Iodotyrosine dehalogenase 1 (DEHAL1) is a transmembrane protein involved in the recycling of iodide close to the thyroglobulin iodination site. *FASEB J. Off. Publ. Fed. Am. Soc. Exp. Biol.* **18**, 1574–1576 (2004).

71. Ortiga-Carvalho, T. M., Chiamolera, M. I., Pazos-Moura, C. C. & Wondisford, F. E. Hypothalamus-Pituitary-Thyroid Axis. *Compr. Physiol.* **6**, 1387–1428 (2016).

72. Medici, M., Visser, W. E., Visser, T. J. & Peeters, R. P. Genetic determination of the hypothalamic-pituitary-thyroid axis: where do we stand? *Endocr. Rev.* **36**, 214–244 (2015).

73. Fonseca, T. L. *et al.* Coordination of hypothalamic and pituitary T3 production regulates TSH expression. *J. Clin. Invest.* **123**, 1492–1500 (2013).

74. Köhrle, J. The deiodinase family: selenoenzymes regulating thyroid hormone availability and action. *Cell. Mol. Life Sci.* **57**, 1853–1863 (2000).

75. Bartalena, L. & Robbins, J. Thyroid hormone transport proteins. *Clin. Lab. Med.* **13**, 583–598 (1993).

76. Feldt-Rasmussen, U. & Rasmussen, Å. K. Thyroid hormone transport and actions. in *Diseases of the Thyroid in Childhood and Adolescence* vol. 11 80–103 (Karger Publishers, 2007).

77. Refetoff, S. Thyroid Hormone Serum Transport Proteins. in (eds. Feingold, K. R. et al.) (2000).

78. Peterson, P. A. Characteristics of a vitamin A-transporting protein complex occurring in human serum. *J. Biol. Chem.* **246**, 34–43 (1971).

79. Palha, J. A. Transthyretin as a thyroid hormone carrier: function revisited. *Clin. Chem. Lab. Med.* **40**, 1292–1300 (2002).

80. Schussler, G. C. The thyroxine-binding proteins. *Thyroid* **10**, 141–149 (2000).

81. Bernal, J., Guadaño-Ferraz, A. & Morte, B. Thyroid hormone transporters--functions and clinical implications. *Nat. Rev. Endocrinol.* **11**, 406–417 (2015).

82. Friesema, E. C. H. *et al.* Identification of monocarboxylate transporter 8 as a specific thyroid hormone transporter. *J. Biol. Chem.* **278**, 40128–40135 (2003).

83. Müller, J. *et al.* Tissue-specific alterations in thyroid hormone homeostasis in combined Mct10 and Mct8 deficiency. *Endocrinology* **155**, 315–325 (2014).

84. Friesema, E. C. H. *et al.* Effective cellular uptake and efflux of thyroid hormone by human monocarboxylate transporter 10. *Mol. Endocrinol.* **22**, 1357–1369 (2008).

85. Visser, W. E. *et al.* Study of the transport of thyroid hormone by transporters of the SLC10 family. *Mol. Cell. Endocrinol.* **315**, 138–145 (2010).

86. Friesema, E. C. *et al.* Thyroid hormone transport by the heterodimeric human system L amino acid transporter. *Endocrinology* **142**, 4339–4348 (2001).

87. Morimoto, E. *et al.* Establishment and characterization of mammalian cell lines stably expressing human L-type amino acid transporters. *J. Pharmacol. Sci.* **108**, 505–516 (2008).

88. del Amo, E. M., Urtti, A. & Yliperttula, M. Pharmacokinetic role of L-type amino acid transporters LAT1 and LAT2. *Eur. J. Pharm. Sci. Off. J. Eur. Fed. Pharm. Sci.* **35**, 161–174 (2008).

89. Visser, W. E., Friesema, E. C. H. & Visser, T. J. Minireview: thyroid hormone transporters: the knowns and the unknowns. *Mol. Endocrinol.* **25**, 1–14 (2011).

90. Davis, P. J., Goglia, F. & Leonard, J. L. Nongenomic actions of thyroid hormone. *Nat. Rev. Endocrinol.* **12**, 111–121 (2016).

91. Oiseth, S., Jones, L. & Maza, E. Thyroid Hormones | Concise Medical Knowledge. (2022).

92. Ortiga-Carvalho, T. M., Sidhaye, A. R. & Wondisford, F. E. Thyroid hormone receptors and resistance to thyroid hormone disorders. *Nat. Rev. Endocrinol.* **10**, 582–591 (2014).

93. Oetting, A. & Yen, P. M. New insights into thyroid hormone action. *Best Pract. Res. Clin. Endocrinol. Metab.* **21**, 193–208 (2007).

94. Kim, H.-Y. & Mohan, S. Role and Mechanisms of Actions of Thyroid Hormone on the Skeletal Development. *Bone Res.* **1**, 146–161 (2013).

95. Yen, P. M. Physiological and molecular basis of thyroid hormone action. *Physiol. Rev.* **81**, 1097–1142 (2001).

96. Brent, G. A. Mechanisms of thyroid hormone action. *J. Clin. Invest.* **122**, 3035–3043 (2012).

97. Saponaro, F., Sestito, S., Runfola, M., Rapposelli, S. & Chiellini, G. Selective Thyroid Hormone Receptor-Beta (TRβ) Agonists: New Perspectives for the Treatment of Metabolic and Neurodegenerative Disorders. *Front. Med.* **7**, 331 (2020).

98. Davis, P. J., Leonard, J. L. & Davis, F. B. Mechanisms of nongenomic actions of thyroid hormone. *Front. Neuroendocrinol.* **29**, 211–218 (2008).

99. Bergh, J. J. *et al.* Integrin alphaVbeta3 contains a cell surface receptor site for thyroid hormone that is linked to activation of mitogen-activated protein kinase and induction of angiogenesis. *Endocrinology* **146**, 2864–2871 (2005).

100. Storey, N. M. *et al.* Rapid signaling at the plasma membrane by a nuclear receptor for thyroid hormone. *Proc. Natl. Acad. Sci. U. S. A.* **103**, 5197–5201 (2006).

101. Davis, P. J., Davis, F. B., Mousa, S. A., Luidens, M. K. & Lin, H.-Y. Membrane receptor for thyroid hormone: physiologic and pharmacologic implications. *Annu. Rev. Pharmacol. Toxicol.* **51**, 99–115 (2011).

102. Campos-Barros, A. *et al.* Phenolic and tyrosyl ring iodothyronine deiodination and thyroid hormone concentrations in the human central nervous system. *J. Clin. Endocrinol. Metab.* **81**, 2179–2185 (1996).

103. Bianco, A. C., Salvatore, D., Gereben, B., Berry, M. J. & Larsen, P. R. Biochemistry, cellular and molecular biology, and physiological roles of the iodothyronine selenodeiodinases. *Endocr. Rev.* **23**, 38–89 (2002).

104. Moreno, M., Giacco, A., Di Munno, C. & Goglia, F. Direct and rapid effects of 3,5-diiodo-L-thyronine (T2). *Mol. Cell. Endocrinol.* **458**, 121–126 (2017).

105. Köhrle, J. The Colorful Diversity of Thyroid Hormone Metabolites. *Eur. Thyroid J.* **8**, 115–129 (2019).

106. Lanni, A., Moreno, M., Cioffi, M. & Goglia, F. Effect of 3,3'-di-iodothyronine and 3,5-di-iodothyronine on rat liver mitochondria. *J. Endocrinol.* **136**, 59–64 (1993).

107. Lombardi, A. *et al.* 3,5-Diiodo-L-thyronine rapidly enhances mitochondrial fatty acid oxidation rate and thermogenesis in rat skeletal muscle: AMP-activated protein kinase involvement. *Am. J. Physiol. Endocrinol. Metab.* **296**, E497-502 (2009).

108. Sacripanti, G. *et al.* 3,5-Diiodo-l-Thyronine Increases Glucose Consumption in Cardiomyoblasts Without Affecting the Contractile Performance in Rat Heart. *Front. Endocrinol. (Lausanne).* **9**, 282 (2018).

109. Accorroni, A., Saponaro, F. & Zucchi, R. Tissue thyroid hormones and thyronamines. *Heart Fail. Rev.* **21**, 373–390 (2016).

110. Saponaro, F. & Zucchi, R. TH Metabolism and Active TH Metabolites in the Heart BT

- Thyroid and Heart : A Comprehensive Translational Essay. in (eds. Iervasi, G., Pingitore, A., Gerdes, A. M. & Razvi, S.) 97–107 (Springer International Publishing, 2020). .

111. Lorenzini, L. *et al.* Assay of Endogenous 3,5-diiodo-L-thyronine (3,5-T(2)) and 3,3'-diiodo-L-thyronine (3,3'-T(2)) in Human Serum: A Feasibility Study. *Front. Endocrinol. (Lausanne).* **10**, 88 (2019).

112. Peeters, R. P.; Visser, T. J. Metabolism of Thyroid Hormone. *ENDText.com, Inc.* (2017).

113. Piehl, S., Hoefig, C. S., Scanlan, T. S. & Köhrle, J. Thyronamines--past, present, and future. *Endocr. Rev.* **32**, 64–80 (2011).

114. Scanlan, T. S. *et al.* 3-Iodothyronamine is an endogenous and rapid-acting derivative of thyroid hormone. *Nat. Med.* **10**, 638–642 (2004).

115. DeBarber, A. E., Geraci, T., Colasurdo, V. P., Hackenmueller, S. A. & Scanlan, T. S. Validation of a liquid chromatography-tandem mass spectrometry method to enable quantification of 3-iodothyronamine from serum. *J. Chromatogr. A* **1210**, 55–59 (2008).

116. Hoefig, C. S. *et al.* Biosynthesis of 3-Iodothyronamine From T4 in Murine Intestinal Tissue. *Endocrinology* **156**, 4356–4364 (2015).

117. Zucchi, R., Rutigliano, G. & Saponaro, F. Novel thyroid hormones. *Endocrine* **66**, 95–104 (2019).

118. Chiellini, G. *et al.* Cardiac effects of 3-iodothyronamine: a new aminergic system modulating cardiac function. *FASEB J. Off. Publ. Fed. Am. Soc. Exp. Biol.* **21**, 1597–1608 (2007).

119. Frascarelli, S. *et al.* Cardiac effects of trace amines: pharmacological characterization of trace amine-associated receptors. *Eur. J. Pharmacol.* **587**, 231–236 (2008).

120. Ghelardoni, S. *et al.* Modulation of cardiac ionic homeostasis by 3-iodothyronamine. *J. Cell. Mol. Med.* **13**, 3082–3090 (2009).

121. Frascarelli, S. *et al.* Cardioprotective effect of 3-iodothyronamine in perfused rat heart subjected to ischemia and reperfusion. *Cardiovasc. drugs Ther.* **25**, 307–313 (2011).

122. Accorroni, A. *et al.* Exogenous 3-Iodothyronamine Rescues the Entorhinal Cortex from β-Amyloid Toxicity. *Thyroid* **30**, 147–160 (2020).

123. Braulke, L. J. *et al.* 3-Iodothyronamine: a novel hormone controlling the balance between glucose and lipid utilisation. *J. Comp. Physiol. B, Biochem. Syst. Environ. Physiol.* **178**, 167–177 (2008).

124. Manni, M. E. *et al.* Pharmacological effects of 3-iodothyronamine (T1AM) in mice include facilitation of memory acquisition and retention and reduction of pain threshold. *Br. J. Pharmacol.* **168**, 354–362 (2013).

125. Manni, M. E. *et al.* 3-Iodothyronamine: a modulator of the hypothalamus-pancreas-thyroid axes in mice. *Br. J. Pharmacol.* **166**, 650–658 (2012).

126. Ghelardoni, S., Chiellini, G., Frascarelli, S., Saba, A. & Zucchi, R. Uptake and metabolic effects of 3-iodothyronamine in hepatocytes. *J. Endocrinol.* **221**, 101–110 (2014).

127. Zucchi, R., Accorroni, A. & Chiellini, G. Update on 3-iodothyronamine and its neurological and metabolic actions. *Front. Physiol.* **5**, 402 (2014).

128. Köhrle, J. & Biebermann, H. 3-Iodothyronamine-A Thyroid Hormone Metabolite With Distinct Target Profiles and Mode of Action. *Endocr. Rev.* **40**, 602–630 (2019).

129. Lorenzini, L. *et al.* Recovery of 3-Iodothyronamine and Derivatives in Biological Matrixes: Problems and Pitfalls. *Thyroid* **27**, 1323–1331 (2017).

130. Musilli, C. *et al.* Histamine mediates behavioural and metabolic effects of 3-iodothyroacetic acid, an endogenous end product of thyroid hormone metabolism. *Br. J. Pharmacol.* **171**, 3476–3484 (2014).

131. Laurino, A. *et al.* In the brain of mice, 3-iodothyronamine (T1AM) is converted into 3-iodothyroacetic acid (TA1) and it is included within the signaling network connecting thyroid hormone metabolites with histamine. *Eur. J. Pharmacol.* **761**, 130–134 (2015).

132. Chaker, L., Bianco, A. C., Jonklaas, J. & Peeters, R. P. Hypothyroidism. *Lancet (London, England)* **390**, 1550–1562 (2017).

133. Patil N, Rehman A, J. I. Hypothyroidism [Updated 2023 Aug 8]. *StatPearls [Internet]. Treasure Isl. StatPearls Publ.* (2023).

134. Bathla, M., Singh, M. & Relan, P. Prevalence of anxiety and depressive symptoms among patients with hypothyroidism. *Indian J. Endocrinol. Metab.* **20**, 468–474 (2016).

135. Bauer, M., Goetz, T., Glenn, T. & Whybrow, P. C. The thyroid-brain interaction in

thyroid disorders and mood disorders. *J. Neuroendocrinol.* **20**, 1101–1114 (2008).

136. Bernal, J., Guadaño-Ferraz, A. & Morte, B. Perspectives in the study of thyroid hormone action on brain development and function. *Thyroid* **13**, 1005–1012 (2003).

137. Eayrs. "The cerebral cortex of normal and hypothyroid rats." *Acto Anat.* **25**, 160–183 (1955).

138. Gothié, J.-D., Demeneix, B. & Remaud, S. Comparative approaches to understanding thyroid hormone regulation of neurogenesis. *Mol. Cell. Endocrinol.* **459**, 104–115 (2017).

139. Correia, N. *et al.* Evidence for a specific defect in hippocampal memory in overt and subclinical hypothyroidism. *J. Clin. Endocrinol. Metab.* **94**, 3789–3797 (2009).

140. Göbel, A. *et al.* Effect of Mild Thyrotoxicosis on Performance and Brain Activations in a Working Memory Task. *PLoS One* **11**, e0161552 (2016).

141. Miller, K. J. *et al.* Verbal memory retrieval deficits associated with untreated hypothyroidism. *J. Neuropsychiatry Clin. Neurosci.* **19**, 132–136 (2007).

142. Montero-Pedrazuela A, Venero C., Lavado-Autric R., Fernandez-Lamo I., Garcia-Verdugo J.M., Bernal J., et A. "Modulation of adult hippocampal neurogenesis by thyroid hormones: Implication in depressive-like behaviour." *Mol. Psychiatry* **11**, 361–371 (2006).

143. Hosseini, M. *et al.* The beneficial effects of olibanum on memory deficit induced by hypothyroidism in adult rats tested in Morris water maze. *Arch. Pharm. Res.* **33**, 463–468 (2010).

144. Alzoubi, K. H., Gerges, N. Z., Aleisa, A. M. & Alkadhi, K. A. Levothyroxin restores hypothyroidism-induced impairment of hippocampus-dependent learning and memory: Behavioral, electrophysiological, and molecular studies. *Hippocampus* **19**, 66–78 (2009).

145. Artis, A. S. *et al.* Experimental hypothyroidism delays field excitatory post-synaptic potentials and disrupts hippocampal long-term potentiation in the dentate gyrus of hippocampal formation and Y-maze performance in adult rats. *J. Neuroendocrinol.* **24**, 422–433 (2012).

146. Yu, T.-S., Dandekar, M., Monteggia, L. M., Parada, L. F. & Kernie, S. G. Temporally regulated expression of Cre recombinase in neural stem cells. *Genesis* **41**, 147–153 (2005).

147. Kapoor, R., Desouza, L. A., Nanavaty, I. N., Kernie, S. G. & Vaidya, V. A. Thyroid hormone accelerates the differentiation of adult hippocampal progenitors. *J. Neuroendocrinol.* **24**, 1259–1271 (2012).

148. Gould, E., Beylin, A., Tanapat, P., Reeves, A. & Shors, T. J. Learning enhances adult neurogenesis in the hippocampal formation. *Nat. Neurosci.* **2**, 260–265 (1999).

149. Schinder, A. F. & Gage, F. H. A hypothesis about the role of adult neurogenesis in hippocampal function. *Physiology (Bethesda).* **19**, 253–261 (2004).

150. Migaud, M., Butruille, L., Duittoz, A., Pillon, D. & Batailler, M. Adult neurogenesis and reproductive functions in mammals. *Theriogenology* **86**, 313–323 (2016).

151. Apple, D. M., Fonseca, R. S. & Kokovay, E. The role of adult neurogenesis in psychiatric and cognitive disorders. *Brain Res.* **1655**, 270–276 (2017).

152. Schroeder, A. C. & Privalsky, M. L. Thyroid hormones, t3 and t4, in the brain. *Front. Endocrinol. (Lausanne).* **5**, 40 (2014).

153. Schreiber, G. *et al.* Thyroxine transport from blood to brain via transthyretin synthesis in choroid plexus. *Am. J. Physiol.* **258**, R338-45 (1990).

154. Wirth, E. K., Schweizer, U. & Köhrle, J. Transport of thyroid hormone in brain. *Front. Endocrinol. (Lausanne).* **5**, 98 (2014).

155. Informatics, I. I. for H. Medicine use and shifting costs of healthcare. (2014).

156. Biondi, B. & Wartofsky, L. Combination treatment with T4 and T3: toward personalized replacement therapy in hypothyroidism? *J. Clin. Endocrinol. Metab.* **97**, 2256–2271 (2012).

157. Hackenmueller, S. A., Marchini, M., Saba, A., Zucchi, R. & Scanlan, T. S. Biosynthesis of 3-iodothyronamine (T1AM) is dependent on the sodium-iodide symporter and thyroperoxidase but does not involve extrathyroidal metabolism of T4. *Endocrinology* **153**, 5659–5667 (2012).

158. Gordon, J. T., Kaminski, D. M., Rozanov, C. B. & Dratman, M. B. Evidence that 3,3',5-

triiodothyronine is concentrated in and delivered from the locus coeruleus to its noradrenergic targets via anterograde axonal transport. *Neuroscience* **93**, 943–954 (1999).

159. James, T. D., Moffett, S. X., Scanlan, T. S. & Martin, J. V. Effects of acute microinjections of the thyroid hormone derivative 3-iodothyronamine to the preoptic region of adult male rats on sleep, thermoregulation and motor activity. *Horm. Behav.* **64**, 81–88 (2013).

160. Bellusci, L. *et al.* New Insights into the Potential Roles of 3-Iodothyronamine (T1AM) and Newly Developed Thyronamine-Like TAAR1 Agonists in Neuroprotection. *Front. Pharmacol.* **8**, 905 (2017).

161. Tozzi, F. *et al.* T1AM-TAAR1 signalling protects against OGD-induced synaptic dysfunction in the entorhinal cortex. *Neurobiol. Dis.* **151**, 105271 (2021).

162. Aldosari, D. I., Malik, A., Alhomida, A. S. & Ola, M. S. Implications of Diabetes-Induced Altered Metabolites on Retinal Neurodegeneration. *Frontiers in neuroscience* vol. 16 938029 (2022).

163. Federation, I. D. IDF Diabetes Atlas. 10th edn. Belgium, Brussels. (2021).

164. Teo, Z. L. *et al.* Global Prevalence of Diabetic Retinopathy and Projection of Burden through 2045: Systematic Review and Meta-analysis. *Ophthalmology* **128**, 1580–1591 (2021).

165. Narayanan, S. P. *et al.* Arginase in retinopathy. *Prog. Retin. Eye Res.* **36**, 260–280 (2013).

166. Amato, R. *et al.* Morpho-functional analysis of the early changes induced in retinal ganglion cells by the onset of diabetic retinopathy: The effects of a neuroprotective strategy. *Pharmacol. Res.* **185**, 106516 (2022).

167. Hernández, C., Dal Monte, M., Simó, R. & Casini, G. Neuroprotection as a Therapeutic Target for Diabetic Retinopathy. *J. Diabetes Res.* **2016**, 9508541 (2016).

168. Rossino, M. G., Dal Monte, M. & Casini, G. Relationships Between Neurodegeneration and Vascular Damage in Diabetic Retinopathy. *Front. Neurosci.* **13**, 1172 (2019).

169. Amato, R., Biagioni, M., Cammalleri, M., Dal Monte, M. & Casini, G. VEGF as a

Survival Factor in Ex Vivo Models of Early Diabetic Retinopathy. *Invest. Ophthalmol. Vis. Sci.* **57**, 3066–3076 (2016).

170. Rossino, M. G. *et al.* Oxidative Stress Induces a VEGF Autocrine Loop in the Retina: Relevance for Diabetic Retinopathy. *Cells* **9**, (2020).

171. Gong, Q., Wang, H., Yu, P., Qian, T. & Xu, X. Protective or Harmful: The Dual Roles of Autophagy in Diabetic Retinopathy. *Front. Med.* **8**, 644121 (2021).

172. Forini, F., Nicolini, G., Kusmic, C. & Iervasi, G. Protective Effects of Euthyroidism Restoration on Mitochondria Function and Quality Control in Cardiac Pathophysiology. *Int. J. Mol. Sci.* **20**, (2019).

173. Cioffi, F., Giacco, A., Goglia, F. & Silvestri, E. Bioenergetic Aspects of Mitochondrial Actions of Thyroid Hormones. *Cells* **11**, (2022).

174. Wrutniak-Cabello, C., Casas, F. & Cabello, G. Thyroid hormone action in mitochondria. *J. Mol. Endocrinol.* **26**, 67–77 (2001).

175. Flamant, F. *et al.* International Union of Pharmacology. LIX. The pharmacology and classification of the nuclear receptor superfamily: thyroid hormone receptors. *Pharmacol. Rev.* **58**, 705–711 (2006).

176. Ng, L., Ma, M., Curran, T. & Forrest, D. Developmental expression of thyroid hormone receptor beta2 protein in cone photoreceptors in the mouse. *Neuroreport* **20**, 627–631 (2009).

177. Ng, L., Liu, H., Liu, Y. & Forrest, D. Biphasic expression of thyroid hormone receptor TRβ1 in mammalian retina and anterior ocular tissues. *Front. Endocrinol. (Lausanne).* **14**, 1174600 (2023).

178. Henning, Y. & Szafranski, K. Age-Dependent Changes of Monocarboxylate Transporter 8 Availability in the Postnatal Murine Retina. *Front. Cell. Neurosci.* **10**, 205 (2016).

179. Arbogast, P., Flamant, F., Godement, P., Glösmann, M. & Peichl, L. Thyroid Hormone Signaling in the Mouse Retina. *PLoS One* **11**, e0168003 (2016).

180. Ng, L. *et al.* Type 3 deiodinase, a thyroid-hormone-inactivating enzyme, controls survival and maturation of cone photoreceptors. *J. Neurosci. Off. J. Soc. Neurosci.* **30**, 3347–3357 (2010).

181. Sawant, O. *et al.* Light-Regulated Thyroid Hormone Signaling Is Required for Rod Photoreceptor Development in the Mouse Retina. *Invest. Ophthalmol. Vis. Sci.* **56**, 8248–8257 (2015).

182. Yang, F., Ma, H., Butler, M. R. & Ding, X.-Q. Deficiency of type 2 iodothyronine deiodinase reduces necroptosis activity and oxidative stress responses in retinas of Leber congenital amaurosis model mice. *FASEB J. Off. Publ. Fed. Am. Soc. Exp. Biol.* **32**, fj201800484RR (2018).

183. Yang, F. *et al.* Targeting iodothyronine deiodinases locally in the retina is a therapeutic strategy for retinal degeneration. *FASEB J. Off. Publ. Fed. Am. Soc. Exp. Biol.* **30**, 4313–4325 (2016).

184. Gao, R. *et al.* Low T3 syndrome as a predictor of poor prognosis in chronic lymphocytic leukemia. *Int. J. cancer* **143**, 466–477 (2018).

185. Lo, J. C., Chertow, G. M., Go, A. S. & Hsu, C.-Y. Increased prevalence of subclinical and clinical hypothyroidism in persons with chronic kidney disease. *Kidney Int.* **67**, 1047–1052 (2005).

186. Huang, G.-Q. *et al.* Low triiodothyronine syndrome is associated with hemorrhagic transformation in patients with acute ischaemic stroke. *Aging (Albany. NY).* **11**, 6385–6397 (2019).

187. Iervasi, G. *et al.* Low-T3 syndrome: a strong prognostic predictor of death in patients with heart disease. *Circulation* **107**, 708–713 (2003).

188. Heidari, Z. & Asadzadeh, R. Subclinical Hypothyroidism Is a Risk Factor for Diabetic Retinopathy in Patients with Type 2 Diabetes Mellitus. *Med. J. Islam. Repub. Iran* **35**, 186 (2021).

189. Hu, Y. *et al.* Association of Thyroid Hormone Levels with Microvascular Complications in Euthyroid Type 2 Diabetes Mellitus Patients. *Diabetes. Metab. Syndr. Obes.* **15**, 2467–2477 (2022).

190. Kong, X. *et al.* Association between Free Thyroxine Levels and Diabetic Retinopathy in Euthyroid Patients with Type 2 Diabetes Mellitus. *Endocr. Res.* **45**, 111–118 (2020).

191. Mantzouratou, P., Lavecchia, A. M., Novelli, R. & Xinaris, C. Thyroid Hormone Signalling Alteration in Diabetic Nephropathy and Cardiomyopathy: a “Switch” to the

Foetal Gene Programme. *Curr. Diab. Rep.* **20**, 58 (2020).

192. Nicolini, G. *et al.* Early and Short-term Triiodothyronine Supplementation Prevents Adverse Postischemic Cardiac Remodeling: Role of Transforming Growth Factor-β1 and Antifibrotic miRNA Signaling. *Mol. Med.* **21**, 900–911 (2016).

193. Forini, F. *et al.* Triiodothyronine prevents cardiac ischemia/reperfusion mitochondrial impairment and cell loss by regulating miR30a/p53 axis. *Endocrinology* **155**, 4581–4590 (2014).

194. Forini, F. *et al.* Integrative analysis of differentially expressed genes and miRNAs predicts complex T3-mediated protective circuits in a rat model of cardiac ischemia reperfusion. *Sci. Rep.* **8**, 13870 (2018).

195. A. Pingitore, F. Mastorci, P. Piaggi, G.D. Aquaro, S. Molinaro, M. Ravani, A. De & Caterina, G. Trianni, R. Ndreu, S. Berti, C. Vassalle, G. I. sefulness of Myocardial, triiodothyronine replacement therapy in patients with ST elevation THIRST, infarction and borderline/reduced triiodothyronine levels (from the study). *Am. J. Cardiol.* **123**, 905–912.

196. Little, A. G. Local Regulation of Thyroid Hormone Signaling. *Vitam. Horm.* **106**, 1–17 (2018).

197. Cicatiello, A. G., Di Girolamo, D. & Dentice, M. Metabolic Effects of the Intracellular Regulation of Thyroid Hormone: Old Players, New Concepts. *Front. Endocrinol. (Lausanne).* **9**, 474 (2018).

198. Vale, C., Neves, J. S., von Hafe, M., Borges-Canha, M. & Leite-Moreira, A. The Role of Thyroid Hormones in Heart Failure. *Cardiovasc. drugs Ther.* **33**, 179–188 (2019).

199. Sawano, E., Negishi, T., Aoki, T., Murakami, M. & Tashiro, T. Alterations in local thyroid hormone signaling in the hippocampus of the SAMP8 mouse at younger ages: association with delayed myelination and behavioral abnormalities. *J. Neurosci. Res.* **91**, 382–392 (2013).

200. Gereben, B. *et al.* Cellular and molecular basis of deiodinase-regulated thyroid hormone signaling. *Endocr. Rev.* **29**, 898–938 (2008).

201. Mastropasqua, R. *et al.* Role of microRNAs in the modulation of diabetic retinopathy. *Prog. Retin. Eye Res.* **43**, 92–107 (2014).

202. Shafabakhsh, R., Aghadavod, E., Mobini, M., Heidari-Soureshjani, R. & Asemi, Z. Association between microRNAs expression and signaling pathways of inflammatory markers in diabetic retinopathy. *J. Cell. Physiol.* **234**, 7781–7787 (2019).

203. Smit-McBride, Z. & Morse, L. S. MicroRNA and diabetic retinopathy-biomarkers and novel therapeutics. *Ann. Transl. Med.* **9**, 1280 (2021).

204. Kowluru, R. A. Mitochondrial Stability in Diabetic Retinopathy: Lessons Learned From Epigenetics. *Diabetes* **68**, 241–247 (2019).

205. Iglesias, A., García-Nimo, L., Cocho de Juan, J. A. & Moreno, J. C. Towards the pre-clinical diagnosis of hypothyroidism caused by iodotyrosine deiodinase (DEHAL1) defects. *Best Pract. Res. Clin. Endocrinol. Metab.* **28**, 151–159 (2014).

206. Pouya Alikhani, Cristian González Guerrero, Andrea Bertolini, Valentina Vitelli, Marco Borsó, Rita M. Regojo, Teresa Peluso, Federico Salas-Lucia, Antonio de la Vieja, Alessandro Saba, Riccardo Zucchi, J. C. M. Dehal1 Deficiency disrupts Thyroglobulin Homeostasis and Impairs Iodine Storage. *Abstr. Conf. 45th Annu. Meet. Eur. Thyroid Assoc.* (2023).

207. Sun, X. *et al.* Expression of Iodotyrosine Deiodinase in Thyroid and Other Organs in Iodine-Deficient and Iodine-Excess Rats. *Biol. Trace Elem. Res.* **167**, 272–279 (2015).

208. Moreno, J. C. Identification of novel genes involved in congenital hypothyroidism using serial analysis of gene expression. *Horm. Res.* **60 Suppl 3**, 96–102 (2003).

209. Gnidehou, S. *et al.* Cloning and characterization of a novel isoform of iodotyrosine dehalogenase 1 (DEHAL1) DEHAL1C from human thyroid: comparisons with DEHAL1 and DEHAL1B. *Thyroid* **16**, 715–724 (2006).

210. Thomas, S. R., McTamney, P. M., Adler, J. M., Laronde-Leblanc, N. & Rokita, S. E. Crystal structure of iodotyrosine deiodinase, a novel flavoprotein responsible for iodide salvage in thyroid glands. *J. Biol. Chem.* **284**, 19659–19667 (2009).

211. Krause, K. *et al.* Characterisation of DEHAL1 expression in thyroid pathologies. *Eur. J. Endocrinol.* **156**, 295–301 (2007).

212. Sun, Z., Su, Q. & Rokita, S. E. The distribution and mechanism of iodotyrosine deiodinase defied expectations. *Arch. Biochem. Biophys.* **632**, 77–87 (2017).

213. Solis-S, J. C. *et al.* Inhibition of intrathyroidal dehalogenation by iodide. *J. Endocrinol.* **208**, 89–96 (2011).

214. Moreno, J. C. *et al.* Mutations in the iodotyrosine deiodinase gene and hypothyroidism. *N. Engl. J. Med.* **358**, 1811–1818 (2008).

215. Moreno, J. C. & Visser, T. J. Genetics and phenomics of hypothyroidism and goiter due to iodotyrosine deiodinase (DEHAL1) gene mutations. *Mol. Cell. Endocrinol.* **322**, 91–98 (2010).

216. Afink, G. *et al.* Molecular characterization of iodotyrosine dehalogenase deficiency in patients with hypothyroidism. *J. Clin. Endocrinol. Metab.* **93**, 4894–4901 (2008).

217. Schulz, E.; Ainhoa, I.; Halit Ilker, A.; Knut, H.; Moreno, J. C. Goitrous Hypothyroidism of Pubertal Onset Caused by a Novel Mutation in Dehal-1 Gene. *54th Annu. Meet. ESPE* (2015).

218. Welsh, K. J. & Soldin, S. J. DIAGNOSIS OF ENDOCRINE DISEASE: How reliable are free thyroid and total T3 hormone assays? *Eur. J. Endocrinol.* **175**, R255–R263 (2016).

219. Thienpont, L. M., Van Uytfanghe, K., Poppe, K. & Velkeniers, B. Determination of free thyroid hormones. *Best Pract. Res. Clin. Endocrinol. Metab.* **27**, 689–700 (2013).

220. Faix, J. D. Principles and pitfalls of free hormone measurements. *Best Pract. Res. Clin. Endocrinol. Metab.* **27**, 631–645 (2013).

221. Midgley, J. E. The free thyroid hormone hypothesis and measurement of free hormones. *Clin. Chem.* **39**, 1342–1344 (1993).

222. Midgley, J. E. Direct and indirect free thyroxine assay methods: theory and practice. *Clin. Chem.* **47**, 1353–1363 (2001).

223. Holm, S. S., Hansen, S. H., Faber, J. & Staun-Olsen, P. Reference methods for the measurement of free thyroid hormones in blood: evaluation of potential reference methods for free thyroxine. *Clin. Biochem.* **37**, 85–93 (2004).

224. Tikanoja, S. H. & Liewendahl, B. K. New ultrafiltration method for free thyroxin compared with equilibrium dialysis in patients with thyroid dysfunction and nonthyroidal illness. *Clin. Chem.* **36**, 800–804 (1990).

225. Bock, J. L. The new era of automated immunoassay. *Am. J. Clin. Pathol.* **113**, 628–646 (2000).

226. van Deventer, H. E., Mendu, D. R., Remaley, A. T. & Soldin, S. J. Inverse log-linear relationship between thyroid-stimulating hormone and free thyroxine measured by direct analog immunoassay and tandem mass spectrometry. *Clin. Chem.* **57**, 122–127 (2011).

227. van Deventer, H. E. & Soldin, S. J. The expanding role of tandem mass spectrometry in optimizing diagnosis and treatment of thyroid disease. *Adv. Clin. Chem.* **61**, 127–152 (2013).

228. Heki, N., Noto, M., Hosojima, H., Takahashi, S. & Murata, T. [Analysis of thyroid hormones in serum and urine by mass fragmentography using GC-MS]. *Nihon Naibunpi Gakkai Zasshi* **52**, 149–157 (1976).

229. Möller, B., Falk, O. & Björkhem, I. Isotope dilution--mass spectrometry of thyroxin proposed as a reference method. *Clin. Chem.* **29**, 2106–2110 (1983).

230. Ramsden, D. B. & Farmer, M. J. Development of a gas chromatographic selected ion monitoring assay for thyroxine (T4) in human serum. *Biomed. Mass Spectrom.* **11**, 421–427 (1984).

231. Siekmann, L. Measurement of thyroxine in human serum by isotope dilution mass spectrometry. Definitive methods in clinical chemistry, V. *Biomed. Environ. Mass Spectrom.* **14**, 683–688 (1987).

232. Thienpont, L. M., De Brabandere, V. I., Stöckl, D. & De Leenheer, A. P. Development of a new method for the determination of thyroxine in serum based on isotope dilution gas chromatography mass spectrometry. *Biol. Mass Spectrom.* **23**, 475–482 (1994).

233. Thienpont, L. M., Fierens, C., De Leenheer, A. P. & Przywara, L. Isotope dilution-gas chromatography/mass spectrometry and liquid chromatography/electrospray ionization-tandem mass spectrometry for the determination of triiodo- L-thyronine in serum. *Rapid Commun. Mass Spectrom.* **13**, 1924–1931 (1999).

234. De Brabandere, V. I., Hou, P., Stöckl, D., Thienpont, L. M. & De Leenheer, A. P. Isotope dilution-liquid chromatography/electrospray ionization-tandem mass spectrometry for the determination of serum thyroxine as a potential reference method. *Rapid Commun.*

Mass Spectrom. **12**, 1099–1103 (1998).

235. Saba, A. *et al.* Tissue distribution and cardiac metabolism of 3-iodothyronamine. *Endocrinology* **151**, 5063–5073 (2010).

236. Tai, S. S.-C., Sniegoski, L. T. & Welch, M. J. Candidate reference method for total thyroxine in human serum: use of isotope-dilution liquid chromatography-mass spectrometry with electrospray ionization. *Clin. Chem.* **48**, 637–642 (2002).

237. Van Uytfanghe, K., Stöckl, D. & Thienpont, L. M. Development of a simplified sample pretreatment procedure as part of an isotope dilution-liquid chromatography/tandem mass spectrometry candidate reference measurement procedure for serum total thyroxine. *Rapid communications in mass spectrometry : RCM* vol. 18 1539–1540 (2004).

238. Zhang, Y., Conrad, A. H. & Conrad, G. W. Detection and quantification of 3,5,3'-triiodothyronine and 3,3',5'-triiodothyronine by electrospray ionization tandem mass spectrometry. *J. Am. Soc. Mass Spectrom.* **16**, 1781–1786 (2005).

239. Wang, D. & Stapleton, H. M. Analysis of thyroid hormones in serum by liquid chromatography-tandem mass spectrometry. *Anal. Bioanal. Chem.* **397**, 1831–1839 (2010).

240. Soukhova, N., Soldin, O. P. & Soldin, S. J. Isotope dilution tandem mass spectrometric method for T4/T3. *Clin. Chim. Acta.* **343**, 185–190 (2004).

241. Sakai, H. *et al.* Correlation between Serum Levels of 3,3',5'-Triiodothyronine and Thyroid Hormones Measured by Liquid Chromatography-Tandem Mass Spectrometry and Immunoassay. *PLoS One* **10**, e0138864 (2015).

242. Saba, A. *et al.* Quantification of thyroxine and 3,5,3'-triiodo-thyronine in human and animal hearts by a novel liquid chromatography-tandem mass spectrometry method. *Horm. Metab. Res. = Horm. und Stoffwechselforsch. = Horm. Metab.* **46**, 628–634 (2014).

243. Richards, K. H. *et al.* A combined LC-MS/MS and LC-MS(3) multi-method for the quantification of iodothyronines in human blood serum. *Anal. Bioanal. Chem.* **411**, 5605–5616 (2019).

244. Jongejan, R. M. S. *et al.* A Mass Spectrometry-Based Panel of Nine Thyroid Hormone

Metabolites in Human Serum. *Clin. Chem.* **66**, 556–566 (2020).

245. Van Uytfanghe, K., Stöckl, D., Ross, H. A. & Thienpont, L. M. Use of frozen sera for FT4 standardization: investigation by equilibrium dialysis combined with isotope dilution-mass spectrometry and immunoassay. *Clin. Chem.* **52**, 1817–1821 (2006).

246. Thienpont, L. M. *et al.* Proposal of a candidate international conventional reference measurement procedure for free thyroxine in serum. *Clin. Chem. Lab. Med.* **45**, 934–936 (2007).

247. Yue, B. *et al.* Free thyroid hormones in serum by direct equilibrium dialysis and online solid-phase extraction--liquid chromatography/tandem mass spectrometry. *Clin. Chem.* **54**, 642–651 (2008).

248. La'ulu, S. L., Rasmussen, K. J. & Straseski, J. A. Pediatric Reference Intervals for Free Thyroxine and Free Triiodothyronine by Equilibrium Dialysis-Liquid Chromatography-Tandem Mass Spectrometry. *J. Clin. Res. Pediatr. Endocrinol.* **8**, 26–31 (2016).

249. Soldin, S. J., Soukhova, N., Janicic, N., Jonklaas, J. & Soldin, O. P. The measurement of free thyroxine by isotope dilution tandem mass spectrometry. *Clin. Chim. Acta.* **358**, 113–118 (2005).

250. Gu, J., Soldin, O. P. & Soldin, S. J. Simultaneous quantification of free triiodothyronine and free thyroxine by isotope dilution tandem mass spectrometry. *Clin. Biochem.* **40**, 1386–1391 (2007).

251. Kiebooms, J. A. L., Wauters, J., Vanden Bussche, J. & Vanhaecke, L. Validated ultra high performance liquid chromatography-tandem mass spectrometry method for quantitative analysis of total and free thyroid hormones in bovine serum. *J. Chromatogr. A* **1345**, 164–173 (2014).

252. Tanoue, R. *et al.* Determination of free thyroid hormones in animal serum/plasma using ultrafiltration in combination with ultra-fast liquid chromatography-tandem mass spectrometry. *J. Chromatogr. A* **1539**, 30–40 (2018).

253. Köhrle, J. & Richards, K. H. Mass Spectrometry-Based Determination of Thyroid Hormones and Their Metabolites in Endocrine Diagnostics and Biomedical Research - Implications for Human Serum Diagnostics. *Exp. Clin. Endocrinol. diabetes Off. journal, Ger. Soc. Endocrinol. [and] Ger. Diabetes Assoc.* **128**, 358–374 (2020).

254. Panici, J. A. *et al.* Early life growth hormone treatment shortens longevity and decreases cellular stress resistance in long-lived mutant mice. *FASEB J. Off. Publ. Fed. Am. Soc. Exp. Biol.* **24**, 5073–5079 (2010).

255. Azrad-Leibovich, T. *et al.* Characterization of Diabetic Retinopathy in Two Mouse Models and Response to a Single Injection of Anti-Vascular Endothelial Growth Factor. *Int. J. Mol. Sci.* **24**, (2022).

256. Bogdanov, P. *et al.* The db/db mouse: a useful model for the study of diabetic retinal neurodegeneration. *PLoS One* **9**, e97302 (2014).

257. Szabadfi, K., Pinter, E., Reglodi, D. & Gabriel, R. Neuropeptides, trophic factors, and other substances providing morphofunctional and metabolic protection in experimental models of diabetic retinopathy. *Int. Rev. Cell Mol. Biol.* **311**, 1–121 (2014).

258. Losi, P. *et al.* Bilayered Fibrin-Based Electrospun-Sprayed Scaffold Loaded with Platelet Lysate Enhances Wound Healing in a Diabetic Mouse Model. *Nanomater. (Basel, Switzerland)* **10**, (2020).

259. Donzelli, R. *et al.* Effect of Hypothyroidism and Hyperthyroidism on Tissue Thyroid Hormone Concentrations in Rat. *Eur. Thyroid J.* **5**, 27–34 (2016).

260. González-Guerrero, C. *et al.* Iodotyrosines Are Biomarkers for Preclinical Stages of Iodine-Deficient Hypothyroidism in Dehal1-Knockout Mice. *Thyroid* **33**, 752–761 (2023).

261. Matuszewski, B. K., Constanzer, M. L. & Chavez-Eng, C. M. Strategies for the assessment of matrix effect in quantitative bioanalytical methods based on HPLC-MS/MS. *Anal. Chem.* **75**, 3019–3030 (2003).

262. Agency, E. M. Guideline on bioanalytical method validation. (2015).

263. Shareef, R. *et al.* Congenital Hypothyroidism in Two Sudanese Families Harboring a Novel Iodotyrosine Deiodinase Mutation (IYD R279C). *Thyroid* **33**, 261–266 (2023).

264. Rutigliano, G. *et al.* Effect of Combined Levothyroxine (L-T(4)) and 3-Iodothyronamine (T(1)AM) Supplementation on Memory and Adult Hippocampal Neurogenesis in a Mouse Model of Hypothyroidism. *Int. J. Mol. Sci.* **24**, (2023).

265. Forini, F. *et al.* Local modulation of thyroid hormone signaling in the retina affects the

development of diabetic retinopathy. *Biochim. Biophys. acta. Mol. basis Dis.* **1870**, 166892 (2024).

266. Livak, K. J. & Schmittgen, T. D. Analysis of relative gene expression data using real-time quantitative PCR and the 2(Δ Δ C(T)) Method. *Methods* **25**, 402–408 (2001).

267. Agardh, E., Bruun, A. & Agardh, C. D. Retinal glial cell immunoreactivity and neuronal cell changes in rats with STZ-induced diabetes. *Curr. Eye Res.* **23**, 276–284 (2001).

268. Walf, A. A. & Frye, C. A. The use of the elevated plus maze as an assay of anxiety-related behavior in rodents. *Nat. Protoc.* **2**, 322–328 (2007).

269. Cruz, A. P., Frei, F. & Graeff, F. G. Ethopharmacological analysis of rat behavior on the elevated plus-maze. *Pharmacol. Biochem. Behav.* **49**, 171–176 (1994).

270. Fernandes, C. & File, S. E. The influence of open arm ledges and maze experience in the elevated plus-maze. *Pharmacol. Biochem. Behav.* **54**, 31–40 (1996).

271. Itoh, K. *et al.* An Nrf2/small Maf heterodimer mediates the induction of phase II detoxifying enzyme genes through antioxidant response elements. *Biochem. Biophys. Res. Commun.* **236**, 313–322 (1997).

272. Hoffmann, A. & Baltimore, D. Circuitry of nuclear factor kappaB signaling. *Immunol. Rev.* **210**, 171–186 (2006).

273. Jornayvaz, F. R. & Shulman, G. I. Regulation of mitochondrial biogenesis. *Essays Biochem.* **47**, 69–84 (2010).

274. McGarry, J. D. & Brown, N. F. The mitochondrial carnitine palmitoyltransferase system. From concept to molecular analysis. *Eur. J. Biochem.* **244**, 1–14 (1997).

275. Westermann, B. Mitochondrial fusion and fission in cell life and death. *Nat. Rev. Mol. Cell Biol.* **11**, 872–884 (2010).

276. Simonides, W. S. *et al.* Hypoxia-inducible factor induces local thyroid hormone inactivation during hypoxic-ischemic disease in rats. *J. Clin. Invest.* **118**, 975–983 (2008).

277. Canale, P. *et al.* Role of miR-133/Dio3 Axis in the T3-Dependent Modulation of Cardiac mitoK-ATP Expression. *Int. J. Mol. Sci.* **23**, (2022).

278. Hansen, G. M. *et al.* Large-scale gene trapping in C57BL/6N mouse embryonic stem

cells. *Genome Res.* **18**, 1670–1679 (2008).

279. Mathi, A. A., Gaupale, T. C., Dupuy, C., Subhedar, N. & Bhargava, S. Expression pattern of iodotyrosine dehalogenase 1 (DEHAL1) during chick ontogeny. *Int. J. Dev. Biol.* **54**, 1503–1508 (2010).

280. Burniat, A. *et al.* Iodotyrosine deiodinase defect identified via genome-wide approach. *J. Clin. Endocrinol. Metab.* **97**, E1276-83 (2012).

281. Pedraza, P. E., Obregon, M.-J., Escobar-Morreale, H. F., del Rey, F. E. & de Escobar, G. M. Mechanisms of adaptation to iodine deficiency in rats: thyroid status is tissue specific. Its relevance for man. *Endocrinology* **147**, 2098–2108 (2006).

282. Yu, D. *et al.* The bidirectional effects of hypothyroidism and hyperthyroidism on anxiety- and depression-like behaviors in rats. *Horm. Behav.* **69**, 106–115 (2015).

283. Buras, A., Battle, L., Landers, E., Nguyen, T. & Vasudevan, N. Thyroid hormones regulate anxiety in the male mouse. *Horm. Behav.* **65**, 88–96 (2014).

284. Venero, C. *et al.* Anxiety, memory impairment, and locomotor dysfunction caused by a mutant thyroid hormone receptor alpha1 can be ameliorated by T3 treatment. *Genes Dev.* **19**, 2152–2163 (2005).

285. Alzoubi, K. H., Aleisa, A. M. & Alkadhi, K. A. Adult-onset hypothyroidism facilitates and enhances LTD: reversal by chronic nicotine treatment. *Neurobiol. Dis.* **26**, 264–272 (2007).

286. Desouza, L. A. *et al.* Thyroid hormone regulates hippocampal neurogenesis in the adult rat brain. *Mol. Cell. Neurosci.* **29**, 414–426 (2005).

287. Davis, J. D., Stern, R. A. & Flashman, L. A. Cognitive and neuropsychiatric aspects of subclinical hypothyroidism: significance in the elderly. *Curr. Psychiatry Rep.* **5**, 384–390 (2003).

288. Ganguli, M., Burmeister, L. A., Seaberg, E. C., Belle, S. & DeKosky, S. T. Association between dementia and elevated TSH: a community-based study. *Biol. Psychiatry* **40**, 714–725 (1996).

289. Stern, R. A. *et al.* Preliminary study of the relationship between thyroid status and cognitive and neuropsychiatric functioning in euthyroid patients with Alzheimer

dementia. *Cogn. Behav. Neurol. Off. J. Soc. Behav. Cogn. Neurol.* **17**, 219–223 (2004).

290. Landucci, E. *et al.* N-(3-Ethoxy-phenyl)-4-pyrrolidin-1-yl-3-trifluoromethyl-benzamide (EPPTB) prevents 3-iodothyronamine (T1AM)-induced neuroprotection against kainic acid toxicity. *Neurochem. Int.* **129**, 104460 (2019).

291. Polini, B. *et al.* T1AM/TAAR1 System Reduces Inflammatory Response and β-Amyloid Toxicity in Human Microglial HMC3 Cell Line. *Int. J. Mol. Sci.* **24**, (2023).

292. Tu, M. *et al.* Notch1 Signaling Activation Contributes to Adult Hippocampal Neurogenesis Following Traumatic Brain Injury. *Med. Sci. Monit. Int. Med. J. Exp. Clin. Res.* **23**, 5480–5487 (2017).

293. Samuels, I. S. *et al.* Deletion of ERK2 mitogen-activated protein kinase identifies its key roles in cortical neurogenesis and cognitive function. *J. Neurosci. Off. J. Soc. Neurosci.* **28**, 6983–6995 (2008).

294. Paquin, A., Barnabé-Heider, F., Kageyama, R. & Miller, F. D. CCAAT/enhancer-binding protein phosphorylation biases cortical precursors to generate neurons rather than astrocytes in vivo. *J. Neurosci. Off. J. Soc. Neurosci.* **25**, 10747–10758 (2005).

295. Hoefig, C. S., Zucchi, R. & Köhrle, J. Thyronamines and Derivatives: Physiological Relevance, Pharmacological Actions, and Future Research Directions. *Thyroid* **26**, 1656–1673 (2016).

296. Efimova, E. V, Katolikova, N. V, Kanov, E. V & Gainetdinov, R. R. Trace amine-associated receptors at the cross-road between innate olfaction of amines, emotions, and adult neurogenesis. *Neural Regen. Res.* **17**, 1257–1258 (2022).

297. Dodd, S. *et al.* Trace Amine-Associated Receptor 1 (TAAR1): A new drug target for psychiatry? *Neurosci. Biobehav. Rev.* **120**, 537–541 (2021).

298. Borowsky, B. *et al.* Trace amines: identification of a family of mammalian G protein-coupled receptors. *Proc. Natl. Acad. Sci. U. S. A.* **98**, 8966–8971 (2001).

299. Lindemann, L. *et al.* Trace amine-associated receptors form structurally and functionally distinct subfamilies of novel G protein-coupled receptors. *Genomics* **85**, 372–385 (2005).

300. Grandy, D. K. Trace amine-associated receptor 1-Family archetype or iconoclast?

Pharmacol. Ther. **116**, 355–390 (2007).

301. Underhill, S. M. *et al.* Amphetamines signal through intracellular TAAR1 receptors coupled to Gα(13) and Gα(S) in discrete subcellular domains. *Mol. Psychiatry* **26**, 1208–1223 (2021).

302. Bradaia, A. *et al.* The selective antagonist EPPTB reveals TAAR1-mediated regulatory mechanisms in dopaminergic neurons of the mesolimbic system. *Proc. Natl. Acad. Sci. U. S. A.* **106**, 20081–20086 (2009).

303. Yang, W., Munhall, A. C. & Johnson, S. W. Dopamine Evokes a Trace Amine Receptor-dependent Inward Current that is Regulated by AMP Kinase in Substantia Nigra Dopamine Neurons. *Neuroscience* **427**, 77–91 (2020).

304. Harmeier, A. *et al.* Trace amine-associated receptor 1 activation silences GSK3β signaling of TAAR1 and D2R heteromers. *Eur. Neuropsychopharmacol. J. Eur. Coll. Neuropsychopharmacol.* **25**, 2049–2061 (2015).

305. Zhang, X. *et al.* Striatal Tyrosine Hydroxylase Is Stimulated via TAAR1 by 3-Iodothyronamine, But Not by Tyramine or β-Phenylethylamine. *Front. Pharmacol.* **9**, 166 (2018).

306. Amato, R. *et al.* Autophagy-mediated neuroprotection induced by octreotide in an ex vivo model of early diabetic retinopathy. *Pharmacol. Res.* **128**, 167–178 (2018).

307. Falkowski, B. *et al.* Higher free triiodothyronine concentration is associated with lower prevalence of microangiopathic complications and better metabolic control in adult euthyroid people with type 1 diabetes. *Endocrine* **60**, 458–465 (2018).

308. Mehalingam, V., Sahoo, J., Bobby, Z. & Vinod, K. V. Thyroid dysfunction in patients with type 2 diabetes mellitus and its association with diabetic complications. *J. Fam. Med. Prim. care* **9**, 4277–4281 (2020).

309. Wei, M. *et al.* Single-cell profiling reveals Müller glia coordinate retinal intercellular communication during light/dark adaptation via thyroid hormone signaling. *Protein Cell* **14**, 603–617 (2023).

310. Gereben, B., Kollár, A., Harney, J. W. & Larsen, P. R. The mRNA structure has potent regulatory effects on type 2 iodothyronine deiodinase expression. *Mol. Endocrinol.* **16**, 1667–1679 (2002).

311. Lourbopoulos, A. *et al.* Changes in thyroid hormone receptors after permanent cerebral ischemia in male rats. *J. Mol. Neurosci.* **54**, 78–91 (2014).

311b. Weltman N *et al*. Low-dose T_3 replacement restores depressed cardiac T_3 levels, preserves coronary microvasculature and attenuates cardiac dysfunction in experimental diabetes mellitus. Mol Med. May 1;**20(1)**:302-12. (2014)

312. Catrina, S.-B. & Zheng, X. Hypoxia and hypoxia-inducible factors in diabetes and its complications. *Diabetologia* **64**, 709–716 (2021).

313. Sullivan, K. M. Iodine deficiency as a cause of autism. *Journal of the neurological sciences* vol. 276 202; author reply 203 (2009).

314. Levie, D. *et al.* Thyroid Function in Early Pregnancy, Child IQ, and Autistic Traits: A Meta-Analysis of Individual Participant Data. *J. Clin. Endocrinol. Metab.* **103**, 2967–2979 (2018).

315. Hay, I., Hynes, K. L. & Burgess, J. R. Mild-to-Moderate Gestational Iodine Deficiency Processing Disorder. *Nutrients* **11**, (2019).

316. Sullivan, K. M. The interaction of agricultural pesticides and marginal iodine nutrition status as a cause of autism spectrum disorders. *Environmental health perspectives* vol. 116 A155 (2008).

317. Lyman, G. H. & Moses, H. L. Biomarker Tests for Molecularly Targeted Therapies--The Key to Unlocking Precision Medicine. *N. Engl. J. Med.* **375**, 4–6 (2016).

318. Rosen, A. & Zeger, S. L. Precision medicine: discovering clinically relevant and mechanistically anchored disease subgroups at scale. *J. Clin. Invest.* **129**, 944–945 (2019).

319. Berbel, P., Navarro, D. & Román, G. C. An evo-devo approach to thyroid hormones in cerebral and cerebellar cortical development: etiological implications for autism. *Front. Endocrinol. (Lausanne).* **5**, 146 (2014).

320. McTamney, P. M. & Rokita, S. E. A mammalian reductive deiodinase has broad power to dehalogenate chlorinated and brominated substrates. *J. Am. Chem. Soc.* **131**, 14212–14213 (2009).

321. Mani, A. R., Moreno, J. C., Visser, T. J. & Moore, K. P. The metabolism and de-

bromination of bromotyrosine in vivo. *Free Radic. Biol. Med.* **90**, 243–251 (2016).

322. McCall, A. S. *et al.* Bromine is an essential trace element for assembly of collagen IV scaffolds in tissue development and architecture. *Cell* **157**, 1380–1392 (2014).

323. Fukuda, A. Chloride homeodynamics underlying modal shifts in cellular and network oscillations. *Neurosci. Res.* **156**, 14–23 (2020).

324. STANBURY, J. B., KASSENAAR, A. A., MEIJER, J. W. & TERPSTRA, J. The occurrence of mono- and di-iodotyrosine in the blood of a patient with congenital goiter. *J. Clin. Endocrinol. Metab.* **15**, 1216–1227 (1955).

325. STANBURY, J. B., MEIJER, J. W. & KASSENAAR, A. A. The metabolism of iodotyrosines. II. The metabolism of mono- and diiodotyrosine in certain patients with familial goiter. *J. Clin. Endocrinol. Metab.* **16**, 848–868 (1956).

326. Medeiros-Neto, G. & Stanbury, J. B. *Inherited Disorders of the Thyroid System*. (Taylor & Francis, 1994).

Publications

- Leri M. **Bertolini A**, Stefani M and Bucciantini M. EVOO Polyphenols Relieve Synergistically Autophagy Dysregulation in a Cellular Model of Alzheimer's Disease. Int J Mol Sci. 2021 Jul 5;22(13):7225. doi: 10.3390/ijms22137225.
- Torrini F, Caponi L, **Bertolini A**, Palladino P, Cipolli F, Saba A, Paolicchi A, Scarano S, Minunni M. A biomimetic enzyme-linked immunosorbent assay (BELISA) for the analysis of gonadorelin by using molecularly imprinted polymer-coated microplates. Anal Bioanal Chem. 2022 Jan 13. doi: 10.1007/s00216-021-0386
- Shareef R, Furman A, Watanabe Y, Bruellman R, Abdullah MA, Dumitresu AM, Refetoff S, **Bertolini A**, Borsò M, Saba A, Zucchi R, Weiss RE. Congenital Hypothyroidism in Two Sudanese Families Harboring a Novel Iodotyrosine Deiodinase Mutation (IYD R279C). Thyroid. 2023 Feb;33(2):261-266. doi: 10.1089/thy.2022.0492.
- Calvigioni M, **Bertolini A**, Codini S, Mazzantini D, Panattoni A, Massimino M, Celandroni F, Zucchi R, Saba A, Ghelardi E. HPLC-MS-MS quantification of short-chain fatty acids actively secreted by probiotic strains. Front Microbiol. 2023 Mar 3; 14:1124144. doi: 10.3389/fmicb.2023.1124144. († **co-first authorship**)
- Lettieri M, Scarano S, Caponi L, **Bertolini A**, Saba A, Palladino P, Minunni M. Serotonin-Derived Fluorophore: A Novel Fluorescent Biomaterial for Copper Detection in Urine. Sensors (Basel). 2023 Mar 10;23(6):3030. doi: 10.3390/s23063030
- Bellini E, Bandoni E, Giardini S, Sorce C, Spanò C, Bottega S, Fontanini D, Kola A, Valensin D, **Bertolini A**, Saba A, Paoli L, Andreucci A, Li M, Varotto C, Sanità di Toppi L. Glutathione and phytochelatins jointly allow intracellular and extracellular detoxification of cadmium in the liverwort Marchantia polymorpha, Environmental and Experimental Botany, Volume 209, 2023, 105303, ISSN 0098-8472, doi: 10.1016/j.envexpbot.2023.105303.
- González-Guerrero C, Borsò M, Alikhani P, Alcaina Y, Salas-Lucia F, Liao XH, García-Giménez J, **Bertolini A**, Martin D, Moratilla A, Mora R, Buño-Soto A, Mani AR, Bernal J, Saba A, de Miguel MP, Refetoff S, Zucchi R, Moreno JC. Iodotyrosines Are Biomarkers for Preclinical Stages of Iodine-Deficient Hypothyroidism in Dehal1-Knockout Mice. Thyroid. 2023 Jun;33(6):752-761. doi: 10.1089/thy.2022.0537.

- Cuffaro, D.; Pinto, D.; Silva, A.M.; **Bertolini, A**.; Bertini, S.; Saba, A.; Macchia, M.; Rodrigues, F.; Digiacomo, M. Insights into the Antioxidant/Antiradical Effects and In Vitro Intestinal Permeation of Oleocanthal and Its Metabolites Tyrosol and Oleocanthalic Acid . *Molecules* 2023, *28*, 5150. https://doi.org/10.3390/molecules28135150.

- Polini, B.; Ricardi, C.; **Bertolini, A**.; Carnicelli, V.; Rutigliano, G.; Saponaro, F.; Zucchi, R.; Chiellini, G. T1AM/TAAR1 System Reduces Inflammatory Response and β-Amyloid Toxicity in Human Microglial HMC3 Cell Line. *Int. J. Mol. Sci.* 2023, *24*, 11569. https://doi.org/10.3390/ijms241411569

- Cuffaro, D.; **Bertolini, A**.; Bertini, S.; Ricci, C.; Cascone, M.G.; Danti, S.; Saba, A.; Macchia, M.; Digiacomo, M. Olive Mill Wastewater as Source of Polyphenols with Nutraceutical Properties. *Nutrients* 2023, *15*, 3746. https://doi.org/10.3390/nu15173746 († **co-first authorship**)

- Rutigliano, G.; **Bertolini, A**.; Grittani, N.; Frascarelli, S.; Carnicelli, V.; Ippolito, C.; Moscato, S.; Mattii, L.; Kusmic, C.; Saba, A.; et al. Effect of Combined Levothyroxine (L-T_4) and 3-Iodothyronamine (T_1AM) Supplementation on Memory and Adult Hippocampal Neurogenesis in a Mouse Model of Hypothyroidism. *Int. J. Mol. Sci.* 2023, *24*, 13845. https://doi.org/10.3390/ijms241813845

- Forini F, Nicolini G, Amato R, Balzan S, Saba A, **Bertolini A**, Andreucci E, Marracci S, Melecchi A, Terlizzi D, Zucchi R, Iervasi G, Lulli M, Casini G. Local modulation of thyroid hormone signaling in the retina affects the development of diabetic retinopathy. Biochim Biophys Acta Mol Basis Dis. 2023 Sep 25;1870(1):166892. doi: 10.1016/j.bbadis.2023.166892